AD NUMBER
AD339904
CLASSIFICATION CHANGES
TO: unclassified
FROM: confidential
LIMITATION CHANGES
TO: Approved for public release, distribution unlimited
FROM: Distribution authorized to U.S. Gov't. agencies and their contractors; Administrative/Operational Use; FEB 1955. Other requests shall be referred to Defense Atomic Support Agency, Washington, DC . Restricted Data.
AUTHORITY
dna-ists ltr dtd 29 aug 1995; dna-ists ltr dtd 29 aug 1995

AD NUMBER

AD339904

CLASSIFICATION CHANGES

TO

confidential

FROM

secret

AUTHORITY

DNA Notice, 3 Feb 1984

AD 339904L

SECRET

WT-733

Copy No.

Operation UPSHOT-KNOTHOLE

NEVADA PROVING GROUNDS

March - June 1953

Project 3.21

STATISTICAL ESTIMATION OF DAMAGE TO ORDNANCE EQUIPMENT EXPOSED TO NUCLEAR BLASTS

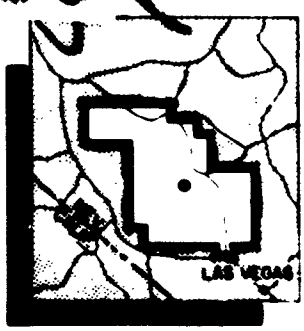

HEADQUARTERS FIELD COMMAND, ARMED FORCES SPECIAL WEAPONS PROJECT
SANDIA BASE, ALBUQUERQUE, NEW MEXICO

SECRE

SECRET

RESTRICTED DATA

Dept. no. WT-733

This document consists of 180 pages

No. 202 of 266 copies, Series A

OPERATION UPSHOT-KNOTHOLE

Project 3.21

STATISTICAL ESTIMATION OF DAMAGE TO ORDNANCE EQUIPMENT EXPOSED TO NUCLEAR BLASTS [U]

REPORT TO THE TEST DIRECTOR

by

Edward Bryant,
Noel Ethridge
Joseph McCoy, ~~1/LT, USA~~

February 1955

RESTRICTED DATA

Ballistic Research Laboratories
Aberdeen Proving Ground, Maryland

SECRET

RESTRICTED DATA

ABSTRACT

This project was concerned with obtaining sufficient data for determination of a method to predict damage to ordnance equipment exposed to nuclear blasts. The additional data were needed in order to increase the scope and reliability of the damage criteria reported in TM 23-200.

The following number of various ordnance items were exposed to provide a means for a statistical estimation of damage:

Trucks, 2-1/2 Ton M-35	27 each
Trucks, 1/4 Ton M-38A1	27 each
57 mm Guns, M-1	27 each
105 mm Howitzers, M-3	5 each
90 mm AA Gun, M-1A1	2 each

In addition, six armored vehicles were obtained from Camp Desert Rock for exposure.

Coordinated with the statistical analysis, an attempt was made to verify the Armour Research Foundation prediction methods for rotational and translational motion of vehicles, with the possibility of further correlating this motion with damage. The test items exposed were also used for verification of the prediction method for damage to ordnance items devised by Ballistic Research Laboratories.

Damage obtained on Shot 9 was within the realm of statistical estimation of damage and agreed to a fair degree of accuracy with the predicted effects based on the Ballistic Research Laboratories' prediction method. The cause for the extensive damage on Shot 10 apparently resulted from dynamic pressures related to side-on pressures of the ideal pressure-distance curve rather than from dynamic pressures related to the low side-on pressures observed. At least, the data strongly suggest this was the case.

The conclusions in general are:

1. Damage within the regular reflection region will be equivalent to or less than the damage resulting from equal overpressures within the Mach region.
2. Equipment exposed in side-on orientation are more vulnerable to blast than either face-on or rear-on orientation.
3. The probability curves obtained from the analysis provide the critera for predicting damage only to the type of equipment tested.
4. The Ballistic Research Laboratories' prediction method was

partly verified and partly contradicted. It is believed, however, that this method, with modifications, will provide a suitable method for predicting damage to equipment other than tested.

5. The calculations based on the Armour Research Foundation's prediction method provided the proper order of magnitude for the response parameters, although in general the response occurring was underestimated.

FOREWORD

This report is one of the reports presenting the results of the 78 projects participating in the Military Effects Tests Program of Operation UPSHOT-KNOTHOLE, which included 11 test detonations. For readers interested in other pertinent test information, reference is made to WT-782, Summary Report of the Technical Director, Military Effects Program. This summary report includes the following information of possible general interest.

a. An over-all description of each detonation, including yield, height of burst, ground zero location, time of detonation, ambient atmospheric conditions at detonation, etc., for the 11 shots.

b. Compilation and correlation of all project results on the basic measurements of blast and shock, thermal radiation, and nuclear radiation.

c. Compilation and correlation of the various project results on weapon effects.

d. A summary of each project, including objectives and results.

e. A complete listing of all reports covering the Military Effects Tests Program.

PREFACE

The main concern of this report is the effects of blast on ordnance equipment exposed to nuclear detonations. The information contained herein represent the findings by the authors up to the time of this writing. Upon additional analytical work and the completion thereof, supplementary reports will be published covering the subject matter.

A concerted effort was made to devise a practical and realistic evaluation of damage affecting the combat use of the ordnance equipment. No attempt was made to ascertain the relative importance of the various components influencing the over-all combat use of the items. In general, if any component was damaged whereby a significant part of the over-all combat efficiency was lost, the item as a whole was considered not usable for immediate combat. The time assigned for repair and the echelon of maintenance to restore the item to combat use serves to indicate the extent of damage.

The development of the prediction method devised by Armour Research Foundation is described thoroughly in their reports submitted to Operations Research Office of the Johns Hopkins University under "Project Attack." Because of the lack of wide distribution of the above reports, the Armour Research Foundation's prediction method as applied for this test is presented briefly herein to give the reader a general idea of the procedure for the analytical approach. The applications of this method to the exposed vehicles were made by Terminal Ballistics Laboratory of Ballistic Research Laboratories and the numerical solutions of the equations for rotational motion was done by the Computing Laboratory of Ballistic Research Laboratories.

It is pointed out that the data presented in this report are more complete and accurate than the data presented in the Preliminary Report, UKP-24. Therefore, it is requested that the preliminary report be no longer used as a reference and the copies be destroyed.

ACKNOWLEDGMENTS

The authors gratefully acknowledge the assistance and support of the many individuals and agencies who have contributed materially to the success of Project 3.21. Particular appreciation is expressed for the active participation by the following personnel from the Development and Proof Services and the Ordnance School of the Aberdeen Proving Ground. These men rendered invaluable aid in the field work and damage evaluation in the capacities noted.

Mr. H. D. Duppstadt - Damage assessment
Mr. C. D. Montgomery - Damage assessment
CWO James R. Norman, USA - Field work and damage assessment
M/Sgt G. W. Eason, USA - Field work and damage assessment
SFC T. H. Murphy, USA - Field work and damage assessment
SFC J. R. Mackey, USA - Field work and damage assessment

Special acknowledgment is gratefully extended to Mr. J. J. Meszaros, Director of Project 3.28.1, and his staff for providing suitable instrumentation. Particular mention is made of the work of Privates J. S. Michalak and G. C. Gunby who designed and constructed the special circuits to effect this instrumentation.

Appreciation is expressed to Maj William Greer and others of Program 9 for the documentary and technical motion picture photography.

Particular and grateful acknowledgment is made to Dr. F. E. Grubbs, Chief of the Surveillance Laboratory, BRL, Dr. C. W. Lampson, Chief of the Terminal Ballistic Laboratory, BRL, and Dr. E. E. Minor, Chief of the Explosion Kinetics Branch, BRL. Dr. Grubbs was responsible for the statistical analysis of the data gathered. Dr. Lampson provided technical suggestions and the wealth of his experience and knowledge of blast phenomena. Dr. Minor rendered technical assistance, encouragement, and guidance throughout the various phases of the project.

Grateful appreciation is expressed for the staff support and coordination rendered by CDR C. E. Langlois, USN, and Capt. C. H. Boyden, USAF, of Program 3, for the field support given by the troops of Camp Desert Rock and for the basic blast measurement data supplied by Program 1 and Project 3.30.

CONTENTS

ILLUSTRATIONS

TABLES

CHAPTER 1

INTRODUCTION

1.1 OBJECTIVES

The test design of Project 3.21 provided a means for three specific objectives; (1) obtain statistical data on damage, (2) verification of the prediction method devised by Armour Research Foundation for rotational and translational motion of ordnance items acted on by external forces, such body motions to be correlated with damage sustained, and (3) verification of the prediction method of damage to ordnance items exposed to atomic blasts as devised by Ballistic Research Laboratories.

The information obtained would lead to the ultimate objective for determining a method for predicting damage to ordnance equipment exposed to nuclear blast.

In a military tactical situation, whether it be a tactical offense or tactical defense, it is of primary importance for a field commander to know just how vulnerable ordnance equipment is to atomic attack and also to be able to estimate the percentages of various types of ordnance equipment which will be inoperable as a result of a nuclear blast. Therefore, the purpose of Project 3.21 was to increase the scope and reliability of damage criteria reported in TM 23-200 whereby the effects of atomic weapons may be judged to a fair degree of accuracy.

1.2 BACKGROUND

In April, 1952, the Ballistic Research Laboratories (BRL) were requested by the Office of the Chief of Ordnance (OCO) to investigate the further need for exposure of ordnance equipment to an atomic blast. The request was made in view of two projects submitted for conduct during Operation UPSHOT-KNOTHOLE. The Project, Determination of Damage Criteria to Critical Items of Military Equipment and Supplies, was submitted by Office of the Chief, Army Field Forces (OCAFF), on the basis that the data reported in TM 23-200 were inadequate to provide reliable damage criteria. The other project, Field Testing of Army Operational Equipment, was submitted through Operations Research Office (ORO) of the John Hopkins University, by Armour Research Foundation (ARF) in order to verify prediction methods for rotational and translational

motion of rigid bodies, evolved under Project Attack. The prediction method by ARF was evolved with the implied belief that there existed a correlation between motion and damage.

A survey of existing information on the effects of ordnance materiel to nuclear blasts was conducted to determine whether or not further exposures were required. An examination of the data indicated that the exposure of ordnance materiel to nuclear blasts has been limited and in many instances such equipment was exposed under conditions where zero damage occurred. Upon completion of the survey and examination thereof, it became apparent that additional information would be required to provide reliable damage criteria.

The BRL proceeded to implement a statistical test in which the requirements set forth by OCAFF could be met. It was also decided to combine the Armour test with the statistical tests wherein the ARF would instrument certain items of equipment to be used in the statistical test. At a later date a mutual agreement was reached between ORO, ARF, and BRL, that BRL instrument the ordnance equipment in order to verify the prediction method evolved under Project Attack and that BRL also retain a member of ARF in order to be assured that the objectives desired by ORO be attained.

The proposal of the combined tests for conduct during UPSHOT-KNOTHOLE was submitted to and approved by the Armed Forces Special Weapons Project (AFSWP), resulting in the authorization of Project 3.21.

1.3 SURVEY

The survey, in brief, represented an attempt to analyse the significant information contained in reports published to date.

The first atomic tests in which equipment was exposed to study effects of equipment to nuclear blasts was during Operation CROSSROADS.1/ The data obtained from this test were not included in the survey since most of the items exposed were secured aboard ships and/or shielded, which led to information not suitable for valid analysis of damage.

During Operation GREENHOUSE 2/ 10 medium tanks (2 ea. M-46 and 8 ea. M-26) were exposed and each tank was instrumented for measuring blast effects, thermal radiation, and gamma radiation. The conclusions reached after this test were limited because of lack of knowledge of the exterior blast conditions on Shot Easy.

An attempt was made to predict damage to items exposed during Operation BUSTER-JANGLE.3/ Most of the predictions for this operation were made in a zone where damage was zero.

A number of items were exposed during Operation TUMBLER-SNAPPER 4/ by the Marine Corps and Sixth Army, Camp DESERT ROCK. The main purpose of these tests was to show participating troops nuclear blast effects on military items, although the tests gave further damage information as a secondary result.

This, in general, constituted the extent to which effects tests on ordnance equipment were conducted. Except for GREENHOUSE, the air blast pressures within the vicinity of items tested were estimated, based on yield and height of burst of weapon.

CHAPTER 2

RESOLUTION OF PROBLEM

2.1 GENERAL

Prior to considering any method for predicting nuclear blast damage to ordnance equipment it was necessary that a suitable system be adapted for evaluating damage. In many cases, items that lose their combat effectiveness as a result of nuclear blasts can be restored to combat use within a short period of time and also, in many cases items although damaged may still be combat usable. The important factors for classification of damage therefore are: (1) the extent of damage affecting the combat use of military items and (2) the time required to restore the damaged items to combat use.

2.2 EVALUATION OF DAMAGE

The system adapted for damage evaluation is based on echelons of maintenance as presently used by the Department of the Army, and the time required to restore the damaged item to combat use.

The Army maintenance system is generally as follows: damaged or below standard items are inspected by qualified personnel and they determine what repairs are needed to bring those items up to the standard condition. These repairs fall into a category of maintenance as determined by the type and/or extent of the repairs required. The items are then sent to the unit or facility of the service that is able to accomplish these repairs.

The present Army system of maintenance is divided into the levels given in the following sections.

2.2.1 Organizational Maintenance

This normally incorporates 1st and 2nd echelons of maintenance. The 1st echelon of maintenance is performed by the driver or crew of the item and includes changing tires, tightening, cleaning, replenishing of oil, fuel, and water, removing rust, etc. The 2nd echelon of maintenance is performed by the trained mechanics within the using unit and

consists of minor repairs, replacement of small or minor sub-assemblies, painting, etc.

2.2.2 Field Maintenance

This incorporates 3rd and 4th echelons of maintenance. It is performed by the mobile unit and semi-mobile Ordnance Maintenance Units and Post Ordnance Shops. The 3rd echelon, performed by mobile units, includes repair work of major items for return to the using units and reclamation of unserviceable assemblies, sub-assemblies, and parts. The 4th echelon, performed by semi-mobile units, includes overflow work from the 3rd echelon units and the repair of major items for return to Utility Stocks. It also includes the reclamation and reconditioning of assemblies, sub-assemblies, and parts. These echelons are usually a Job Shop operation.

2.2.3 Depot Maintenance

This is 5th echelon maintenance. It is performed by semi-mobile and fixed type Ordnance Maintenance Units and by Class II Ordnance Installations on equipment for Depot Stocks. It includes the rebuilding of major items and the reconditioning of assemblies, sub-assemblies, and parts. It is usually a production line operation.

2.2.4 Salvage

In addition, another classification is that of Salvage which applies to the damaged items which cannot be economically repaired and to items damaged beyond repair.

2.2.5 Time for Repair

After study by personnel with field experience in maintenance, the following repair time limits for organizational maintenance were chosen:

Type of Equipment	Time Limit for Organizational Maintenance (Man Hours)
1/4 Ton Truck	6
2-1/2 Ton Truck	6
105 mm Howitzer	6
Tanks (M4A3, M26, M46)	12

It is pointed out that the time limit indicated includes the time to restore damaged items to combat use only. Thus, for example, if the damage to a 1/4 ton truck was such that the vehicle was made combat ineffective but could be repaired and made combat effective in 6 man hours or less, then it was said that only organizational maintenance would be required.

The following economical repair time limits applied in a normal military operation were taken from FM9-10, Maintenance and General Supply in the Field.

Type of Equipment	Field Maintenance (Man Hours)	Depot Maintenance (Man Hours)
Medium and Heavy Artillery	16	48
Wheeled Vehicles	32	96
Tanks	64	128
Power Train Assemblies		16
Engines		32

The man hours indicated above refer to a complete rebuilding of the equipment.

It was desired to generalize this method of damage evaluation to degrees of damage (light, moderate and severe) to conform with the present criteria used in TM 23-200, Capabilities of Atomic Weapons. Hence, light damage will constitute that damage which will not affect the combat use of the items; moderate, that damage requiring from organizational up to and including field maintenance to restore the item to combat use; and severe, that damage requiring depot maintenance and damage classified as salvage.

Tables A.1 and A.2 shown in Appendix A, delineate echelon of maintenance and time required to replace or restore damaged components of 105 mm howitzers and medium tanks. The table for the 105 mm howitzers is also applicable to the 57 mm guns. The time estimates in the above tables are based on the personal experience of several officers and ordnance mechanics with field experience. Standard time estimates to replace or restore damaged components for wheeled vehicles (2-1/2 ton and 1/4 ton trucks) are presented in TBORD-173, Unit Replacement and Repair Time Guide for Wheeled Vehicles.

2.3 STATISTICAL ESTIMATION OF DAMAGE 5/

The initial problem was to select appropriate positions or distances from ground zero where various types of ordnance equipment were to be placed for Shots 9 (8 May) and 10 (25 May). It was desired to place items where the expected damage would vary between 100 per cent and zero per cent as related to combat effectiveness. It was decided to estimate the probability of damage as a function of overpressure from existing but rather inconclusive data. Discussions with Army Field Forces indicated that the most desired information was (1) data that would allow prediction of the proportion of vehicles which would be available for combat within a given time after exposure to nuclear blasts, and (2) information in terms of distances from ground zero which would indicate a region encompassing 100 per cent to zero per cent damage as related to combat effectiveness for different types of equipment. It was also desirable to know the proportion of military items of a given type which are rendered ineffective for immediate combat but can be restored to combat use within a short period of time and with a minimum of maintenance. The time parameter for repair was chosen to be zero.

As a result of past tests, specific damage for a given blast overpressure was recorded and estimates were simply made of time required to restore the damaged piece of ordnance equipment to combat use.

These times were estimated to a best approximation by qualified personnel based on information of damage recorded in various test reports. By this method, a quantitative analysis of data has been made, based on overpressure and the estimated time for restoration to combat effectiveness in accordance with the two parameters of organizational maintenance time limit and immediate combat ineffectiveness (zero hours).

Using this assumption that the probability of damage varies normally with the value of overpressure and tabulating whether or not organizational maintenance is required, it then becomes possible to estimate the mean and standard deviation of the assumed normal curve (see BRL Technical Note No. 151, On Estimating Ballistic Limit and Its Precision).

Curves have been drawn and are herein included which indicate for four types of ordnance equipment the proportion of items which would be combat ineffective immediately after exposure and the proportion of items that will require maintenance beyond organizational capabilities to restore to combat use. These curves show plots of probability of damage between unity and zero as a function of the overpressure. Figures 2.1 and 2.2 give probabilities that a 1/4 ton truck will not be combat usable within 6 hours and zero hours respectively, as a function of overpressure. Figures 2.3 and 2.4 give the proportions of 2-1/2 ton trucks which will not be combat usable within 6 hours and zero hours respectively. Figures 2.5 and 2.6 give the proportions of the 105 mm howitzers which will not be combat usable within 6 hours and zero hours respectively. Finally, Figs. 2.7 and 2.8 present the chance that the tanks of the type M4A3, M-26, and M-46 (considered collectively) will not be combat usable within 12 hours and zero hours respectively. These curves are not very well established because of the paucity of data and, therefore, the curves were used as guides only. The estimated standard deviations for the parameters (mean and standard deviation) of the normal distribution fitted are given in Table 2.1.

TABLE 2.1 - Parameters of the Normal Distribution for Probability of Organizational Maintenance (6 Hours and Zero Hours) as a Function of Overpressure

Item	Time	Figure	Mean	Std. Dev.
1/4 Ton Truck	6	2.1	23.1	7.6
1/4 Ton Truck	0	2.2	12.0	2.0
2-1/2 Ton Truck	6	2.3	14.9	4.8
2-1/2 Ton Truck	0	2.4	13.4	6.4
105 mm Howitzers	6	2.5	47.1	2.1
105 mm Howitzers	0	2.6	24.6	11.3
Medium Tank	12	2.7	76.0	33.5
Medium Tank	0	2.8	38.0	20.5

The equation to fit the curves of Fig. 2.1 through Fig. 2.8 is:

$$P = \frac{1}{\sqrt{2\pi}} \int_{-\infty}^{t} e^{(-1/2)t^2} \, dt \qquad (2.1)$$

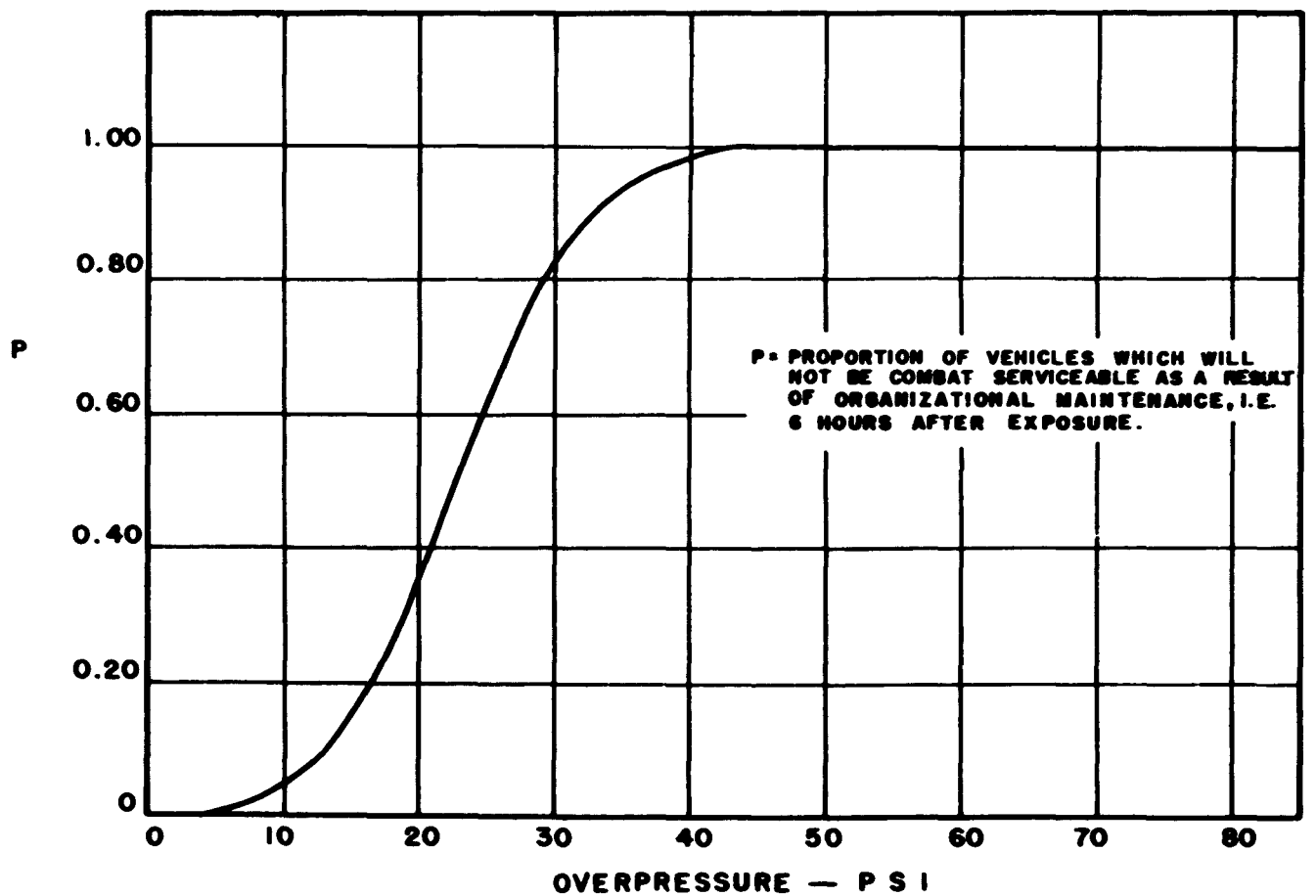

Fig. 2.1 Probability of Damage vs Overpressure
(1/4 Ton Truck) (6 Hours)

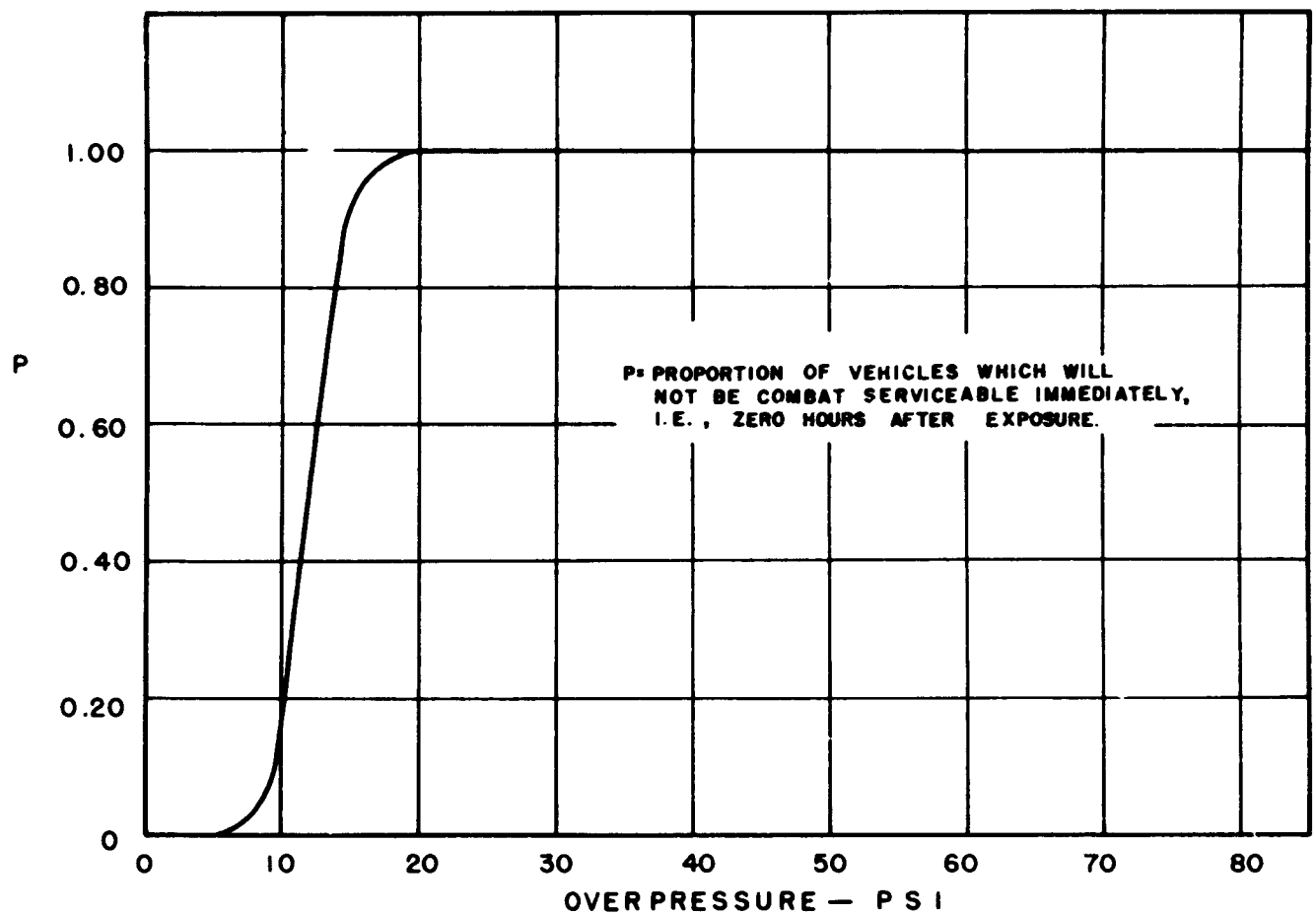

Fig. 2.2 Probability of Damage vs Overpressure
(1/4 Ton Truck) (0 Hours)

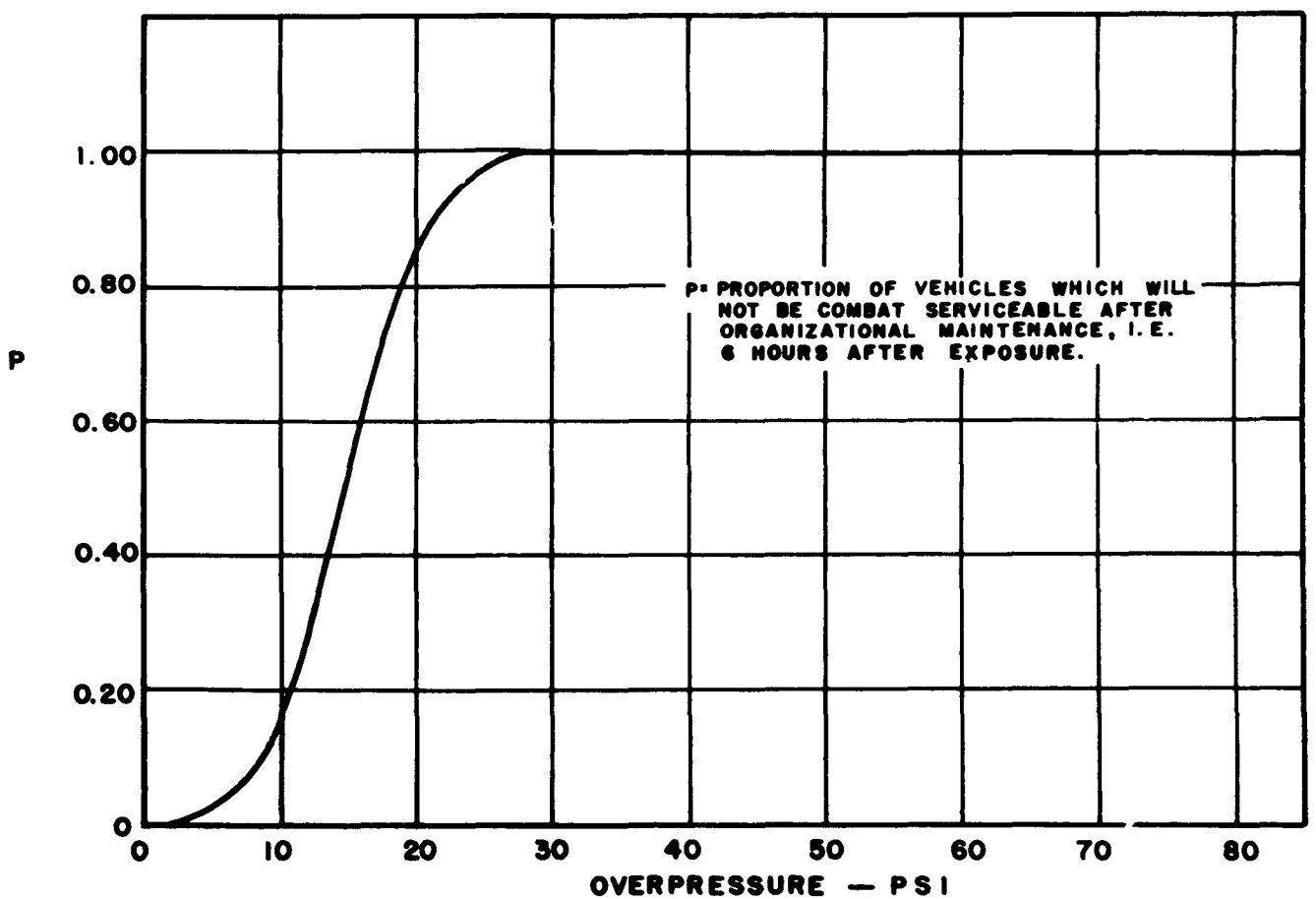

Fig. 2.3 Probability of Damage vs Overpressure
(2-1/2 Ton Truck) (6 Hours)

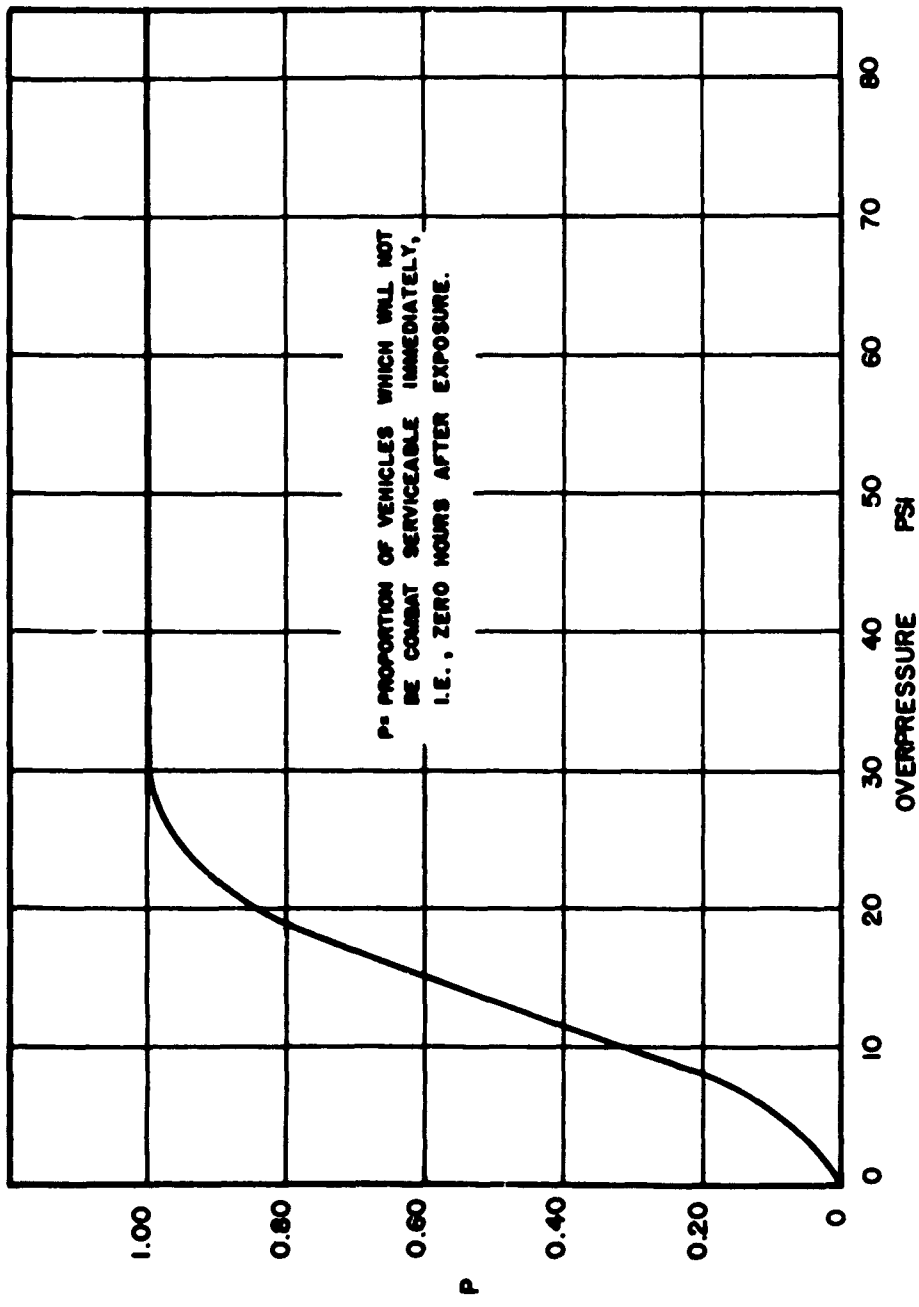

Fig. 2.4 Probability of Damage vs. Overpressure (2-1/2 Ton Truck) (0 Hours)

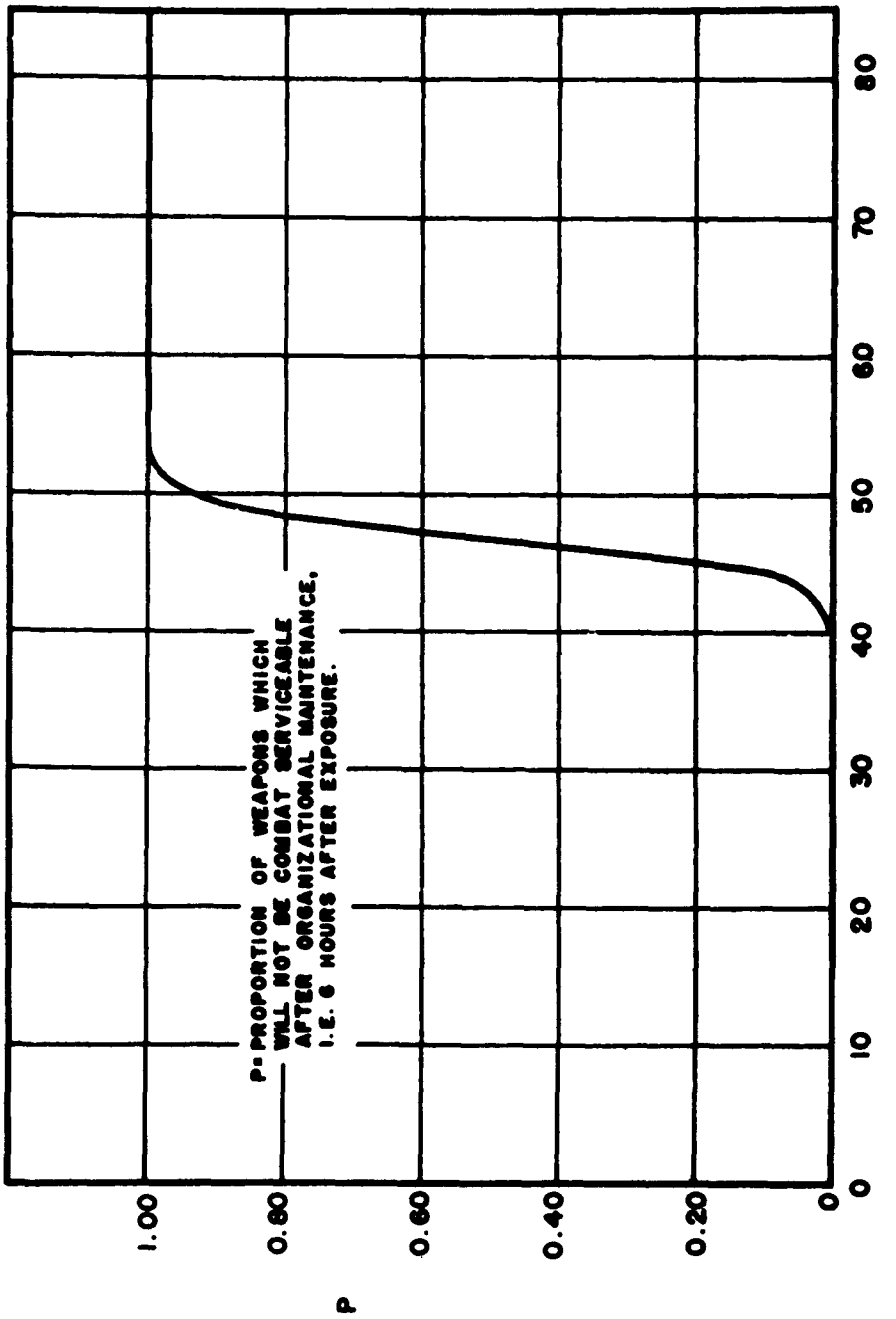

Fig. 2.5 Probability of Damage vs Overpressure (105 mm Howitzers) (6 Hours)

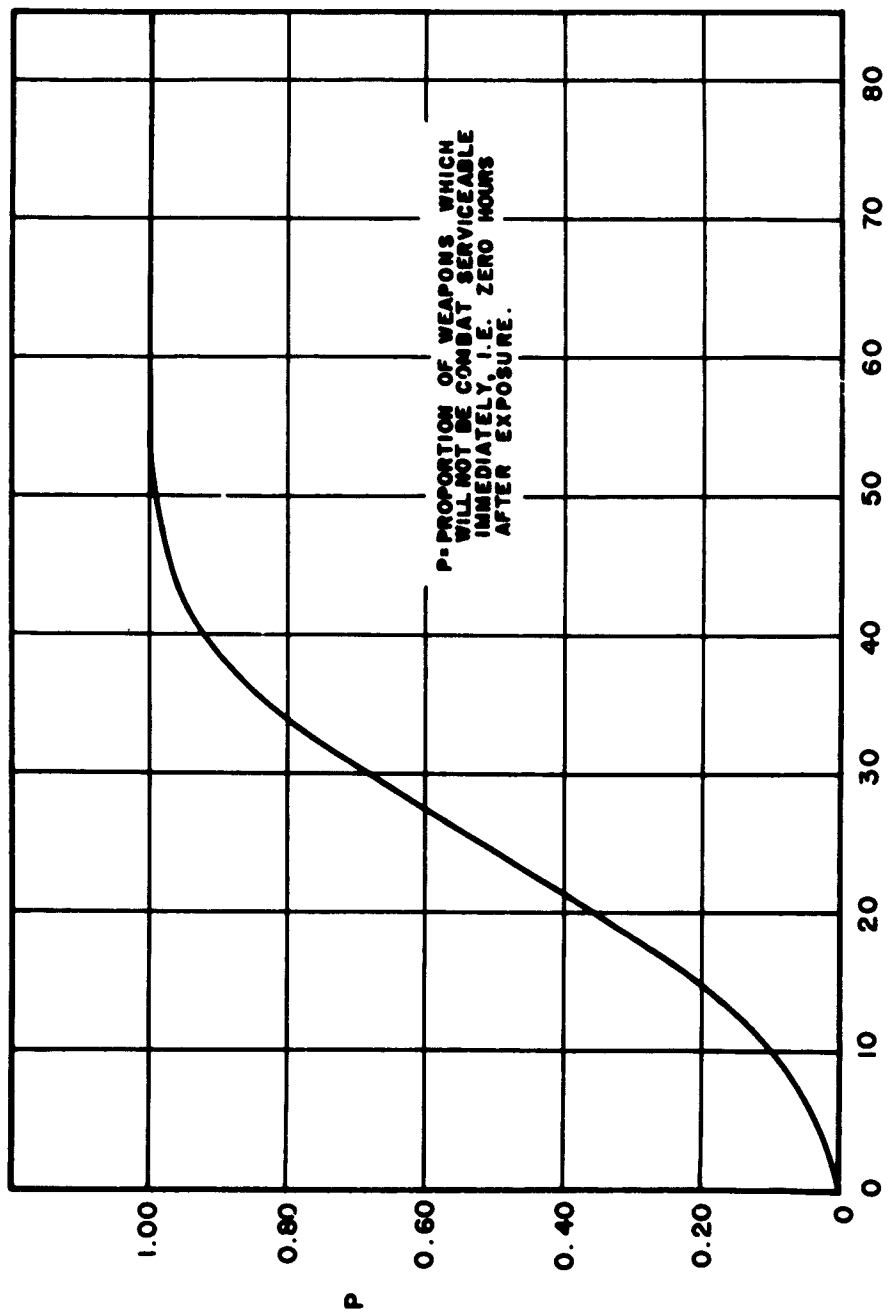

Fig. 2.6 Probability of Damage vs. Overpressure (105 mm Howitzers) (0 Hours)

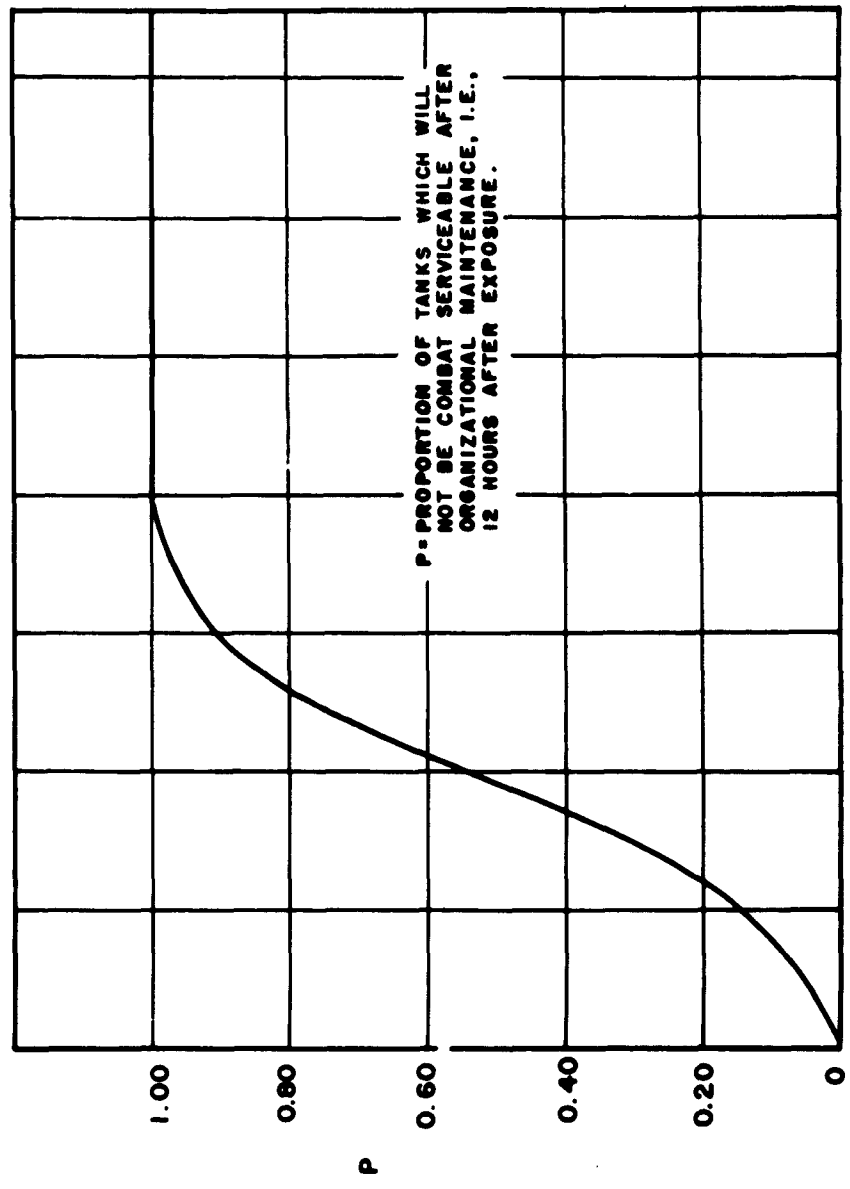

Fig. 2.7 Probability of Damage vs Overpressure (Medium Tanks) (12 Hours)

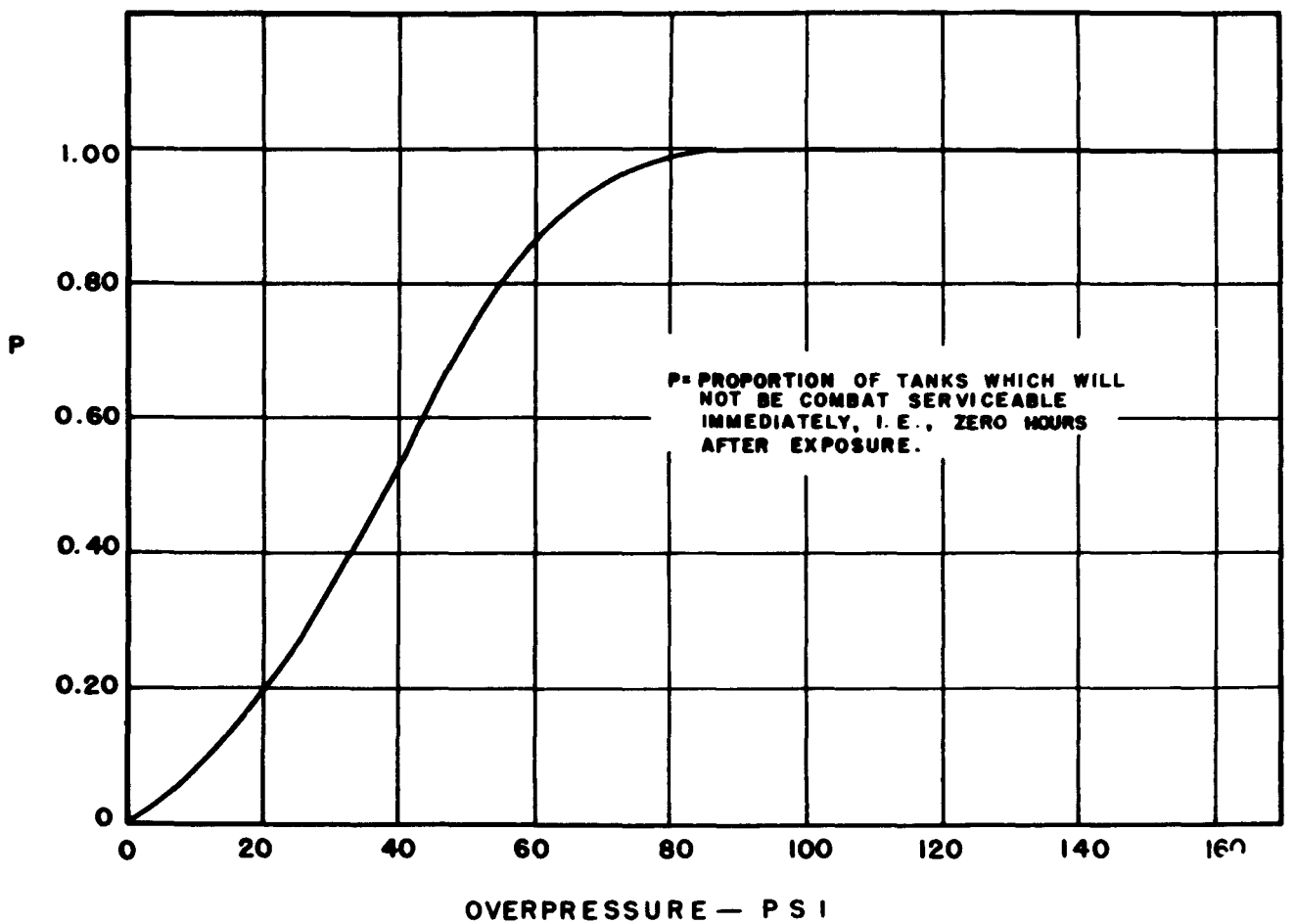

Fig. 2.8 Probability of Damage vs Overpressure (Medium Tanks) (0 Hours)

where:

P = Probability

$t = \frac{\text{overpressure} - \mu}{\sigma}$

and: μ = mean value

σ = standard deviation

A completely satisfactory solution showing exactly where to place various types of ordnance equipment so that the probability of damage curve may be estimated with best accuracy has not been obtained because of the theoretical difficulties involved. It is clear, however, that the majority of the pieces of equipment should be placed within a zone so that there results a mixture of cases where damage occurs on some pieces and does not occur on other units. Also, a definite loss in precision results, if half of the vehicles are placed so close to ground zero that these are all damaged and the other half are placed so far away that no damage results. Therefore, it appeared desirable for the method of analysis employed to place pieces of equipment within a zone where the probability of damage varies from about 0.05 to 0.95 for items requiring maintenance beyond organizational to restore to combat use. In this manner a mixture of results will occur, i.e., the repair time parameter will be varied. For a given available number of pieces of equipment, the problem of best distribution within such a zone in order to obtain the most precise damage curve remains to be investigated. It was decided that the pieces of equipment would be placed at approximately equal intervals of pressure over the 0.05 to 0.95 probability zone.

2.4 BALLISTIC RESEARCH LABORATORIES PREDICTION METHOD FOR DAMAGE

This particular method of predicting damage [6] was empirically obtained based on results of previous tests. The following equation is extracted from Reference 6 to present briefly this prediction method.

$$r = \left[(P_s/e)\ C_d\ \frac{A}{W} - 0.7\right]\ k_1\ k_2 \qquad (2.2)$$

where:

A = Projected area of items normal to the direction of propagation.

C_d = Drag coefficient, assumed to vary from 0.5 for a cylindrical shape to 1.2 for a flat plate.

e = Exponential function, 2.72.

k_1 = Length of item along line of shock wave propagation normalised to some arbitrary unit of length. The width of the M-26 tank (11.5 ft) is the normalising factor used.

k_2 = A dimensionless number characteristic of a particular item. This number is shown as a function of log W in Fig. 2.9.

W = Net weight in pounds of the exposed item.

p_s = Overpressure in psi.

$\mathcal{F}$ = A factor related to combat effectiveness as shown in Fig. 2.10.

The pressures P_s to be correlated with damage in the regular reflection region are the pressures of the incident wave, and as the critical angle for Mach formation is approached the measured reflected overpressures are used. Within the region of Mach formation the Mach overpressures are to be correlated with damage.

For all vehicles and large guns (equal to or larger than 105 mm howitzers) the length used in computing k_1 is essentially the tread of the item (side exposed). For all 30 caliber machine guns and smaller items, the characteristic length for guns (not mounted on motor carriers) between 30 caliber machine guns and 105 mm howitzers is somewhere between the barrel diameter and the tread of the weapon. In general, if the carriage of the weapon is large in weight or area compared to the gun itself the value k_1 corresponds to a length of approximately two-thirds of the tread of the carriage. If the reverse is true, k_1 corresponds more nearly to the barrel diameter of the gun.

Because of the limited time available prior to the test, the computations made for predicting damage were attempted for the 1/4 ton trucks only. However, for completeness of this report the computations for predicting damage to all of the items exposed were made after the test and are included in Table 2.2.

Table 2.2 indicates the extent of damage as a function of overpressure for the items exposed in Shots 9 and 10. Using the information contained in the BRL report,[6] the lethal radius of effect has been computed. The values of pressure used for computing the lethal radius were taken from Fig. 7 of TM 23-200 corrected to test altitude.

TABLE 2.2 - Predicted Effects Using BRL Prediction Method

Shot	Item	Orientation	% C.E.*	Overpressure (psi)	Lethal Radius (ft)
9	1/4 ton truck	Side-on	60	8.8	2970
9	1/4 ton truck	Face-on	60	8.2	3230
9	2-1/2 ton truck	Side-on	60	8.12	3220
9	2-1/2 ton truck	Face-on	60	10.16	2480
10	1/4 ton truck	Side-on	10	21.5	1420
10	2-1/2 ton truck	Side-on	10	18.9	1670
10	Medium Tank (M4A3)	Side-on	10	52.1	880
10	57 mm AT Gun	Side-on	10	67.8	810

* C.E. denotes combat effectiveness

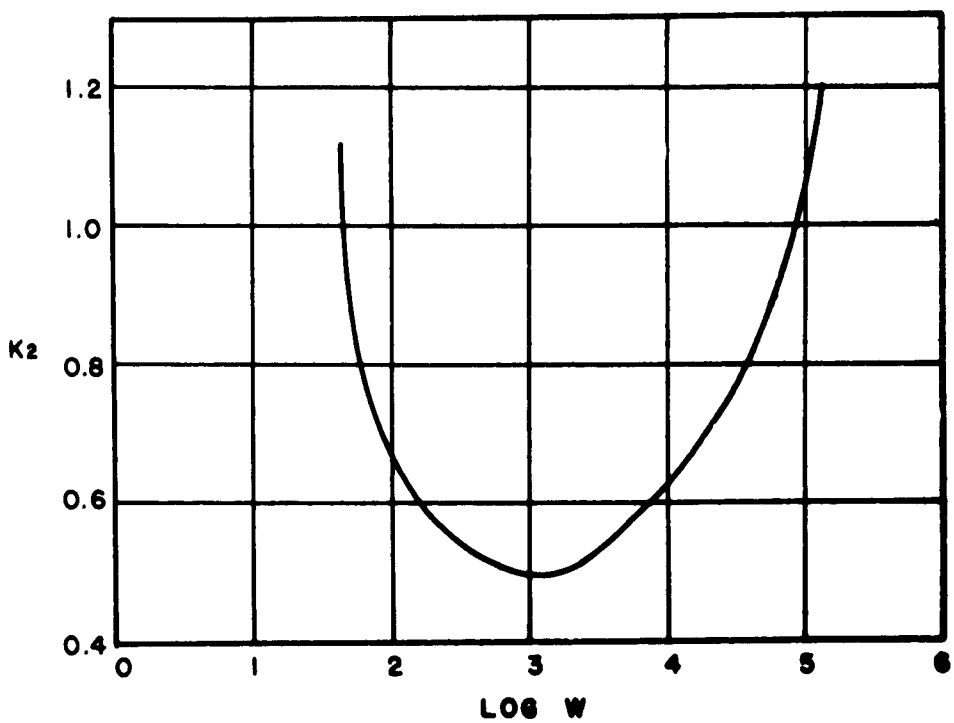

Fig. 2.9 Dimensionless Parameter K_2 as a Function of Log W

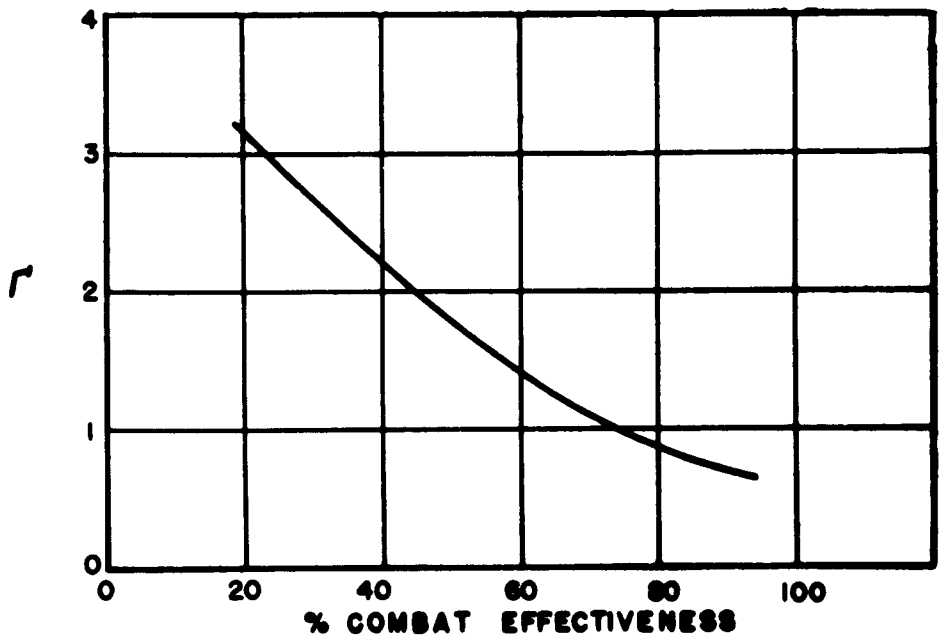

Fig. 2.10 Factor Γ as a Function of Per Cent Combat Effectiveness

2.5 THE ARMOUR RESEARCH FOUNDATION PREDICTION METHOD

2.5.1 General

The approach of the Armour Research Foundation to the damage prediction problem was to devise a method for predicting the loading and response of bodies exposed to nuclear blasts, assuming that there exists a correlation between the motion of a rigid body and the damage occurring to the body. If the proper correlation were established then the method would provide the means for predicting damage.

The development of the method for predicting the loading and response on movable targets is contained in the ARF reports 7, 8, 9, 10, and 11 for Project Attack. The problem was similar to that of estimating loading on stationary buildings, except in addition the effects of translations and rotations on the loading and the various types of motion response were considered. The damage resulting from the motion can be expected to vary with the type of motion resulting (translation, rotation, or a combination thereof). The method was developed from a limited amount of data and discrepancies can result from many causes. Therefore, experimental confirmation was necessary to establish its usefulness.

To provide this experimental confirmation it was necessary to verify the predictions of loading and response for rigid bodies and then to establish the relations between the motion parameters and the damage to the body. The usefulness of the method will be determined by the degree of correlation between a predictable parameter and the actual damage inflicted. The necessary information for damage inflicted on particular targets was obtained in fulfilling the other objectives of the project. Therefore the field work of the ARF phase of the project resolved into obtaining necessary loading and response data.

It was desirable to verify the predicted pressure loadings on the test targets in addition to investigating their motion. However, to obtain a true picture of the pressure loading on an odd-shaped target such as the truck would have required more instrumentation channels than were available for this project. Therefore, it was decided to restrict the instrumentation to measuring the response instead of loading. It was expected that the loading data obtained by other projects will provide further insight into the loading process for the vehicles.

The response variables selected for measurement were the displacement, the angular velocity about an axis parallel to the expected turning axis, and the horizontal and vertical components of acceleration. Motion photography was used in an attempt to record displacement versus time.

The ARF method was developed specifically for a shock wave with a plane wave front. On Shot 9 a major portion of the vehicles were placed in the regular reflection region, and some prediction of the effects to be expected was desired. It was reasonable to expect that the effects in the regular region for a given pressure would be less than the effects caused by a Mach wave of the same pressure and duration because of the reduction in the horizontal component of wind

velocity in the regular reflection region. Therefore to obtain an approximate upper bound on the effects to be expected, the calculations were made assuming the targets were struck by a Mach wave of the same pressure and duration as the expected reflected wave. To obtain an idea of the reduction in effects possible a very simple modification was performed. The diffraction loading characteristics were assumed to be the same, but the expression for the drag pressure in the equations of motion was reduced in the same proportion that the horizontal wind velocity would be reduced for acoustic reflection. The gage ranges were selected so that insofar as possible a satisfactory reading would be obtained for the effects calculated for both cases.

Predictions of loading and response were made for the vehicular targets at the five test stations suitable for instrumentation on Shot 9. Values were obtained for the total displacements, accelerations, and angular velocities, and these values were considered in the selection of gage ranges. No calculations were made for Shot 10 prior to the test. Because of the expected slightly shorter pressure phase durations the values of the response parameters were expected to be approximately the same or slightly less than those derived for Shot 9 at corresponding Mach pressure levels.

Necessary information for the performance of the calculations was knowledge of the shape of the pressure-time decay curve, the duration of the positive phase, the shock front velocity, the velocity of the rarefaction wave in the reflected region, and the peak reflected pressure developed by the shock striking a perpendicular wall. The pressures expected at the stations of interest and the durations were obtained from scaled data of TUMBLER 1. The expressions used for the calculations of the other data were obtained from a GREENHOUSE report.[12]

The targets for which the calculations were made were the 1/4 ton truck M38A1 and the 2-1/2 ton truck M-135. When the calculations were well under way the 2-1/2 ton truck M-35 was substituted because the M-135 became unavailable. There was not sufficient time prior to the test for recalculation. However, because of the basic similarity of the vehicles the loading and response characteristics of the M-135 were assumed to apply to the M-35 as well.

Characteristic data on the guns were not received in time for application of the Armour method to these weapons. The application of the method to the gun and to the M-35 is in progress, and the results will be placed in supplementary reports.

2.5.2 Loading

The ARF method for calculation of loading on an odd-shaped target such as a vehicle is an adaption of the loading scheme for a rectangular parallelepiped, or cuboid. The target is divided into a number of appropriate cuboids which are estimated to receive as a whole loading equivalent to that received by the actual vehicle. The loading on each cuboid is determined from its assigned dimensions and the characteristics of the shock wave striking it. The values for each cuboid are appropriately summed to obtain total loading.

The loading on a single cuboid on the ground plane is presented in the Armour reports(9)and(10)as follows: A rigid cuboid fixed to the ground is assumed to be struck by a plane shock wave moving with the plane of the wave front parallel to the face of the cuboid. The time the wave strikes the front face is designated as zero time.

On the front face the pressure rises instantly to the value of peak reflected pressure. This pressure decreases to overpressure plus two-thirds the drag pressure in a time equal to three times the time necessary for a sound signal in the reflected region to travel the minimum of height or one-half the width of the front face of the cuboid, whichever dimension is smallest. This pressure decreases as the shock front passes the front face and reaches zero at a time equal to the duration of the shock wave. The upper curve in Fig.2.11 represents this pressure.

The rear of the cuboid remains at atmospheric pressure until the shock front travels the length of the cuboid. As the shock front passes the rear face, the pressure begins to rise on the rear from atmospheric to overpressure minus one-third the drag pressure in the time required for the sound signal to travel a distance eight times the minimum of height or one-half the width of the rear face. This pressure decreases and reaches atmospheric pressure at a time equal to the duration of the shock wave. The lower curve in Fig.2.11 represents this pressure.

Insufficient information is available to describe the loading on the top surface accurately, and the forces are assumed to make only a negligible contribution to the motion of the cuboid.

The resultant force/in^2 acting on the cuboid then is the pressure on the front face minus the pressure on the rear face. The impulse/in^2 is the area under the curve of pressure on the front face minus the area under the curve of pressure on the rear face. The period from $t = 0$ to the time t_D is called the shock loading period. At the time t_D the pseudo-steady state is reached and forces acting are drag forces only. The resultant area under the curves up to the time t_D at which pseudo-steady state is reached represents the shock loading impulse/in^2. The resultant area from the time t_D to the time t_o represents the impulse/in^2 due to drag pressure. Refer to Fig. 2.11.

For the calculation of impulse the area under the curve is divided into several parts. These are indicated in Fig. 2.16. From the figure it is apparent that:

$$A_1 - A_2 + A_3 + A_4 = \text{Total Impulse/in}^2 \qquad (2.3a)$$

$$A_1 - A_2 + A_3 = \text{Shock Loading Impulse/in}^2 \qquad (2.3b)$$

$$A_4 = \text{Impulse due to Drag Pressure/in}^2 \qquad (2.3c)$$

$$Y(A_1 - A_2 + A_3) = \text{Angular Shock Loading Impulse/in}^2 \qquad (2.3d)$$

The areas can be expressed as follows:

$$A_1 = 1/2\ (Pr + P_B)\ t_B \tag{2.4a}$$

$$A_2 = 1/2\ P_D\ (t_D - t_C) \tag{2.4b}$$

$$A_3 = 1/2\ (P_B + P_E)\ (t_D - t_B) \tag{2.4c}$$

$$A_4 = C_D \int_{t_D}^{t_o} Pd\ (t)\ dt \tag{2.4d}$$

where:

$$P_B = Ps\ (t_B) + 2/3\ Pd\ (t_B) \tag{2.5a}$$

$$P_D = Ps\ (t_D) - 1/3\ Pd\ (t_D) \tag{2.5b}$$

$$P_E = Ps\ (t_D) + 2/3\ Pd\ (t_D) \tag{2.5c}$$

$$t_B = 3h/C_r \tag{2.6a}$$

$$t_C = L/U \tag{2.6b}$$

$$t_D = t_C + 8h/U \tag{2.6c}$$

and:

P_B, P_D, P_E = Pressures at the times indicated by the subscript

Ps = Overpressure in lb/in^2

Pr = Reflected pressure in lb/in^2

Pd = Drag pressure in lb/in^2

U = Velocity of the shock front

C_D = Coefficient of drag

t_o = Duration of positive phase

Y = Distance from ground plane to center of front face of cuboid

C_r = Velocity of the rarefaction wave

h = Minimum of height or 1/2 width of the cuboid, whichever is smaller

L = Length of the cuboid along shock path

Thus the total impulse, the shock loading impulse, and the drag loading impulse can be calculated for a cuboid.

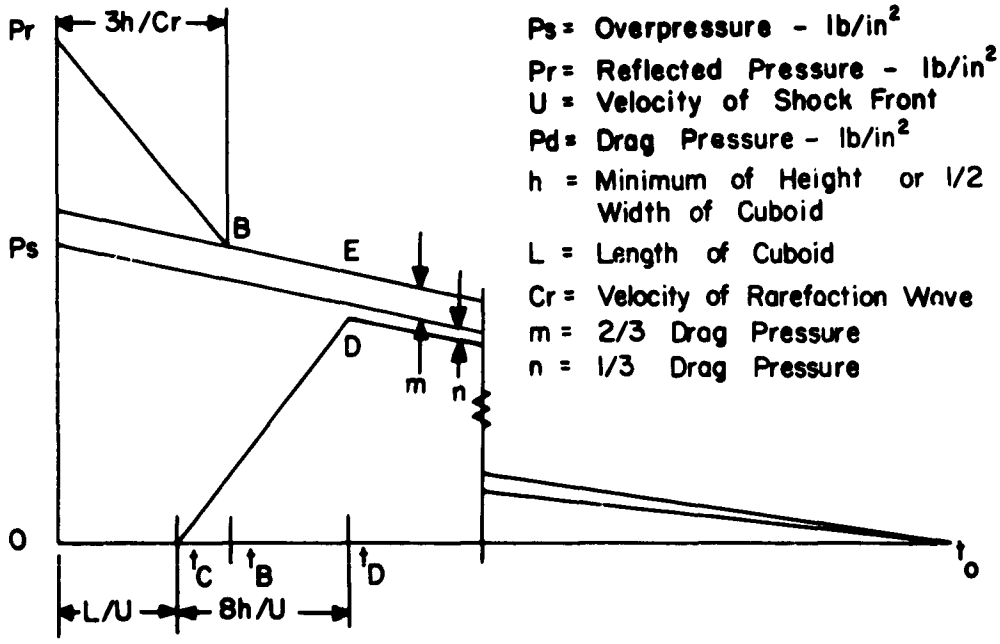

Fig. 2.11 Pressure Loading vs Time on a Cuboid

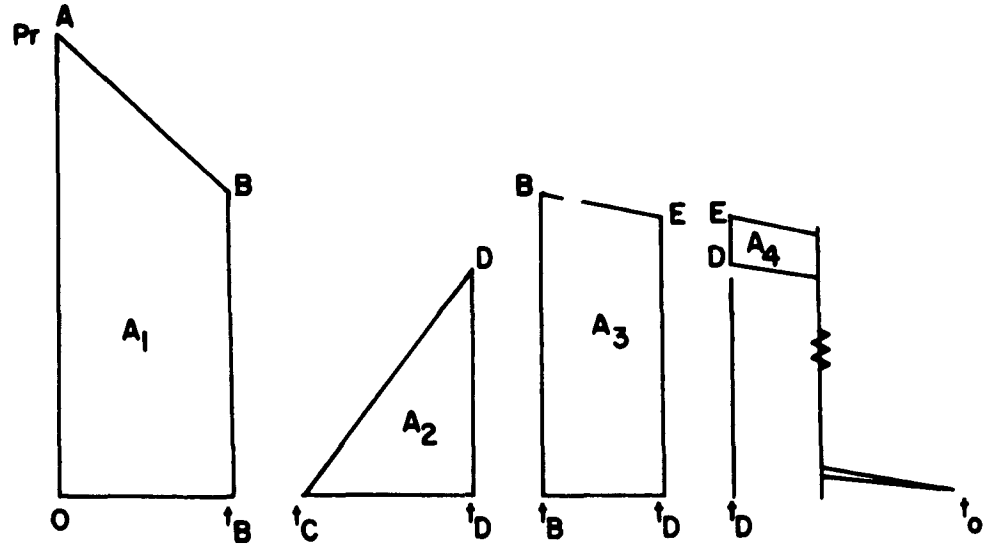

Fig. 2.12 Areas for Impulse Calculation for a Cuboid

The loading on a target of irregular shape (such as a vehicle) is approximated by constructing a cuboid representation of the target so that the expected loading on the target and on the cuboid representation is equivalent. For a given target the choice of cuboid representation will vary depending upon the person applying the method because of varying estimations of the cuboid dimensions to duplicate the actual component loading characteristics. The equivalent cuboid is clear in the case of such parts as the tail gate or the gas tank of a truck. But in the case of the under body and chassis parts the estimation of a suitable equivalent cuboid is difficult. The accuracy of the method does not justify considering every part of the vehicle individually.

When the cuboid representation of the target is constructed then the loading scheme as described for a single cuboid is applied separately to each component cuboid, where the clearing times for the front face, the loading times on the rear face, and the drag coefficients are adjusted according to the location and characteristics of each component cuboid.

The total impulse imparted to the target during the period of the diffraction of the shock around the target is termed the total shock loading impulse, and it is assumed to be the sum total of the shock impulse for this period for each cuboid. The total drag impulse for the target is the impulse received from the end of the shock loading period to the end of the positive duration of the blast wave. The total impulse is assumed to be the sum of the drag impulse of the component cuboids. The time t_w at which the shock loading is over and drag loading begins is fixed by taking the maximum time of shock loading of the component cuboids.

The angular impulse imparted to a component cuboid about an axis in the ground plane is found by multiplying the linear impulse for the cuboid by the distance from the center of pressure for the area of the front face to the ground plane. The angular impulse imparted to the target then is assumed to be the sum of the angular impulse for the various component cuboids.

As indicated in the ARF reports there are several sources of possible errors in the ARF prediction method. For the vehicular target, which is supported above the ground, the force acting on the underside of the vehicle is assumed to be equal and opposite to the force on the top at all times, for lack of data indicating the true situation. For the same reason the method does not take into account vortex and turbulence phenomena. The estimation of the drag coefficients may introduce major discrepancies. The effect of the motion of the targets on their loading was investigated in the ARF reports and the conclusion was reached that if the target moved at velocities less than 100 ft/sec the effect on loading forces could be neglected at the present stage of development of the method. An additional factor that will produce discrepancies is the non-rigidity of the vehicular target. The method is designed for rigid bodies and the effects on a vehicle may be different due to elastic and inelastic deformation.

2.5.3 Response

The response of the target to the loading forces is calculated under simplifying assumptions, namely, that the target responds as a rigid body, that no motion occurs during envelopment by the shock wave, and that the response is in the form of sliding or rotation but not a combination of the two motions.

If the target is assumed to move a negligible distance during the shock loading period (justified by the short time length of the period and the large mass of the target) then the loading occurring during this period can be considered impulsively applied, and the resulting change of momentum computed from the equation:

$$mv_1 - mv_0 = Ft^* = \text{Impulse} \qquad (2.7)$$

Here m is the mass of the target, v_0 is its velocity at zero time, v_1 is the velocity at the end of the shock loading period, F is the force applied, and t^* is the time length of the shock loading period. Since the velocity of the target is initially zero, then the result of the shock loading impulse is the imparting of the velocity v_1 to the target.

After the end of the shock loading period only drag forces are considered to be acting and the resulting motion is expressed in an equation involving these time-dependent drag forces. The value of velocity produced by the shock loading impulse is applied as an initial condition on this equation. If the variable involved in the equation of motion is linear displacement then the velocity resulting from the linear shock loading impulse can be computed from equation 2.7 by substituting the appropriate values of impulse and mass and solving for the velocity.

If the variable under consideration is the angle denoting the rotation of the center of gravity about a selected axis, then the initial angular velocity at the beginning of the drag loading period is obtained from equation 2.7 by substituting values for the angular shock loading impulse, and for moment of inertia rather than the mass, and solving for the angular velocity.

The equation of motion describing translation over the surface ground plane is derived as follows: A cuboid supported above the ground plane is assumed to slide over the ground plane with no rotation occurring as shown in Fig. 2.13.

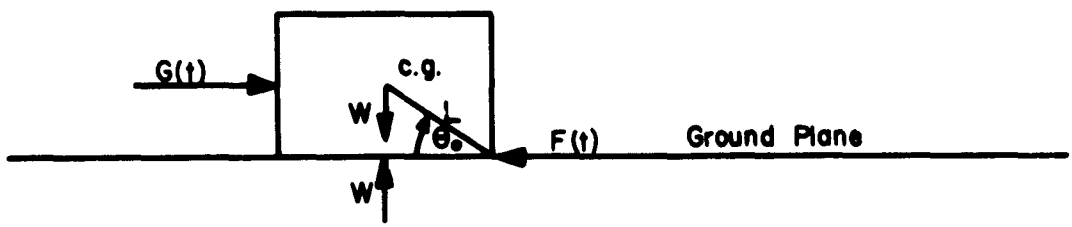

Fig. 2.13 Forces Acting on a Sliding Cuboid

Here G(t) is considered the positive force due to drag pressure, and F(t) is the opposing frictional force. The moments are assumed to be such that no rotation occurs. Then the force G(t) is opposed by an equal force F(t) until G(t) exceeds the maximum value of F(t). Then sliding occurs, and the equation of motion is:

$$(W/g)\ d^2x/dt^2 = G(t) - F(t)$$

Now $G(t) = Pd(t)\ A_s$, where Pd(t) is the drag pressure as a function of time, and A_s is the drag area presented by the target to the dynamic pressure, and $F(t) = \mu(t)\ W$, where $\mu(t)$ is the coefficient of friction and W = weight of the target. Then substituting:

$$d^2x/dt^2 = (g/W)\ Pd(t)\ A_s - (g/W)W\mu(t)$$

$$= g\left[\ Pd(t)\ (A_s/W) - \mu(t)\right] \qquad (2.8)$$

The integration limits are taken from an initial time t_* to t, and the coefficient of friction μ is assumed to be a constant. The result is:

$$dx/dt = (gA_s/W)\int_0^t Pd(t)\ dt - \mu g(t-t_*)$$

$$- (g\ A_s/W)\int_0^{t_*} Pd(t)dt + (dx/dt)_* \qquad (2.9)$$

Here t_* is taken as the end of the shock loading period. Then $(dx/dt)_*$ is the velocity derived from equation 2.7.

The value for the displacement was obtained by integrating expression 2.9 and the result is as follows:

$$x = (g\ A_s/W)\int_0^{t'}\left[\int_0^t Pd(t)dt\right]dt - (g\ A_s/W\int_0^{t_*}\left[\int_0^t Pd(t)dt\right]dt$$

$$-(t' - t_*)\left[(\mu g/2)\ (t' - t_*) + (g\ A_s/W)\int_0^{t_*} Pd\ (t)dt - (dx/dt)_*\right] \qquad (2.10)$$

The second term was found to be negligible for the vehicular targets. For the total displacement the time t' is the time at which the velocity reaches zero and is derived from equation 2.9:

$$\int_0^{t'} Pd(t)dt = \mu g(W/g\ A_s)\ (t' - t_*) + \int_0^{t_*} Pd(t)dt - (W/g\ A_s)\ (dx/dt)_* \qquad (2.11)$$

The intersection of the straight line given by the right-hand expression with the integral curve on the left yields t' for the total displacement calculation.

No additional constant appears after integrating the velocity since at $t = t_*$ the displacement is assumed to be zero. The double integral term can be obtained by use of Simpson's Rule. Equations 2.8, 2.9, and 2.10 then describe the case of pure translational motion.

It is useful to examine the conditions necessary for no rotation to occur. Consider the turning moments acting on the cuboid in Fig. 2.13. The overturning couple is determined by the magnitude of the frictional force. Equating moments:

$$I\, d^2\theta/dt^2 = F(t)\, Y_d - Wl \cos\theta_o$$

At $t = t_*$ $Y_d = Y_s$ (the distance from the ground plane to the point of application of the drag force on the side of the target). $F(t) = \mu W$ where μ is the coefficient of friction. $G(t) = Pd(t)A_s$ where $Pd(t)$ is the drag pressure. Then for no turning to occur:

$$\mu(t)\, W\, Y_s \leq Wl \cos\theta_o \qquad (2.12)$$

For no sliding:

$$G(t) \leq F(t)$$

$$Pd(t)A_s \leq \mu(t)\, W \qquad (2.13)$$

Now the case for rotation only is considered. If rotation of the target occurs then it is assumed to take place about a horizontal axis through the bottom rear edge of the cuboid target. The resulting equation of motion is of the form:

$$I\,(d^2\theta/dt^2) = M(t)$$

where M(t) is the turning moment versus time; I is the moment of inertia. The derivation of the form of the equation for vehicular targets as presented in the ARF reports is now given. In this derivation the vehicular target is considered as a cuboid structure supported on structures of relatively small area and height. As the vehicle rotates the angles of its side and bottom planes change and the total are presented to drag changes. The assumption is made that the force acting on a body plane is directly proportional to the area projected into the plane of the shock front.

From Fig. 2.14, the force F_b acting on the bottom plane is:

$$F_b = Pd(t)\, A_b \sin(\theta - \theta o)$$

where Pd(t) is the drag force per in^2 for a drag coefficient of unity, A_b is the drag area of the bottom in in^2 and $(\theta - \theta o)$ is the angle through which the target has rotated.

The force F_s acting on the side is:

$$F_s = Pd(t)\ A_s \cos(\theta - \theta o)$$

where A_s = the drag area of the side of the target in in^2. From the figure:

$$d_b = r' \sin\theta'$$

$$\theta - \theta o = \theta' - \theta''$$

$$\theta' = \theta - \theta o + \theta''$$

$$d_b = r' \sin(\theta - \theta o + \theta'')$$

$$d_s = w \sin(\theta - \theta o) + Y_s \cos(\theta - \theta o)$$

where w is the width of the target. In addition, let $d_1 = r\cos\theta$. Now to examine the moments about the horisontal axis oc taken through the bottom rear edge of the structure:

$$Wd_1 = -W r\cos\theta \qquad W = \text{Weight}$$

$$F_s d_s = Pd(t)\ A_s w \sin(\theta - \theta o)\cos(\theta - \theta o) + Pd(t)\ A_s Y_s \cos^2(\theta - \theta o)$$

$$F_b d_b = Pd(t)\ A_b r' \sin(\theta - \theta o)\sin(\theta - \theta o + \theta'')$$

The resulting overturning moment M(t) becomes:

$$M(t) = -W r\cos\theta + Pd(t)\left[wA_s \sin(\theta - \theta o)\cos(\theta - \theta o) + A_s Y_s \cos^2(\theta - \theta o) + r' A_b \sin(\theta - \theta o)\sin(\theta - \theta o + \theta'')\right]$$

Now:

$$\sin(\theta - \theta o + \theta'') = \sin(\theta - \theta o)\cos\theta'' + \cos(\theta - \theta o)\sin\theta''$$

Then $M(t) = -Wr\cos\theta + Pd(t)\left[wA_s \sin(\theta - \theta o)\cos(\theta - \theta o) + + A_s Y_s \cos^2(\theta - \theta o) + r' A_b \cos\theta'' \sin^2(\theta - \theta o) + + r' A_b \sin\theta'' \sin(\theta - \theta o)\cos(\theta - \theta o)\right]$

The expression in brackets reduces to:

$$\left[1/2\ (w A_s + r' A_b \sin\theta'')\sin 2(\theta - \theta o) + A_s Y_s + (r' A_b \cos\theta'' - A_s Y_s)\sin^2(\theta - \theta o)\right]$$

Then $I\, d^2\theta/dt^2 = -Wr \cos\theta + Pd(t)\, A_s\, Y_s \left\{ 1 \right.$

$$+ \left[(w/2\, Y_s) + (r'\, A_b/2Y_sA_s) \sin\theta'' \right] \sin 2(\theta - \theta o)$$

$$+ \left. \left[(r'A_b/A_s\, Y_s) \cos\theta'' - 1 \right] \sin^2 (\theta - \theta o) \right\} \qquad (2.14)$$

Equation 2.14 then describes the motion of the body when rotation about axis cc is assumed to be the only motion occurring.

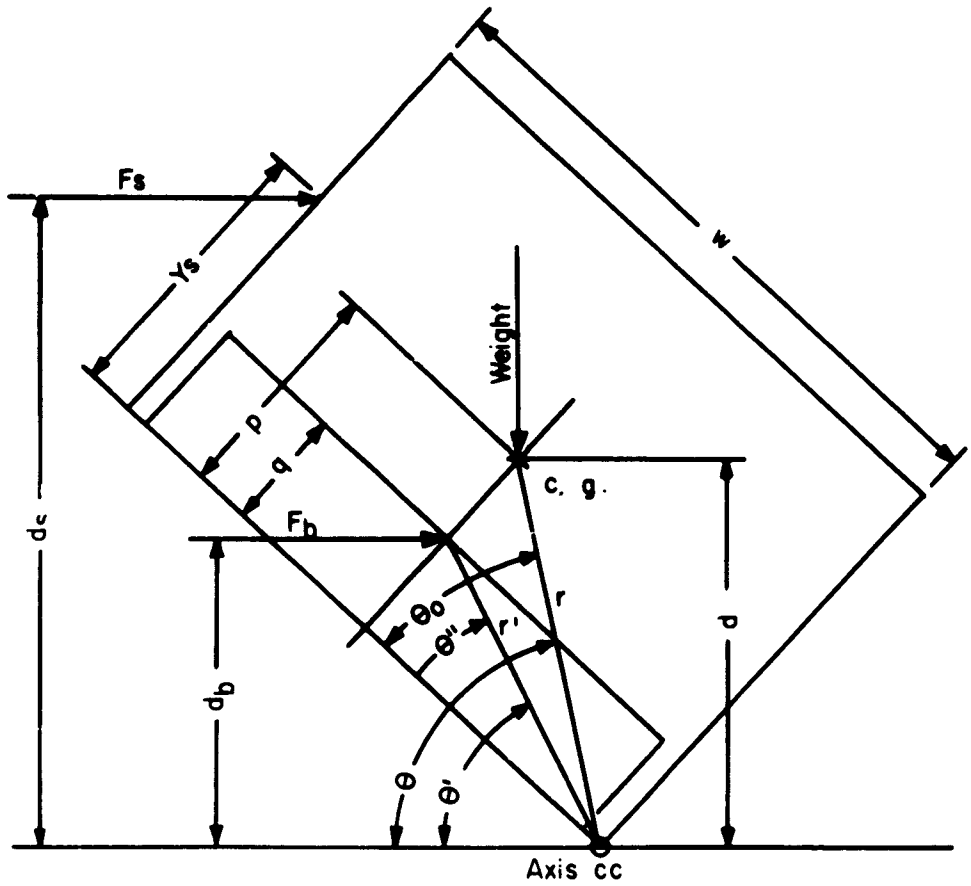

Fig. 2.14 Forces Acting on an Overturning Vehicular Target

2.5.4 Loading on the Test Targets

For the test under consideration the majority of the vehicles were placed either side-on to the blast or face-on to the blast. These were the two orientations considered in the application of the loading methods. Guns and tanks were included in the target items, but only vehicles were in such locations that they could be instrumented. Therefore, attention was concentrated on pr dictions for the vehicles.

The two vehicular targets cons d were the 1/4 ton truck M-38A1 and the 2-1/2 ton truck M-135. . calculations were performed for Shot 9 assuming the blast wave striking the vehicles to be a Mach wave. For those pressure levels occurring in the regular reflection region the solution was obtained using a Mach wave of the corresponding pressure and duration. For the regular reflection region the response solutions obtained in this manner should be greater in magnitude than the response experienced because of the reduced horizontal drag component in the regular region. A simple modification taking into account this reduction in drag component was performed on the Mach solutions.

The overpressure levels selected were 5, 7.2, 9.2, 14.0 and 20.0 psi. The values were determined by the expected placement of the vehicles in relation to instrument shelters.

The application of the methods to the M-38A1 side-on and face-on and to the M-135 side-on and face-on follows. The specific objective of the loading calculations as applied for this test was to obtain values for the linear and angular shock loading impulse for determining the initial conditions for the equations of motion, and for determining the areas presented to drag pressure for use in deriving the equations of motion.

The cuboid representation of the target is dependent upon the construction of the target item, of course. The representation for one orientation may differ from that of another orientation because of the change in the relative importance of various parts of the vehicle as the orientation is changed. The number of resulting cuboids for a given orientation depends upon how many cross-sectional areas of importance have different loading characteristics. Drawings and photographs and the actual items were studied in the attempt to arrive at a realistic cuboid representation.

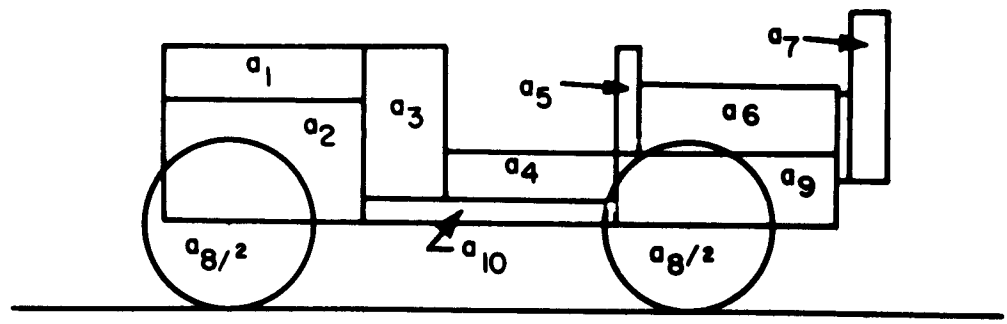

Fig. 2.15 Division of 1/4 Ton Truck M38A1 into Cross-sectional Areas for the Side-on Orientation

The cuboid representation for the M38A1 1/4 ton truck in side-on orientation is shown in Fig. 2.15, where a_1, a_2, etc., indicate the cross-sectional areas. Table 2.3 lists the dimensions of the cuboids and the loading constants assigned to each. The cuboids are identified by their cross-sectional areas.

The drag coefficient for a cube resting on the ground plane is taken as 1.0, and the values assigned to the component cuboids are varied around this value depending upon whether the actual component is streamlined, hence reducing drag, or irregular to the extent that flow is impeded more than for a simple cube.

In the Armour loading method the clearing time of the front face is expressed in terms of the length of time for the rarefaction wave to travel three times the distance from the top of the cuboid to the ground plane or from the sides to the center of the front face, whichever is the lesser distance. In the case of cross-sectional area a_1 the appropriate distance h is the height of a_1, since the rarefaction wave can travel no shorter distance to relieve the face completely. No impediment is offered to the build-up of pressure on the rear face, and this was assumed to take place in the normal time of 8h/U. The drag coefficient was chosen as 1.0.

In the case of a_2 the fender prevents normal clearing upward and to the right. Any impediment to normal flow around the cuboids is compensated for by adjusting the clearing times and the rear loading times. Clearing of the front face was assumed to take the more than normal time of 4h/Cr, where h is the height of a_2 and Cr is the velocity of the rarefaction wave in the reflected region. The drag coefficient was chosen as 1.5 because of the action of the fenders in impeding the flow.

The clearing and loading of a_3 was assumed to be normal with h the width of a_3. This distance is the shortest that the rarefaction wave could travel to relieve the reflected pressure on the front face. The drag coefficient was assumed to be the normal 1.0.

The clearing and rear loading of a_4 was also assumed normal, with h taken to be 1/2 the height of a_4, since the rarefaction wave will start from each edge. The drag coefficient was assumed to be 1.2, since the area is irregular.

Area a_5, representing the upper part of the driver's seat, is duplicated by the passenger seat. This passenger seat was assumed to receive an impulse equal to 0.75 the a_5 impulse. Clearing and loading for a_5 were assumed to be normal, with h taken as the width of the area. Drag coefficient was chosen as 1.0.

The area a_6 was assumed normal with h taken as 6 in. for the front face and 12 in. for the rear face. Clearing for the front face begins from the top and bottom edges, while loading on the rear begins from one edge. The drag coefficient was assumed to be 1.0. The a_6 is duplicated, and the rear area was assigned 0.75 the a_6 impulse.

Area a_7, representing the spare tire and gas can, was assumed to be normal, with h as 4 in., and the drag coefficient 1.0.

Area a_8 represents the wheels. Clearing of the front face is assumed normal, but loading on the rear face should be longer than normal because of interference from the fender housing and the concavity

of the rear face. The value h is taken as the radius of the wheel and the time for loading on the rear face is taken to be 10h/U, and the drag coefficient is 1.0. The area is duplicated by about 1/2 the area of the opposite wheels and the secondary area is assigned an impulse of 0.25 a_8 to allow for assumed attenuation of the shock wave in traveling under the vehicle. Y for this secondary area is taken to be 9.0 in.

Area a_9 is the area under the rear fender housing, and clearing and rear loading is assumed to be impeded by the fenders. The time for clearing was taken to be 4h/Cr, and the time for loading the rear face was taken to be 12h/U, where h is the height of a_9. A drag coefficient of 1.5 was assigned, since the fender housing should add considerable resistance to flow.

Area a_{10} was assumed to be normal, with h taken as the height of a_{10}. A drag coefficient of 1.2 was assigned because of the irregularity of the objects represented.

The values assumed for the various quantities are listed in Table 2.3. The time for clearing the front face is denoted by t_B and the time for loading the rear face is $t_D - t_C$. If h for the rear face differs from the h for the front face the numerical value is listed in the expression for $t_D - t_C$.

Now the desired results from the loading calculations are values for the linear shock loading impulse and angular shock loading impulse. In the ARF reports these quantities are computed by applying the relations presented in Section 2.5.2 to each component cuboid.

TABLE 2.3 Cuboid Characteristics for M-38A1 Side-on

Area	Area (in^2)	Width (in.)	Ht. (in.)	L (in.)	Y (in.)	h (in.)	T_B (sec)	T_D-T_C (sec)	C_D
a_1	327.8	34.5	9.5	52.5	41.2	9.5	3h/C_r	8h/U	1.0
a_2	752.5	35.0	21.5	29.5	25.7	21.5	4h/C_r	12h/U	1.5
a_3	441.0	14.0	31.5	59.1	34.7	14.0	3h/C_r	8h/U	1.0
a_4	270.0	30.0	9.0	59.1	[illegible].4	4.5	3h/C_r	8h/U	1.2
a_5	74.0	4.0	18.5	18.0	37.2	4.0	3h/C_r	8h/U	1.0
a_6	408.0	34.0	12.0	6.0	33.9	6.0	3h/C_r	8(12)/U	1.0
a_7	240.0	8.0	30.0	43.0	35.9	4.0	3h/C_r	8h/U	1.0
a_8	1461.2	30.5 dia.		7.0	14.4	15.3	3h/C_r	10h/U	1.0
a_9	507.0	39.0	13.0	32.0	21.4	13.0	4h/C_r	12h/U	1.5
a_{10}	176.0	44.0	4.0	29.5	16.9	4.0	3h/C_r	8h/U	1.2

Then the values of linear and angular shock loading impulse for each component cuboid are added to obtain the total shock loading impulse on the vehicle.

This procedure was followed for the vehicles and the shock loading impulse values were obtained. The computation of the impulse values for each component cuboid was tedious, and therefore once the values were available to check the effects of any change in procedure, the computational process was simplified for further calculations which might be done.

The simplification introduced was the averaging of the component cuboid characteristics to obtain a single cuboid which would experience a shock loading impulse equivalent to the sum of the loading of the component cuboids. The characteristics of the equivalent cuboid are given by the following relations:

$$\text{Area} = \Sigma a_n \qquad (2.15)$$

$$\text{Height} = 2H_f \qquad (2.16)$$

$$\text{Width} = A/(2H_f) \qquad (2.17)$$

$$\text{Length} = (\Sigma L_n a_n)/(\Sigma a_n) \qquad (2.18)$$

$$Y = \frac{\Sigma\left[(L_n + (bh)_n + (ch)_n)\ a_n Y_n\right]}{\Sigma\left[(L_n + (bh)_n + (ch)_n)\ a_n\right]} \qquad (2.19)$$

$$H_f = (\Sigma a_n\ (bh)_n)/(3\Sigma a_n) \qquad (2.20)$$

$$H_r = (\Sigma a_n\ (ch)_n)/(8\Sigma a_n) \qquad (2.21)$$

$$t_B = (\Sigma a_n\ (bh)_n)/(C_r \Sigma a_n) \qquad (2.22)$$

$$t_D - t_C = (\Sigma a_n (ch)_n)/(U\Sigma a_n) \qquad (2.23)$$

The subscript n identifies the component cuboid, H_f is the minimum distance for the rarefaction wave to travel in clearing the front face, H_r in the minimum distance for loading wave to travel in loading the rear face, Y is the approximate distance from the ground plane to the center of pressure of the equivalent cuboid, t_B is the clearing time of the front face for the equivalent cuboid, $t_D - t_C$ is the loading time of the rear face for equivalent cuboid, $(bh)_n$ is the numerator of the expression for T_B for a component cuboid n, such as is listed in Table 2.3, and $(ch)_n$ is the numerator of the expression for $t_D - t_C$ for a component cuboid n, such as is listed in Table 2.3. The equations weigh the dimensions of the component cuboids according to the cross-sectional area of each cuboid.

The value of angular shock loading impulse on the vehicles obtained by multiplying the value of Y given by Equation 2.19 times the linear shock loading impulse differs from the values obtained by considering the component cuboids individually and summing. This difference was less than five per cent and was considered sufficiently small to neglect in comparison to errors which may result from the basic assumptions of the method. The value of linear shock loading impulse is the same as that obtained by the individual treatment.

The equivalent cuboid dimensions for the M-135 and M38A1 vehicles in side-on and face-on orientation were computed and are contained in Table 2.4. These equivalent cuboids may be used for the

TABLE 2.4 Equivalent Cuboid Dimensions and Loading Parameters

Vehicle	Orientation	Area (in^2)	Width (in.)	Ht. (in.)	L (in.)	Y (in.)	H_f (in.)	H_r (in.)	T_B (sec)	$T_D - T_C$ (sec)	A_s (in.)	Y_s (in.)	T_* (sec)
M38A1	Side-on	5384	192.7	27.9	24.62	23.2	13.97	16.76	$41.91/C_T$	134.07/U	4646	26.02	288/U
M38A1	Face-on	4698	156.5	30.0	27.12	37.0	15.01	18.43	$45.03/C_T$	147.5/U	4079	32.23	381/U
M-135	Side-on	16,540	410	40.3	31.8	35.2	21.1	20.1	$63.4/C_T$	181.5/U	15,550	38.23	276/U
M-135	Face-on	6632	216	30.7	70.25	49.5	15.3	17.15	$46.01/C_T$	137.2/U	5782	46.90	348/U

computation of shock loading impulse for a given overpressure and duration on the M38A1 and M-135 by the process described in Section 2.5.2.

Figure 2.16 shows the equivalent cuboid for the M38A1 in side-on orientation. The calculations of the linear and angular shock loading impulse on this cuboid for one particular overpressure level is listed here. At an overpressure of 9.2 psi, 57 degrees C, 12.2 psi atmospheric pressure, P_r = 23.77 psi, U = 1428 ft/sec, Cr = 1304.8 ft/sec. Then:

$$t_B = 41.91/C_r = 0.00268 \text{ sec}, \quad t_D - t_C = 134.07/U = 0.00782 \text{ sec}$$

$$t_C = L/U = 24.62/U, \quad t_D = 134.07/U + 24.62/U = 158.69/U = 0.00926 \text{ sec}$$

Then $t_D - t_B = 0.00658$ sec.

For the times involved the corresponding pressures are obtained from Friedrich's modified equation listed in the GREENHOUSE report.[12]

Then $P_B = P_s(t_B) + 2/3\ P_d(t_B) = 10.57$ psi

$$P_D = P_s(t_D) - 1/3\ P_d(t_D) = 8.19 \text{ psi}$$

$$P_E = P_s(t_D) + 2/3\ P_d(t_D) = 10.29 \text{ psi}$$

$$A_1 = 1/2\ (P_r + P_B)\ t_B = 0.0460 \text{ lb-sec/in}^2$$

$$A_2 = 1/2\ P_D(t_D - t_C) = 0.0320 \text{ lb-sec/in}^2$$

$$A_3 = 1/2\ (P_B + P_D)(t_D - t_B) = 0.0686 \text{ lb-sec/in}^2$$

Thus the shock loading impulse/in^2 is $A_1 - A_2\ A_3 = 0.0826$ lb-sec/in^2. The total shock loading for the equivalent cuboid and hence for the vehicle is given by the product of the total area and the shock loading impulse/in^2 found above, and the result is 445 lb-sec.

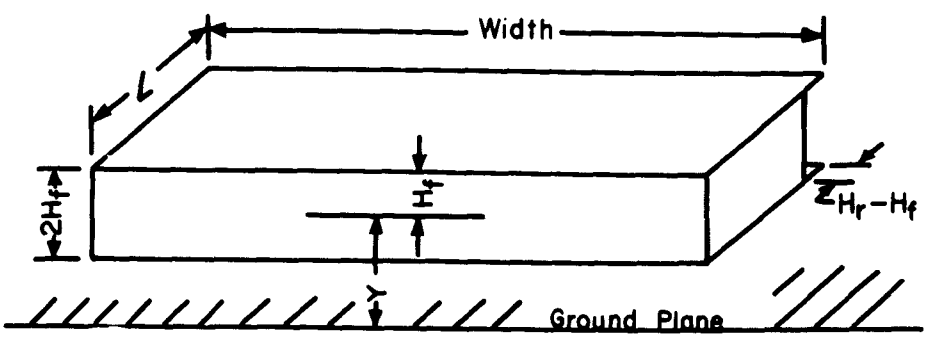

Fig. 2.16 Equivalent Cuboid for M38A1 Side-on

The angular shock loading impulse is, from Equation 2.3d, where Y is the averaged value for the equivalent cuboid:

$$Y\ (445\ \text{lb-sec}) = (23.2\ \text{in})(445\ \text{lb-sec}) = 860\ \text{lb-sec-ft}$$

The area presented to drag flow by the vehicle is chosen less than that concerned in shock loading, since the duplicated areas will have small effect.

The following areas were assumed to compose the area presented to drag: a_1, a_2, a_3, a_4, a_5, a_6, a_7, $0.5a_8$, a_9, and a_{10}. Only 1/2 the wheel area was used since 1/2 the area overlaps the body area.

The object of the calculations was to obtain A_s, where $A_s = AC_d$ (where C_d is the drag coefficient and A is the sum of the cross-sectional areas of the above components), and Y_s, the distance above the ground plane of the point of application of the drag force.

$$A_s = \Sigma\, a_n C_d = 4646\ \text{in}^2$$

$$\Sigma a_n C_d Y = 120{,}900\ \text{in}^3$$

$$Y_s = (\Sigma a_n C_d Y)/(\Sigma a_n C_d) = 26.02\ \text{in} = 2.17\ \text{ft} \qquad (2.25)$$

$$\text{For the equivalent cuboid, } C_d = (\Sigma a_n C_d)/(\Sigma a_n) = 1.18 \qquad (2.26)$$

The values for A_s and Y_s for the other orientations and vehicles were obtained in the same manner.

The application of the loading method at other pressure levels and to the M38A1 face-on and the M-135 side-on and face-on was carried out in a similar manner using the relations appropriate for each case. The values obtained for the linear and angular shock loading impulse are shown in Figs. 2.17 and 2.18. These curves apply for the test vehicles struck by a Mach wave which has the ideal pressure-time decay with the duration equal to that predicted for the Mach and regular reflection regions for Shot 9.

The values of linear and angular shock loading impulse as read from these curves were used to calculate the initial velocities from equation 2.7 to be applied as a condition on the equations of motion describing the response of the vehicles.

2.5.5 Response of the Test Targets

Sufficient loading data were obtained in the previous section for setting up the equations of motion. The additional physical characteristics required for the equations except for the moment of inertia of the vehicles about the assumed axes of rotation were determined from manuals and body builders' drawings. Since no means were available whereby the moments of inertia could be determined experimentally they were approximated by calculations described in Appendix B.

Since only sliding or rotation was assumed to occur for a given orientation, each case was investigated to determine the type of motion

most likely to occur. For the M38A1 in face-on orientation the condition for no turning to occur is, from Equation 2.12:

$$\mu Y_s \leq L \cos\theta_o$$

Substituting $Y_s = 2.7$ ft, $L = 4.2$ ft, and $\cos\theta_o = 0.847$, then the result appears that for no turning $\mu \leq 1.3$ (assuming μ to be constant). Now all vehicles exposed were parked with the gears disengaged, in neutral, and with the hand brake applied. The hand brakes are designed to hold the weight of the vehicles, that is, to provide $\mu = 1.0$. Then if 1.0 represents about the maximum value of the coefficient the vehicle in this orientation can be expected to slide only.

For the M-135 truck face-on $Y_s = 4.1$ ft, $L = 8.5$ ft, and $\cos\theta_o = 0.931$. Then the condition for no turning is that $\mu \leq 1.93$. Therefore, since the hand brakes provide a μ of 1.0 maximum the M-135 can be expected to slide only.

For the M38A1 side-on $Y_s = 2.2$ ft, $L = 3.2$ ft, and $\cos\theta_o = 0.712$. Then the condition for no turning is that $\mu \leq 1.02$. Because of the loose surface of the soil at the test site it seemed likely that the coefficient of friction would increase as the truck slid sideways. Thus although sliding occurs at first rotation may predominate very shortly after sliding begins.

If the condition for no rotation is examined for the M-135 side-on the result is that $\mu \leq 0.9$ for no turning to occur. If the coefficient of friction is 1.0 as assumed then rotation should occur initially and a combination of the two types of motion can be expected, with rotation probably predominating.

For the side-on orientation a combination of the two types of motion seems most probable. In any case the equations for sliding only and for rotation only are investigated, and since the appearance of one mode of motion should decrease the energy expended in the other mode, the solutions for sliding only and for rotation only should bound the motion actually occurring.

For each case there is a limiting pressure for a given coefficient of friction below which no sliding occurs. The condition for no sliding is Equation 2.13:

$$Pd(t)\ A_s \leq \mu W$$

From this condition the limiting pressure at which the drag pressure alone will produce no sliding can be obtained. Assuming a coefficient of $\mu = 1.0$, the limiting pressure for the M38A1 side-on is 4.5, for the M38A1 face-on is 4.8, for the M-135 side-on is 5.0, and for the M-135 face-on is 8.4. The shock loading impulse will cause movement of 0.1 ft maximum at these limiting pressures for $\mu = 1.0$. Since the lowest pressure at which vehicles were placed was 5.0 psi, then movement should occur at all positions by all the vehicles except the M-135 face-on, in which case the movement is negligible. For all vehicles to move at the 5.0 psi level then the coefficient of friction should be less than 0.4.

The equations of rigid body motion for rotation only for the vehicles in side-on orientation were obtained by substituting the appropriate quantities listed in Table 2.5 in the previously derived Equation 2.14.

TABLE 2.5 Vehicle Parameters Used in the Equation for Overturning

	I_{cc} slug-ft^2	A_b ft^2	A_s ft^2	Y_s ft	n ft	w ft	r ft	θ_o deg.	sin θ^*	cos θ^*	W lb
M38A1	983	48.34	32.26	2.17	2.76	4.92	3.16	44.6	0.5775	0.8164	2,620
M-135	9290	146.50	108.00	3.19	3.97	5.73	4.27	47.9	0.6926	0.7215	12,380

The equation resulting for the M38A1 side-on is as follows:

$$d^2\theta/dt^2 = -480.8\cos\theta + 326\,Pd(t)\left[1.80 + 3.03\sin 2(\theta-\theta o) + \sin^2(\theta-\theta o)\right] \quad (2.25)$$

The resulting equation for the M-135 side-on was:

$$d^2\theta/dt^2 = -326.1\cos\theta + 66.7\,Pd(t)\left[4.59 + 6.80\sin 2\theta(-\theta o) + \sin^2(\theta-\theta o)\right] \quad (2.26)$$

In each equation Pd(t) is in lb/in^2, θ is in degrees, and t is in seconds.

The initial angular velocities applied as a condition on these equations were obtained from Equation 2.7.

$$(d\theta/dt)_* = (\text{shock loading angular impulse}/ I_{cc})\ 57.3°/\text{rad.} \quad (2.27)$$

The values are listed in Table 2.6

The solutions for the pressures tabulated were computed by the BRL Computing Laboratory. The resulting curves for angular velocity and angular displacement are shown in Figs. 2.19, 2.20, 2.21, and 2.22. The curves are terminated abruptly because the computations were ended when the vehicle had rotated through an angle of 90 degrees or returned to its initial position of zero displacement. The computations could be extended beyond 90 degrees by using the angular velocity at this point as an initial condition on a second equation of motion of the same type but with different constants (due to the changed physical characteristics in this position). However, the calculations required for this extension were not considered justified by the precision of the results to be expected.

Since many of the test items were placed in the regular reflection region, a simple modification of the equation was attempted to approximate the effects to be expected in this region. The shock loading

impulse was considered to be the same as for a Mach wave of the same pressure and duration as the predicted reflected wave. The horizontal component of drag was reduced in the following manner: The horizontal wind component of the reflected wave was considered dependent on the angle of reflection. The angle of reflection was assumed equal to the angle of incidence. Expressing this horizontal wind component U_h in terms of the angle of incidence α and the wind velocity V behind the shock front:

$$U_h = V \sin \alpha$$

Now: $Pd(t) = 1/2\ \rho\,(t)\ V(t)^2$ where $\rho\,(t)$ = density

The horizontal component of the drag force $Pd(t)_h$ is found by substitution of the horizontal component of the wind velocity U_h into Pd(t):

$$Pd(t)_h = 1/2\ \rho\,(t)\ U_h^2 = 1/2\ \rho\,(t)\ \ (V \sin \alpha)^2 = \sin^2 \alpha\, Pd(t) \tag{2.28}$$

Then the drag pressure in the regular region is considered as the drag pressure for a Mach wave multiplied by the square of the angle of incidence. The equations were modified accordingly for the tabulated pressures and angles of incidence. The values of α as obtained from the predicted curves are listed in Table 2.6.

Solutions for the angular velocities obtained with this modification for the side-on orientation are shown in Figs. 2.23 and 2.24. It is evident that a considerable reduction in effect results.

The equations of motion for the vehicles for sliding only were obtained by substituting the values for A_s and W from Table 2.3 into the equations 2.9, 2.10, and 2.11 derived for translations. The resulting equations for the accelerations were:

M38A1 Side-on: $d^2x/dt^2 = g(1.78\ Pd(t) - \mu)$ (2.29)

M38A1 Face-on: $d^2x/dt^2 = g(1.56\ Pd(t) - \mu)$ (2.30)

M-135 Side-on: $d^2x/dt^2 = g(1.26\ Pd(t) - \mu)$ (2.41)

M-135 Face-on: $d^2x/dt^2 = g(0.47\ Pd(t) - \mu)$ (2.31)

Here x is in feet, t is in seconds, g is the acceleration due to gravity, μ is the coefficient of friction, and Pd(t) is the dynamic pressure in psi.

When the equations are integrated the following relations were obtained for the sliding velocities:

M38A1 Side-on:

$$dx/dt = 57.2 \int_0^t Pd(t)dt - \mu g(t - t^*) - 57.2 \int_0^{t^*} Pd(t)dt + (dx/dt)^* \tag{2.33}$$

M38A1 Face-on:

$$dx/dt = 50.2 \int_0^t Pd(t)dt - \mu g(t - t*) - 50.2 \int_0^{t*} Pd(t)dt + (dx/dt)* \qquad (2.34)$$

M-135 Side-on:

$$dx/dt = 40.4 \int_0^t Pd(t)dt - \mu g(t - t*) - 40.4 \int_0^{t*} Pd(t)dt + (dx/dt)* \qquad (2.35)$$

M-135 Face-on:

$$dx/dt = 15.0 \int_0^t Pd(t)dt - \mu g(t - t*) - 15.0 \int_0^{t*} Pd(t)dt + (dx/dt)* \qquad (2.36)$$

The values of $(dx/dt)*$ are derived from the linear shock loading impulse as indicated by Equation 2.7. The expression for $t*$ for each case is tabulated in Table 2.4. The values obtained for $(dx/dt)*$ for Shot 9 are given in Table 2.7.

TABLE 2.6 Angular Velocities and Angles of Incidence at Given Overpressure

psi	M38A1 deg/sec	M-135 deg/sec	α degrees
5.0	26.97	18.42	
7.2	39.32	26.64	
9.2	50.68	34.54	
12.0	67.00	45.33	40.26
14.0	78.93	53.04	37.12
16.0	90.6	60.87	32.39
20.0	114.8	76.78	22.94

TABLE 2.7 Initial Velocities Derived from Linear Shock Loading Impulse

psi	M38A1 Side-on (ft/sec)	M38A1 Face-on (ft/sec)	M-135 Side-on (ft/sec)	M-135 Face-on (ft/sec)
5.0	2.9	2.8	2.6	1.0
7.2	4.2	4.0	3.7	1.5
9.2	5.5	5.2	4.9	1.9
14.0	8.5	8.1	7.5	3.0
20.0	12.4	11.8	10.9	4.3

The equations resulting for displacement are, from Equation 2.10, omitting the negligible second term:

M38A1 Side-on:

$$x = 57.2 \int_0^{t'} \left[\int_0^{t} Pd(t)dt \right] dt - (t' - t_*) \left[(\mu g/2)(t' - t_*) + 57.2 \int_0^{t_*} Pd(t)dt - (dx/dt)_* \right] \quad (2.37)$$

M38A1 Face-on:

$$x = 50.2 \int_0^{t'} \left[\int_0^{t} Pd(t)dt \right] dt - (t' - t_*) \left[(\mu g/2)(t' - t_*) + 50.2 \int_0^{t_*} Pd(t)dt - (dx/dt)_* \right] \quad (2.38)$$

M-135 Side-on:

$$x = 40.4 \int_0^{t'} \left[\int_0^{t} Pd(t)dt \right] dt - (t' - t_*) \left[(\mu g/2)(t' - t_*) + 40.4 \int_0^{t_*} Pd(t)dt - (dx/dt)_* \right] \quad (2.39$$

M-135 Face-on:

$$x = 15.0 \int_0^{t'} \left[\int_0^{t} Pd(t)dt \right] dt - (t' - t_*) \left[(\mu g/2)(t' - t_*) + 15.0 \int_0^{t_*} Pd(t)dt - (dx/dt)_* \right] \quad (2.40)$$

The integral terms are evaluated from calculated pressure-time decay curves, t* is calculated from the relation given in Table 2.3, and t' is found as indicated in section 2.5.3, Equation 2.11.

The values of total displacement were calculated assuming coefficients of friction of 0.25, 0.5, and 1.0. The displacements plotted against overpressure are shown in Figs. 2.25 through 2.28. Since a Mach wave was assumed, the dynamic pressure required for a given displacement is determined from the overpressure by the usual relation between the overpressure and the dynamic pressure in a plane wave.

When plotted on log log paper versus overpressure the displacements form almost a straight line curve up to about 15 psi. Thus displacement as a function of overpressure is of the following approximate form for the region from 5.0 to 15.0 psi: $x = C P^b$ where x is the displacement, C is a constant, P is the overpressure, and b is a constant $3<b<4$.

The displacements represent the effect of a Mach wave of the same pressures and durations expected for Shot 9. Beyond about 11.0 psi the regular reflection region is entered on Shot 9, and the displace-

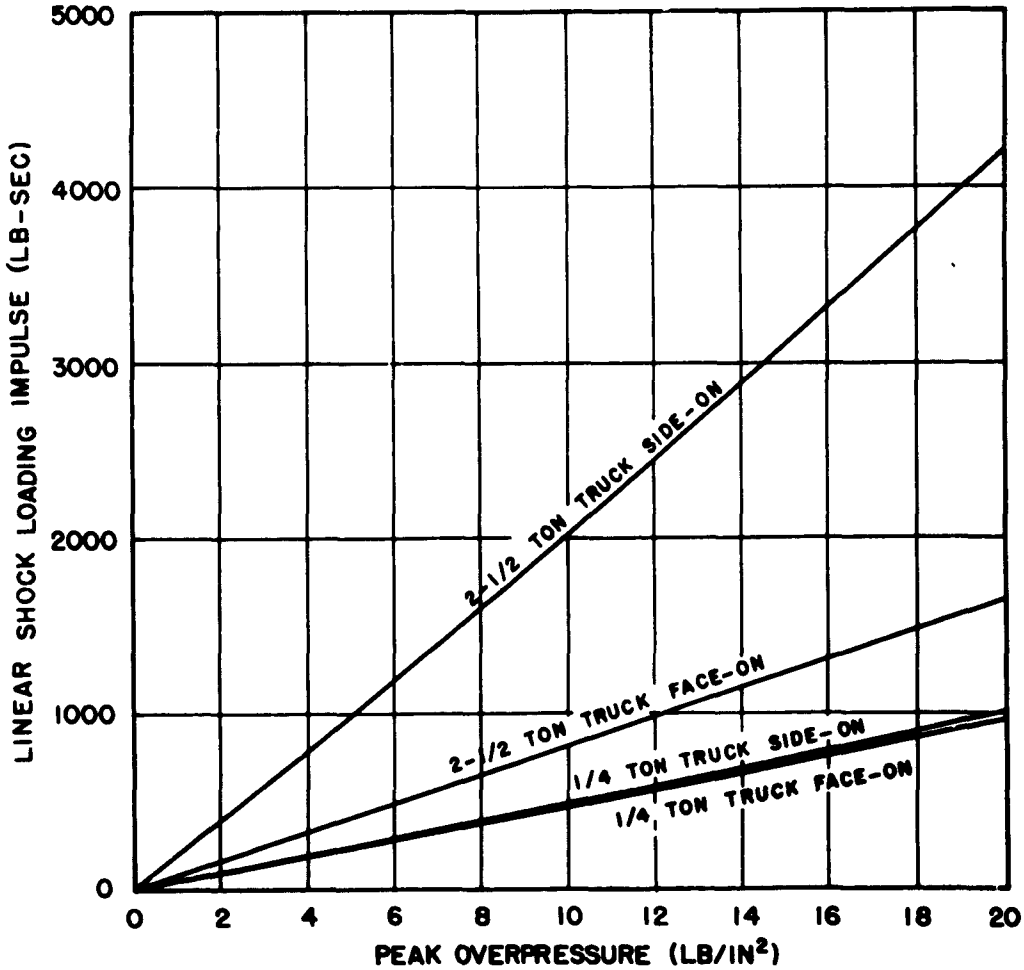

Fig. 2.17 Linear Shock Loading Impulse on Test Vehicles

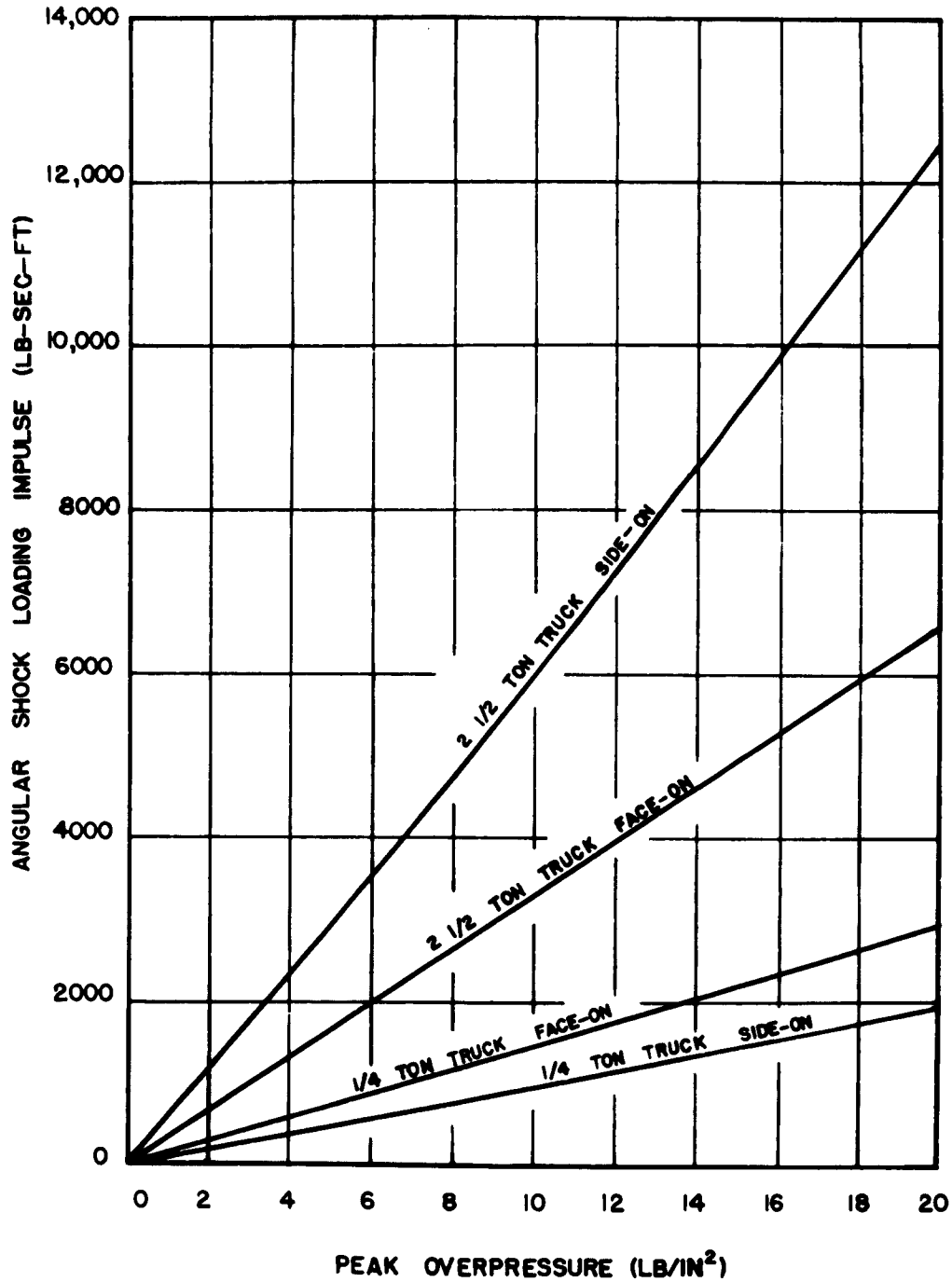

Fig. 2.18 Angular Shock Loading Impulse on Test Vehicles

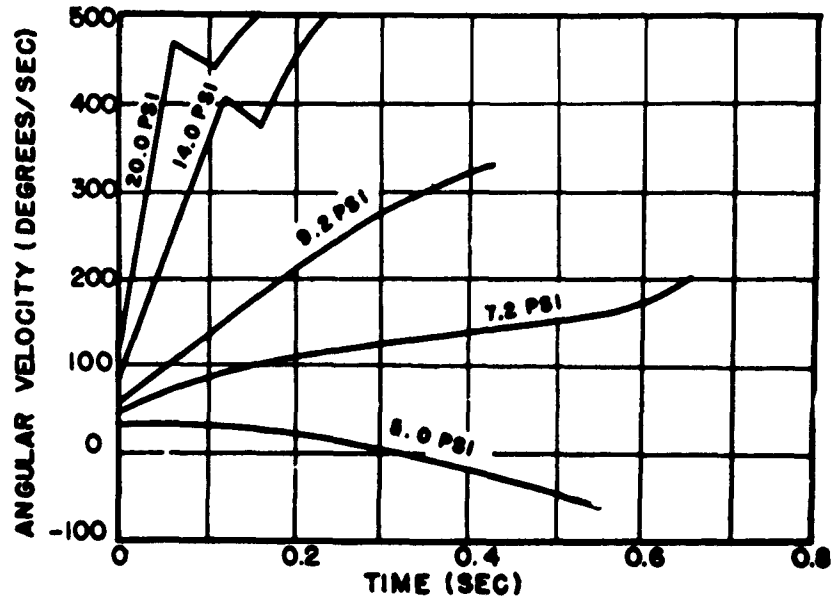

Fig. 2.19 Angular Velocities of M38A1 1/4 Ton Truck Struck Side-on by Mach Wave (Calculated)

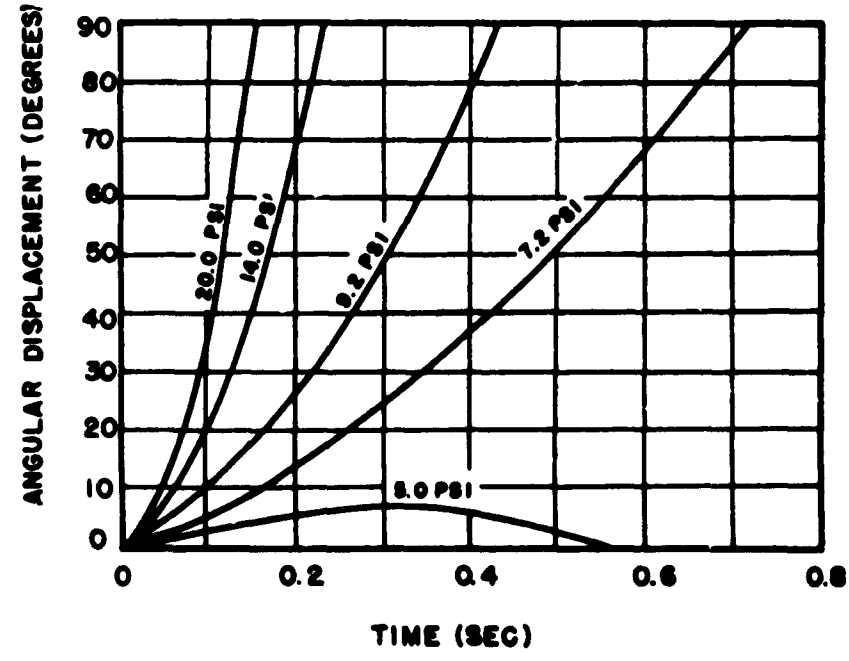

Fig. 2.20 Angular Displacement of M38A1 1/4 Ton Truck Struck Side-on by Mach Wave (Calculated)

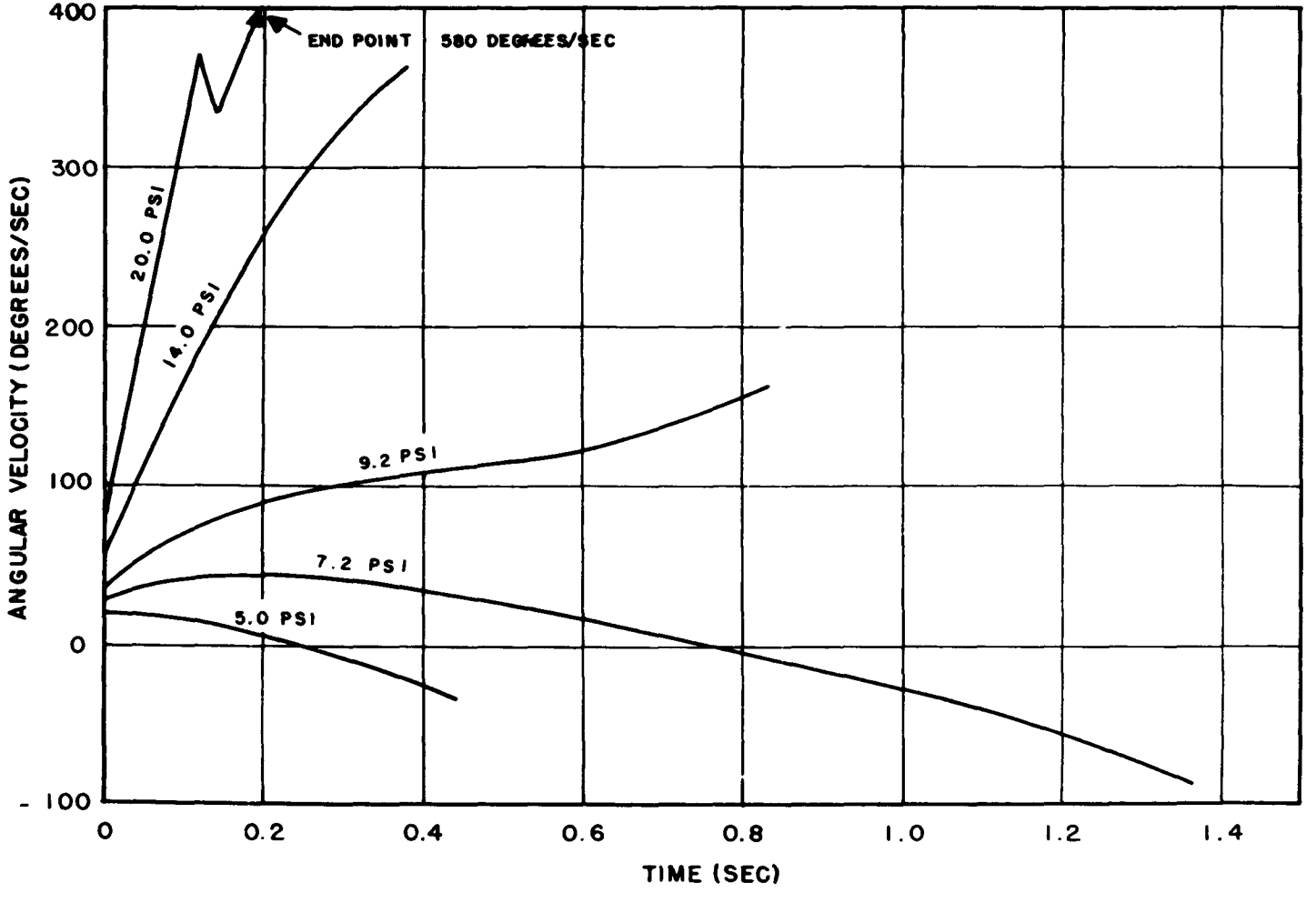

Fig. 2.21 Angular Velocities of M-135 2-1/2 Ton Truck Struck Side-on by Mach Wave (Calculated)

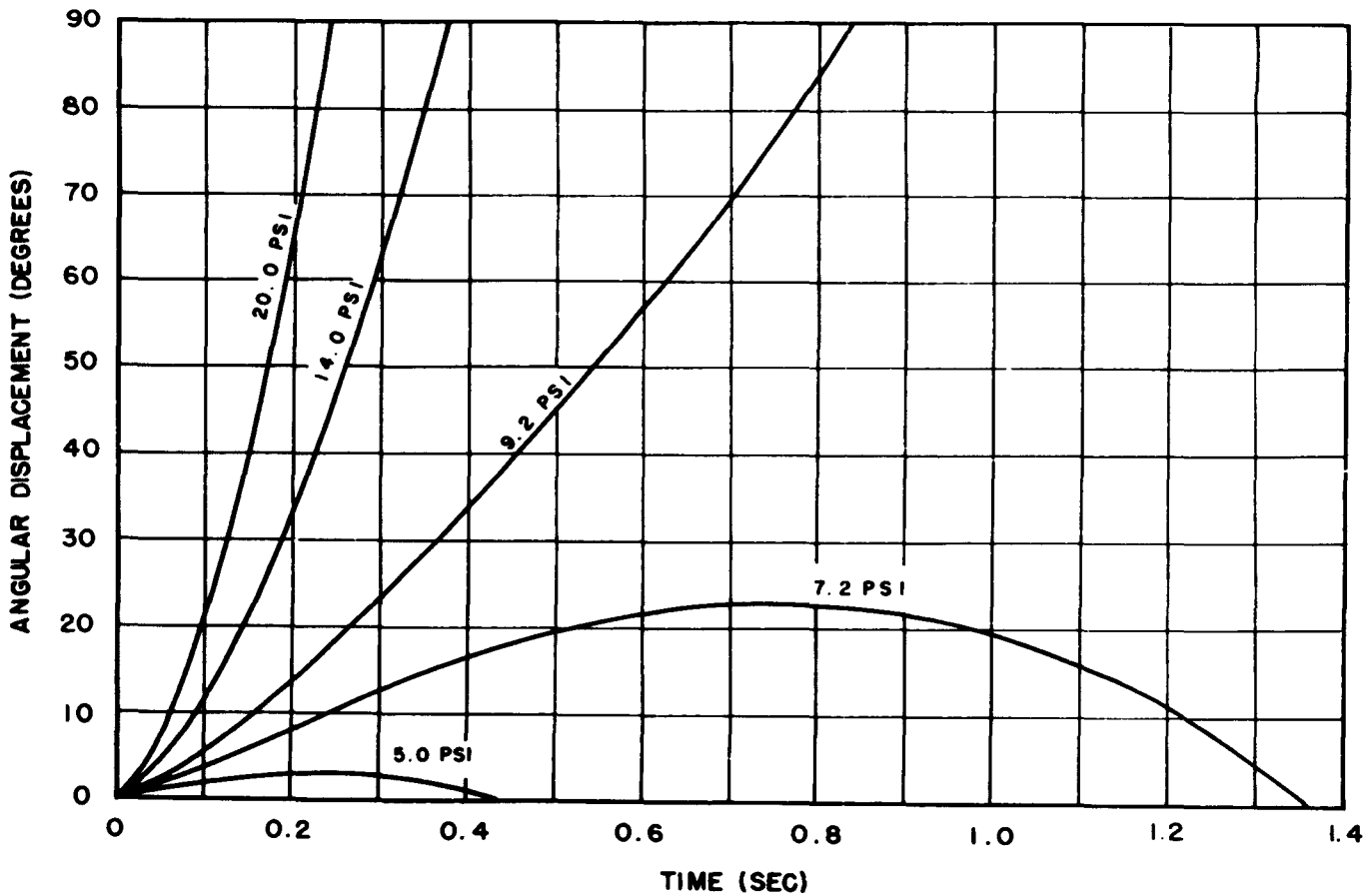

Fig. 2.22 Angular Displacement of M-135 2-1/2 Ton Truck Struck Side-on by Mach Wave (Calculated)

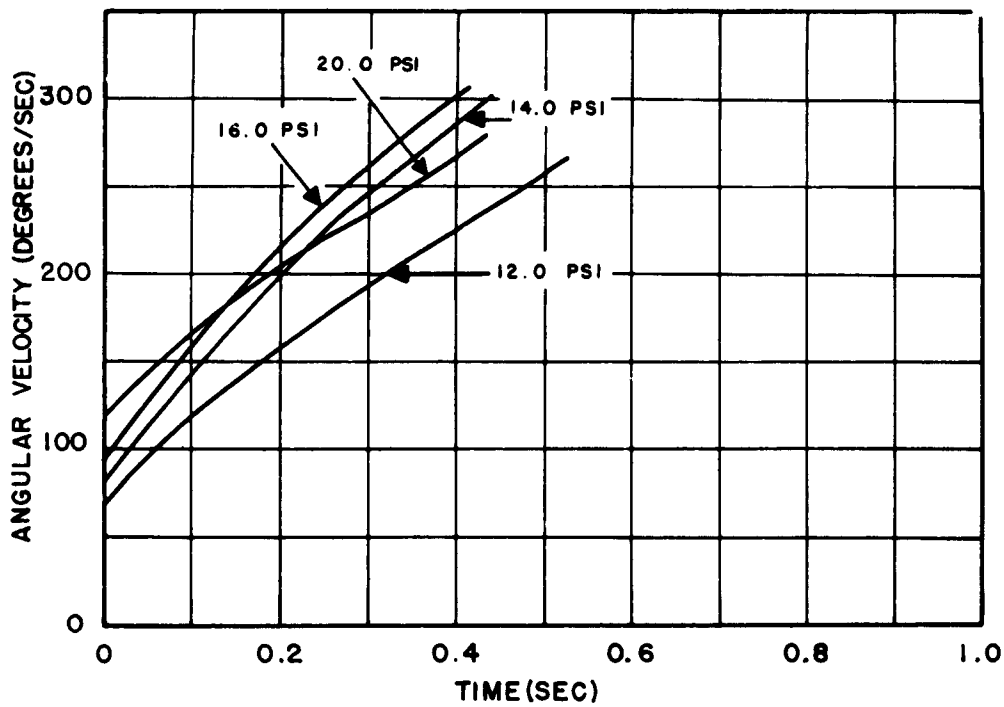

Fig. 2.23 Calculated Angular Velocities of M38A1 1/4 Ton Truck Struck Side-on by Wave in Regular Region

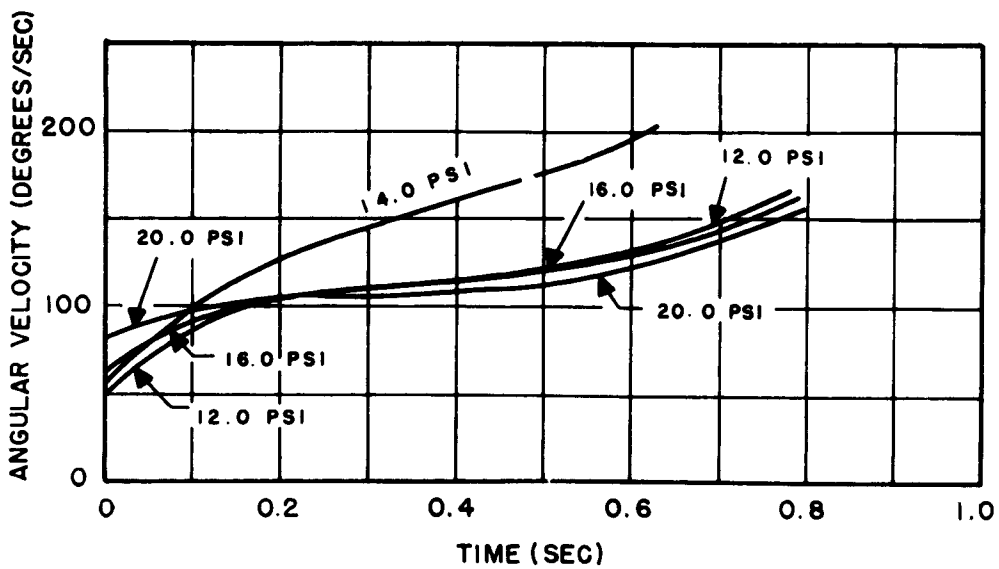

2.24 Calculated Angular Velocities of M-135 2-1/2 Ton Truck Struck Side-on by Wave in Regular Region

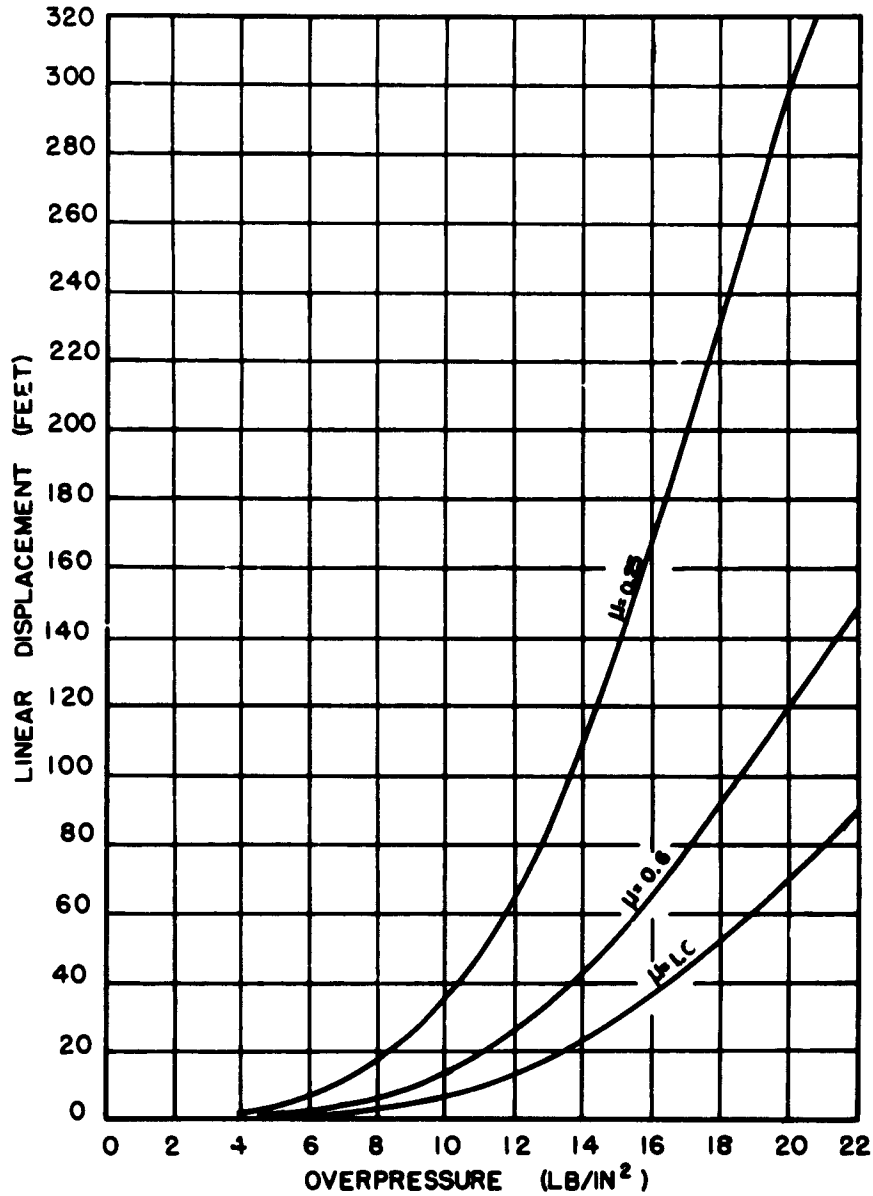

Fig. 2.25 Calculated Linear Displacement vs Overpressure for M-38A1 1/4 Ton Truck Struck Side-on by Mach Wave (Assuming Sliding Only)

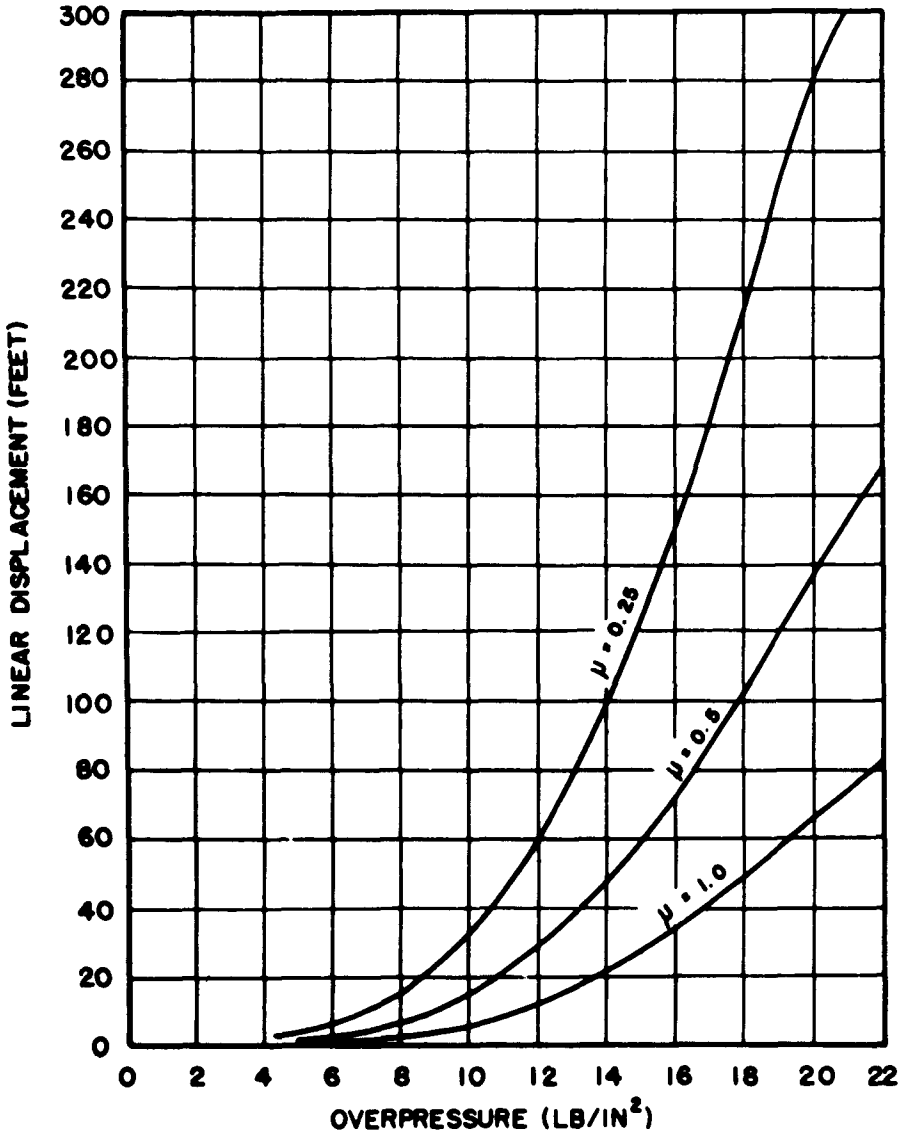

Fig. 2.26 Calculated Linear Displacement vs Overpressure for M-38A1 1/4 Ton Truck Struck Face-on by Mach Wave (Assuming Sliding Only)

ments observed can be expected to decrease below the curve values as the horizontal wind component decreases.

No calculations were made for Shot 10. However, because of the expected slightly shorter durations the calculated displacements for Shot 10 should be about the same or less than the displacements recorded in Figs. 2.25 through 2.28.

It is emphasized that the linear displacements presented in the figures listed were calculated assuming sliding only. If rotation occurs the total sliding should be reduced. If the vehicle overturns the original construction of a simple cuboid sliding over a plane no longer applies, and the values from the curves cannot be applied accurately to the actual test situation. Thus if the vehicle remains upright the values for the linear displacement given by the curves should bound those actually occurring, and above the pressure required for overturning the curves can only be considered to give an indication of the magnitude of the displacement that would result.

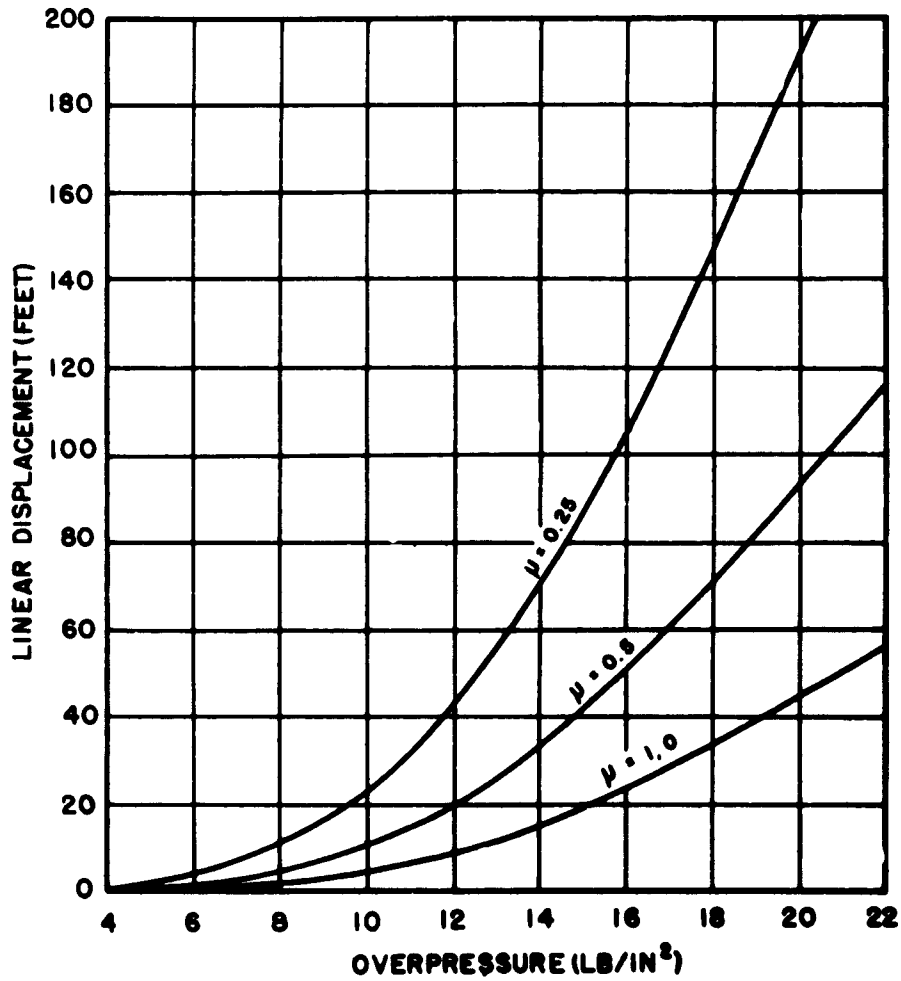

Fig. 2.27 Calculated Linear Displacement vs Overpressure for M-135 2-½ Ton Truck Struck Side-on by Mach Wave (Assuming Sliding Only)

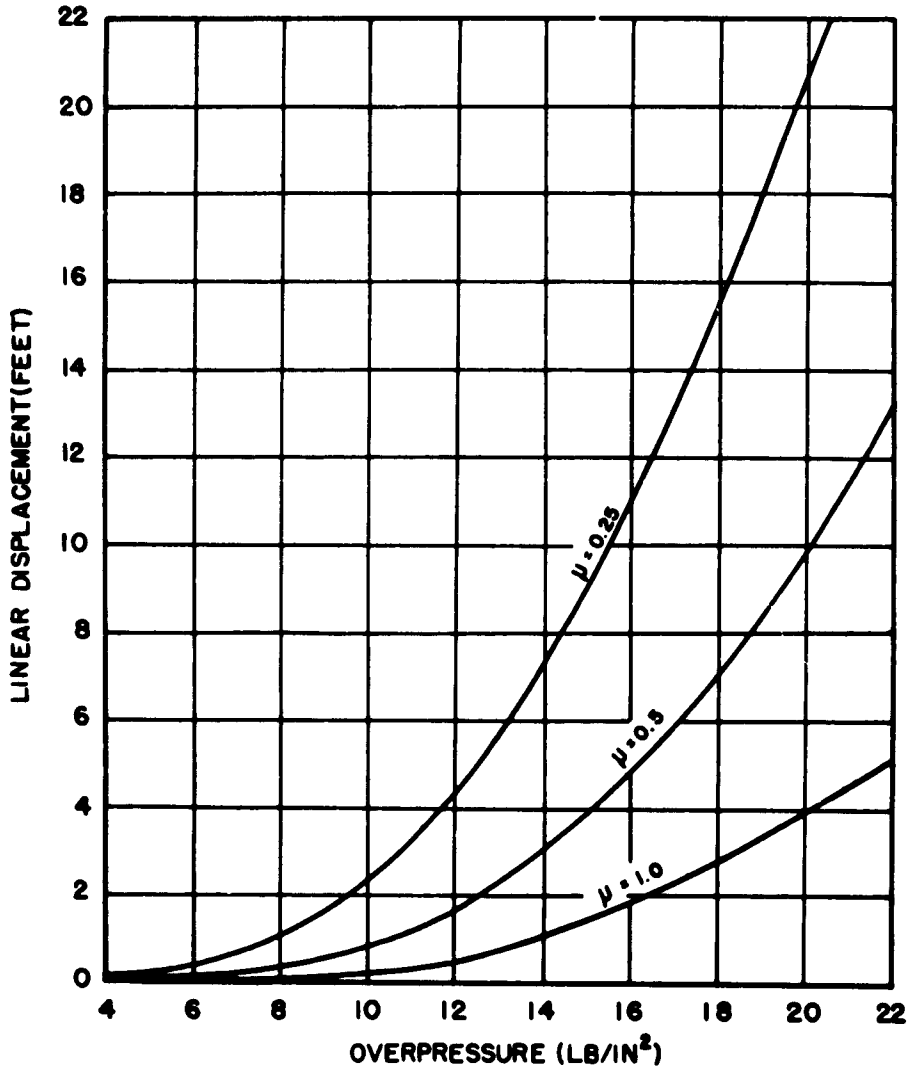

Fig. 2.28 Calculated Linear Displacement vs Overpressure for M-135 2-1/2 Ton Truck Struck Face-on by Mach Wave (Assuming Sliding Only)

CHAPTER 3

EXPERIMENTAL PROCEDURE

3.1 FIELD LAYOUT - SHOT 9 AND SHOT 10

The equipment exposed in Shot 9 and Shot 10 consisted of the following:

1. Trucks, 2-1/2 ton M-35. . . . . .27 each
2. Trucks, 1/4 ton M38A1 . . . . . .27 each
3. 57 mm guns, M-1 . . . . . .27 each
4. 105 mm howitzers, M-3 . . . . . 5 each
5. Tanks (M4 - 3 ea.) (M24 - 1 ea.) (M3 - 3 ea.) (M7 - Sp 1 ea.) . . . . . 7 each
6. 90 mm AA Guns (M1A1) . . . . . 2 each

It was intended to use 105 mm howitzers (M2A1), but these were in short supply and in lieu thereof 57 mm guns were used. For the purpose of this report, it was assumed that the damage characteristics of the 57 mm gun are similar to those of the 105 mm howitzer. The location and orientation of the items exposed are listed in Table 3.1 and Table 3.2, for Shot 9 and Shot 10 respectively. Field layout of equipment exposed is shown in Figs. 3.1, 3.2, and 3.3. The 90 mm guns were located in the DESERT ROCK Sector to coordinate the weapons effectiveness test with troop indoctrination. Only vehicles were exposed on Shot 9, since the maximum pressures expected were insufficient to cause damage to either guns or tanks.

The vehicles and guns were placed side-on, rear-on, and face-on. It was assumed that side-on orientation would cause greater target vulnerability and face-on least target vulnerability. The items in rear-on orientations would be in the intermediate category between least and greatest vulnerability. Because of the small number of tanks available, these were put in side-on and face-on orientation only.

The guns and howitzers were tactically emplaced. The emplacements were similar to the standard Corps of Engineers hasty field emplacements for light artillery (see Engineers Field Manual FM-25). The guns were located at higher pressure regions than seemed necessary to obtain 100 per cent damage probability as indicated by the statistical analysis. The survey of 105 mm howitzers has shown that a majority

of the pieces were placed on the surface for exposure and since all of the 57 mm guns were to be tactically emplaced to obtain shielding effects, it appeared that higher pressures would be necessary to obtain 100 per cent damage.

The 105 mm howitzers (M-3) were used to compare effects upon items similar in shape but different in size.

On both shots, two stakes were driven into the ground near each item for marking their position prior to the shot. After each shot, these stakes were used as reference points for displacement measurements.

3.2 INSTRUMENTATION

3.2.1 General

The gages used to measure the linear horizontal and vertical accelerations were Wiancko accelerometers and the self-recording ERA accelerometers. The gage chosen for measuring angular velocity was the Giannini Rate-Gyro, Type 3611 F. This instrument employs a D. C. driven gyro which is restrained in its zero position by a spring. As the rotational velocity about an axis perpendicular to the axis of the gyro increases, the gyro deflects against the spring and sweeps a contact across a potentiometer. Damping on the order of 0.4 or 0.5 is built into the instrument. The gyro is designed to be highly resistant to linear accelerations and vibrations. The potentiometer resistance is 2000 ohms, linearity is $\pm$ 2 per cent of full range, and resolution is 0.5 per cent of full range. The gage was employed in an A. C. bridge circuit for use with the Webster-Chicago recording equipment. The D. C. power supply to the gyro was provided by the vehicle batteries.

For further details of the gages used refer to the report of Project 3.28.1 (WT-738), since this project provided all instrumentation for Project 3.21.

Table 3.3 and Table 3.4 delineate the range and type of gage used at each pressure level on Shot 9 and Shot 10 respectively. The letters TSO indicate the 2-1/2 ton truck in the side-on orientation. TFO and JSO, (J, for jeeps) are interpreted in a like manner. RG indicates the rate gyro, WcA indicates the Wiancko accelerometer, and ERA is the self-recording accelerometer.

On Shot 9, twelve Wiancko gages and twenty accelerometers were placed on the instrumented vehicles for measuring linear accelerations. Simultaneously eight channels were used for recording angular velocities for the same vehicles.

On Shot 10, eight Wiancko gages and eight ERA accelerometers were placed on the instrumented vehicles for measuring linear accelerations. Simultaneously eight channels were used for recording angular velocities for the same vehicles.

3.2.2 Placement and Mounting of Gages

The frame of the vehicle was selected as reference for indicating

displacement and orientation of the vehicles. Therefore, it was desirable to attach all gages to the frame if possible. In addition, placement close to the center of gravity was desired to reduce any effects of rotation on the linear accelerometers. In most cases mountings were constructed in order to obtain proper orientation and rigid attachment to the vehicles. In all cases the Wiancko accelerometer and rate gyros were attached to the outside of the left frame member of the 2-1/2 ton truck in line with the center of gravity, and to the outside of the right frame member of the 1/4 ton truck in line with the center of gravity. For the 2-1/2 ton truck face-on, the ERA gage was mounted in the center of the cargo body as far forward as possible. For the 1/4 ton truck side-on, the ERA gage was mounted on the floor of the tool box located under the right front seat. For other orientations, the ERA gage was attached to the frame members as described above.

The vehicles were expected to move considerable distances in some cases. It was desired that the gages record at least during the initial stages of this motion; thus it was necessary to provide for about 50 ft of free cable at the vehicle locations. This free cable was coiled in a box about 2 ft square under the vehicle and covered with about 2 in. of loose sand. The cables were tied securely to the bottom of the vehicles with slack between the secured point and the gage.

3.3 PHOTOGRAPHY

Motion picture photography of the various positions was attempted in order to provide information about the environment of the vehicles while under test, to display the motion of the vehicles, and possibly indicate the time of occurrence of damage. Any data obtained should aid in the interpretation of the acceleration and angular velocity records. White crosses were painted on the vehicles near the center of gravity and bars were painted at the end of the vehicles to facilitate interpretation of the films. The viewing axis was perpendicular to the path of the shock waves. The cameras were operated at a speed of approximately 64 frames/sec. The table below indicates the positions photographed:

Position	Target	Shot No.	No. of Cameras
3.21m	vehicles	9	1
3.21k	vehicles	9	2
3.21i	vehicles	9	2
3.21e	vehicles	9	2
3.21k	vehicles	10	2
3.21af	vehicles	10	2
3.21y	57 mm guns	10	2

(Cont'd)

Position	Target	Shot No.	No. of Cameras
3.21i	vehicles	10	2
3.21e	vehicles	10	2

All items except position 3.21e were on stabilized areas.

Still photographs were taken of the items before and after each shot. Since many of the items were of identical condition prior to shot time, still pictures were taken of the most representative items before each shot. After each shot as many pictures were taken of the items as was practical.

All photography was provided by Program 9.

TABLE 3.1 Shot 9 Field Layout

Position	Dist (ft) Corrected to Actual GZ	Measured Over-pressure (psi)	1/4 Ton Truck		No/ Pos	2-1/2 Ton Truck		No/ Pos
3.21a	1195	17.8	1-FO	1-RO	2	1-RO		1
3.21b	1320	16.8	1-FO		1	1-SO	1-FO	2
3.21c	1480	15.6	1-SO	1-RO	2	1-SO	1-RO	2
3.21d	1640	14.5	1-SO	1-RO	2	1-SO	1-FO	2
3.21e	1640	14.5	1-SO	1-FO	2	1-SO	1-FO	2
3.21f	1740	14.0	1-SO	1-RO	2	1-SO	1-SO	2
3.21g	1830	13.4	1-SO	1-FO	2	1-SO	1-RO	2
3.21h	875	21	1-RO	1-FO	2	2-FO		2
3.21i	2480	10.8	1-SO	1-RO	2	1-SO	1-RO	2
3.21j	2860	10.6				1-SO	1-FO	2
3.21ia	3060	10.2	1-SO	1-FO	2			
3.21ib	3930	8.3	1-FO	1-RO	2	1-RO	1-FO	2
3.21k	4360	7.4	1-SO	1-FO	2	1-SO	1-FO	2
3.21l	5590	6.3	1-SO	1-FO	2	1-SO	1-FO	2
3.21m	6550	4.4	1-SO	1-FO	2	1-SO	1-FO	2
				Total	27		Total	27

TABLE 3.1 Shot 9 Field Layout (Cont'd)

Position	Dist (ft) Corrected to Actual GZ	Measured Over-pressure (psi)	90 mm AA Gun	No/ Pos.	2-1/2 Ton Truck	No/ Pos.
3.21 f	1500	15.4	1-FO	1		
3.21 l	5200	6.8	1-FO	1		
			Total	2		

TABLE 3.2 Shot 10 Field Layout

Position	Dist (ft) Corrected to Actual GZ	Actual Measured Overpressure (psi)		Item			
				1/4 Ton Truck		2-1/2 Ton Truck	
3.21 d	995	*58.0	**	1-FO	1-RO	1-FO	1-RO
3.21 e	1130	39.0		1-FO	1-SO	1-FO	1-SO
3.21 ad	1600	12.5	17.2	1-SO			1-SO
3.21 i	1920	9.0	11.5	1-SO			1-SO
3.21 af	2415	8.4	10.3	1-SO			1-SO
3.21 ag	2770	7.6	7.0	1-SO			1-SO
3.21 k	4380	4.0		1-SO			1-SO
3.21 t	900	78.0	97.5	1-FO	1-RO	1-FO	1-RO
	Total			11		11	

TABLE 3.2 Shot 10 Field Layout (Cont'd)

Position	Dist. (ft) Corrected to Actual GZ	Actual Measured Overpressure (psi)		57 mm Gun AT (M2)	105 mm How. (M3)	90 mm AA Gun (M1)	Tanks (M4A3, (M24)
3.21 n	380	* >300	**				1-FO
3.21 o	570	200					1-FO 1-SO
3.21 p	645	160		2-FO			
3.21 q	715	130	112	1-FO 1-SO 1-RO	1-RO	1-FO	1-FO
3.21 r	850	90		1-FO 1-SO 1-RO	1-RO		
3.21 t	900	78	97.5	1-FO 1-SO 1-RO	1-RO		
3.21 u	1045	51	60.0	1-FO 1-SO 1-RO			1-FO 1-SO
3.21 v	1100	43	36.8	1-FO 2-SO 2-RO	1-RO		
3.21 w	1265	27	26.0	1-FO 1-SO 1-RO	1-RO		
3.21 x	1415	18	25.2	1-FO 1-SO 1-RO			1-SO
3.21 y	2140	8.6	10.5	1-SO 1-RO			
3.21 z	3000	7.2				1-FO	
		Totals		27	11	2	7

* Main blast line
** BRL mechanical gages

TABLE 3.3 Instrumentation (Shot 9)

Over-pressure (psi)	Vehicle Orientation	Type Gage	Range	ERA Range h-v (g's)
5.0	TSO	RG	± 60°/sec	2-1
	JSO	RG	± 100°/sec	2-1
	JFO			2.5-1
	TFO			1.5-1
7.2	TSO	RG	± 100°/sec	2.5-1
		RG	± 200°/sec	
	TFO	WcA	5g	2-1
	JFO	WcA	5g	6-2
	JSO	RG	± 300°/sec	5-2
9.2	TSO	RG	± 200°/sec	6-1
		RG	± 500°/sec	
		WcA	10g	
		RG	± 500°/sec	10-6
		RG	± 1000°/sec	
		WcA	10g	
	JFO	WcA	10g	10-3
		WcA	25g	
	TFO	WcA	5g	2-1
		WcA	10g	
14.0	TSO	RG	± 500°/sec	10-2
	TFO	WcA	10g	5-2
	J O	WcA	15g	20-6
	JSO	RG	± 1500°/sec	20-10
20.0	TSO	RG	± 1000°/sec	30-10
	TFO	WcA	15g	10-5
	JFO	WcA	30g	30-10
	JSO	RG	± 1500°/sec	50-10

TABLE 3.4 Instrumentation (Shot 10)

Peak Over-pressure (psi)	Vehicle Orientation	Type Gage	Range	ERA Range h-v (g's)
7.2	TSO	RG	± 100°/sec	2-1
		WcA	1g	
		RG	± 200°/sec	2-1
9.2	TSO	RG	± 200°/sec	2.5-1
		WcA	2g	
	JSO	RG	± 300°/sec	5-2
		WcA	3g	
14.0	TSO	RG	± 300°/sec	6-1
		WcA	5g	
	JSO	RG	± 700°/sec	10-3
		WcA	8g	
20.0	TSO	RG	± 500°/sec	10-2
		WcA	10g	
	JSO	RG	± 1000°/sec	20-6
		WcA	15g	

Fig. 3.1 Field Layout of Vehicles for Shot 9

Fig. 3.2 Field Layout of Vehicles for Shot 10 (Area West of G

Fig. 3.3 Field Layout of Ordnance Materiel For Shot 10 (Area South of GZ)

CHAPTER 4

RESULTS AND OBSERVATIONS

4.1 EVALUATION AND RECOVERY - SHOT 9

The second day following the atomic blast, a complement of seven men with one 5 ton wrecker (M-62) went into the area to evaluate and recover 54 vehicles and two 90 mm AA guns. Generally, the 5 ton wrecker was used to upright all vehicles that were overturned. In the case of the 1/4 ton trucks turned on the side four men put the trucks back in an upright position.

It took approximately 65 man-hours to recover and evaluate the vehicles. It is believed that if recovery took place after the shot, as soon as practical, this time could be decreased by several man-hours. Additional time was required to release the hydrostatic engine lock developed by the overturned trucks. While a truck was on its back, oil flowed between the piston and the cylinder head preventing piston motion. Spark plugs were removed and the engine cranked in order to release the hydrostatic lock.

Two teams, composed of qualified personnel, were organized to evaluate and record the damage. A quick inspection was conducted to determine whether or not vehicles were combat usable. Upon ascertaining the extent of damage affecting the combat use of a vehicle an attempt was made to have a realistic repair and repair time, by actually performing the work required to restore vehicle to combat use and recording the time taken.

Out of 54 vehicles exposed, 15 were immediately combat usable. Thirty-eight vehicles required repair time ranging from 1/2 to 2 man-hours of organizational maintenance to restore to combat use. Only one truck required depot maintenance and this was apparently due to a secondary effect. A tire was ignited and the sustained fire spread to the electrical system.

Each vehicle (combat usable) was driven approximately 17 miles to a parking lot where a thorough evaluation was conducted to determine the man-hours needed to restore the vehicle to original condition. In Appendix C, Table C.1 presents a copy of the cover sheet for on-the-spot evaluation and Table C.2 illustrates the procedure for thorough evaluation of damage. It is to be understood that the time for repair

in above tables is based on immediate availability of parts and tools as well as skilled mechanics performing the work. The results of Shot 9 are tabulated in Appendix C, Table C.3. The distances have been corrected to actual ground zero.

4.2 EVALUATION AND RECOVERY - SHOT 10

The same procedure described in section 4.1 was followed for evaluation and recovery of vehicles in Shot 10. Six out of 22 vehicles exposed were in good enough condition that recovery was possible. The rest of the vehicles were completely demolished.

While on-the-spot checks were suitable to determine the combat usability of vehicles, it was necessary that a thorough evaluation be conducted to determine the combat use of guns, since the various components of the gun form an integral whole for reliable and accurate operation.

It was the policy to indicate the lowest echelon of maintenance required to restore damaged items to combat use. This posed a special problem in the case of 57 mm guns. According to the echelon of maintenance established for guns, very little repair work is done by the using unit. In general, most of the maintenance to repair or restore damaged components is by Field Ordnance Units. Therefore, regardless of the damage to guns, the echelon of maintenance assigned in the majority of the cases was field. This somewhat introduces discrepancies in generalizing damage to categories of light, moderate, and severe. To circumvent this discrepancy, it was decided to assign the additional classification of salvage whereby the gun could be restored to combat use, but it would not be economical to do so. This mode of classification wherever applicable is shown in the tabulated results of Shot 10, Appendix C, Table C.4.

The distances of each position shown in the above table have been corrected to the actual ground zero. The outline for evaluating damage to guns is shown in Table C.5 and the evaluation of damage for tanks is shown in Table C.6.

4.3 DAMAGE COMMENTS - SHOT 10

In the words of the Test Director, Dr. E. B. Doll, "The damage effects of Shot 10 were spectacular, both in magnitude and character, even to a casual or untrained observer." Some comments regarding these spectacular effects of Shot 10 seem appropriate in order to give to the reader an idea of the damage resulting from this atomic detonation.

The test equipment consisted of trucks, tanks, and artillery. As might be expected in field conditions only the latter was entrenched. Despite a high degree of dispersion and a hasty field fortifications virtually all of the equipment was unusable.

Practically nothing was left intact of the trucks out to a radius of 2000 ft from ground zero. Beyond this point trucks were picked up and hurled through the air from 10 to 30 ft. It is impossible to say how far trucks placed within the 2000 ft radius were moved, since they

were torn into pieces and scattered up to distances of 2000 ft from their original position.

The chassis of one truck was thrown 600 ft through the air, smashing a hole in a 4 in. reinforced concrete roof of a test structure. Generally, engines were ripped from the frames, the chassis bent and twisted, and in some cases the armature was torn from inside the generator case.

Despite their greater strength the tanks suffered equally, as they were in general closer to the point of detonation. One M4A3 tank weighing 30 tons was thrown back 120 ft and the turrent was ripped off and found lying an additional 120 ft further back. A lighter tank (M24) was moved 148 ft and stripped of its turrent, threads, and road wheels. At a lower pressure region an 18 ton self-propelled howitzer (M7) was tossed 170 ft through the air and slid 80 ft more after landing.

The artillery which consisted of 57 mm guns and 105 mm howitzers were virtually all knocked out. Some guns were thrown about 200 ft and usually suffered extreme damage. Tubes and trails were ripped off carriages, wheels were sheared cleanly off their axles, and in at least one case the recoil mechanism was blown completely away from the tube and carriage.

This does not tell the whole story of the damage occuring as a result of this atomic blast. It must be kept in mind that these items were dispersed throughout the area for test purposes so it can only be imagined what havoc and chaos would be created if items were more concentrated in one region such as depots, railroad marshalling yards, etc. Without a doubt, secondary damage effects would be as great. Such secondary effects as flying debris striking other items were not operative in this test.

4.4 DISPLACEMENTS

4.4.1 Displacements on Shot 9

The final position of all vehicles exposed on Shot 9 was recorded by triangulation measurements from the stakes marking the preshot position of the vehicles. The displacements of the center of gravity (regardless of the final orientation) was determined from the measurements and the results are presented in Tables 4.1 and 4.2. The accuracy of the displacements listed is ± 5 per cent. The various sources of the pressure data quoted in Tables 4.1 and 4.2 are discussed in sections 5.1 and 5.2 of this report.

In general the motion of the vehicles was directed approximately radially out from actual ground zero. The deviation from intended orientation listed in Tables 4.1 and 4.2 roughly indicates the change in the direction of motion from that anticipated.

The final angular displacement of the vehicles was observed and recorded. The figures listed in Tables 4.1 and 4.2 represent the number of degrees rotation about the longitudinal axis of the vehicle required to produce the final angular orientation with respect to this axis. If the vehicle turned on its side, then 90 degrees is listed, if the vehicle made one complete revolution returning to an upright position,

360 degrees is listed. The figure does not represent the maximum angular displacement, since a vehicle found on its side may have turned almost on its back before falling to rest finally on its side. The same uncertainty prevailed for other orientations.

The 90 mm AA guns exposed on Shot 9 in hasty field emplacements exhibited no displacement whatever.

4.4.2 Displacements on Shot 10

The majority of the vehicles exposed on Shot 10 were dismembered to the extent that a displacement measurement was not feasible. These vehicles are denoted by dem. (demolished) in Tables 4.3 and 4.4. At position 3.21i the frames of the vehicles remained roughly intact and their displacement is listed. The majority of the vehicle parts, representing a large part of the total weight, were scattered over a wide area. At those positions at a greater distance from ground zero than 3.21i the vehicles remained intact and their displacements were determined by reference to stakes in the same manner as for Shot 9. The accuracy of the figures given for displacements is ± 5 per cent. The source of pressure noted in Tables 4.3 and 4.4 is given in sections 5.1 and 5.2.

At position 3.21af a clear imprint of the side and wheels of the 2-1/2 ton truck were found in the stabilized surface about 36 ft from the original position. No other marks were evident closer to the original position. Apparently the truck rotated 270 degrees with little or no contact with the ground, landed squarely on the side which originally faced ground zero, then continued its turn to come to rest on its back.

After Shot 10 the gun emplacements were found to be partially filled in with dirt so that all the reference stakes were completely covered (except for 3.21y, a stabilized area). The original position of the center of gravity was estimated from the configuration of the emplacement and the distance from this point to the center of the gun remains was recorded. The error for the values in Table 4.5 is ± 15 per cent for displacements of 10 ft or less, decreasing to ± 7 per cent for displacements greater than 150 ft. Where the tube and gun carriage were separated and could be identified the displacements of each are recorded. The displacements of those guns exposed in rear-on position were found to exceed those of face-on or side-on orientations, and the displacements for the face-on orientation were generally less than those for the other orientations.

The displacements of the 105 mm howitzers on Shot 10 are contained in Table 4.6. The same conditions prevailed for displacement measurements as for the 57 mm guns. The values are considered accurate to ± 7 per cent. These guns were all emplaced rear-on.

The tank displacements were recorded in the same manner as the displacements of the vehicles. The marker stakes were not buried, and the values in Table 4.7 are considered accurate to ± 5 per cent. Those tanks that overturned are noted in the table. It is not certain whether the M-7 self-propelled howitzer at position 3.21x rolled. Although the howitzer was found upright and reasonably intact, it

traversed a considerable distance from its original side-on position, and it seems quite possible that overturning did occur during movement.

The 90 mm AA guns exposed on Shot 10 were not discernibly displaced.

4.5 INSTRUMENTATION AND PHOTOGRAPHY

4.5.1 Instrumentation

Because of initiation failure one-half of the self-recording ERA accelerometer channels were lost on Shot 9 and Shot 10. Of the 20 channels that initiated on Shot 9, 15 channels were usable. Six out of the eight channels that initiated on Shot 10 were usable.

Twenty-five channels were employed on Shot 9 to record the output of the Wiancko accelerometers and Giannini rate gyros that were attached to the vehicles. Four channels were not usable because of electrical failure of undetermined origin. The rate gyros apparently recorded satisfactorily. The accelerometer records, however, contain a considerable amount of high frequency oscillations. Electrical or graphical filtering may be required to obtain the proper data from some of the records. The gage ranges selected were satisfactory. The free cable that was buried under a few inches of sand under the vehicles apparently pulled out of the ground and followed the movement of the vehicles satisfactorily.

Sixteen channels were employed on Shot 10 to record the output of the accelerometers and rate gyros. Five of the channels indicated electrical failure as soon as the shock wave arrived. It seems possible that at the closer stations some cables broke immediately. The accelerometer records are characterized by an extreme amount of high frequency oscillations up to the time of cable break. The rate gyro gage ranges, although satisfactory for similar pressures on Shot 9, were evidently considerably lower than required to record the extent of the phenomena on Shot 10. At position 3.21af, for example, the output from the rate gyro on the 1/4 ton truck rose to its peak range of 300 degrees/sec in 0.2 sec and remained off scale until the connecting cable was broken when the vehicle movement exceeded the length of available free cable. The output from the rate gyro attached to the 2-1/2 ton truck at the same position rose to its peak range of 200 degrees/sec in 0.1 sec and remained off scale until the connecting cable broke.

The analysis of the records is in progress. For further information on the gages used and typical records refer to the report of Project 3.28.1, which provided the instrumentation for this project.

4.5.2 Photography

The objective of the technical photography requested was to obtain a quantitative description of the motion of the vehicles exposed and general environmental information during exposure. The success of the photography was restricted by the action of dust, even on stabilized areas.

On Shot 9 photographs were made of stations with two cameras each at positions 3.21m, 3.21k, 3.21i, and 3.21e. The ground at

position 3.21m was stabilized over about 2/3 of the length of arc constituting the position, at position 3.21k the stabilization extended over 1/3 the position arc, at position 3.21i the stabilization covered 1/2 the position arc, and at position 3.21e there was no stabilization at all.

Stations at all positions apparently operated properly, and the amount of useful information recorded was determined by the degree that visibility was affected by dust. Visibility was reduced least at position 3.21m, where some part of the nearest vehicle was visible at all times. At 3.21k visibility was more affected, but parts of the nearest vehicle were visible for the majority of the time. At position 3.21i and position 3.21e the obscuration was sufficient to prevent the derivation of any displacement-time information from the films.

On Shot 10 photographs were made by stations of two cameras each at positions 3.21k, 3.21af, 3.21i, 3.21e, and 3.21y. Positions 3.21af and 3.21y were stabilized over the full position arc. The camera station at position 3.21e was destroyed and the films lost. The camera tower at position 3.21i was severely bent, but the films were recovered and provide views of the position up to the time of shock arrival. At position 3.21af the camera tower was bent but camera operation was not interrupted. Some parts of the vehicles were visible in the initial phases of the motion immediately after the shock arrival. At position 3.21y the camera tower was bent very slightly, but the cameras continued to operate. Shock arrival at the target items was recorded but obscuration occurred as the shock wave reached the camera. At position 3.21k the camera station was apparently unaffected, and parts of the nearest vehicle were in view for about half the positive phase.

The dust quantity and rate of rise prior to shock arrival as indicated in the films seems to be greater for Shot 9 than for Shot 10, which is consistent with the fact that thermal radiation at the positions photographed was higher on Shot 9. Dust level remained below camera level during most of the positive phase on Shot 9. In the precursor region on Shot 10 reduction in visibility occurred as soon as the shock wave arrived at the camera, indicating that dust extended well above the camera levels.

For reading purposes the films were projected on white cardboard perpendicular to the axis of the projector. The linear enlargement experienced was about 35 times. The positions of the marker pole and vehicles prior to disturbance were traced on the cardboard screen. Then in successive frames when it was desired to record the positions, the screen was adjusted so that the image of the marker pole was superimposed on the drawing of the image from the original frame. The features of the vehicles were traced using various colors to provide necessary coding. Measurements of the movement of the vehicles then were made from these drawings.

The angular position of selected parts of the vehicles were measured with respect to the original position. This angle was read directly from the drawing. Readings taken from different parts of the vehicles and from different films of the same subject were plotted, and it was found that the points in general were randomly interspaced, indicating that the error in making the traces and reading the angles overrides errors due to different positioning in the film plane, film

TABLE 4.1 Displacement of M-38A1 1/4 Ton Truck Shot 9

Position	Range (ft)	Pressure Side-on (psi)	Pressure Dynamic (psi)	Deviation from Intended Orientation (Degrees)	Displacement Side-on (ft)	Displacement Face-on (ft)	Displacement Rear-on (ft)	Angl. Displ. S. O. (Degrees)	Angl. Displ. F. O. (Degrees)	Angl. Displ. R. O. (Degrees)
3.21 h	875	21.0	0.98	19		3.9	5.9		0	0
3.21 a	1190	17.8	1.43	34		15.9	15.5		90	180
3.21 b	1320	16.8	1.55	30		17.0			0	
3.21 c	1480	15.6	1.69	25	29.5		19.8	360		90
3.21 d	1640	14.5	1.80	23	25.2	13.6		270	0	
3.21 e	1640	14.5	1.80	29	27.1	17.6		270	0	
3.21 f	1740	14.0	1.85	26			26.3			90
3.21 g	1830	13.4	1.90	26	32.9	22.0		180	180	
3.21 i	2480	10.8	2.13	16	23.8	8.0		180	0	
3.21 ia	3060	10.2	2.58	18	22.4	7.5		180	0	
3.21 ib	3930	8.3	1.73	12		6.9	16.0		0	0
3.21 k	4360	7.4	1.40	11	9.6	1.4		90	0	
3.21 l	5590	5.4	0.77	8	0.9	0.5			0	
3.21 m	6550	4.4	0.49	7	0.6	0.0			0	

TABLE 4.2 Displacement of M-35 2-1/2 Ton Truck Shot 9

Position	Range (ft)	Pressure Side-on (psi)	Pressure Dynamic (psi)	Deviation from Intended Orientation (Degrees)	Displacement Side-on (ft)	Displacement Face-on (ft)	Displacement Rear-on (ft)	Angl. Displ. S. O. (Degrees)	Angl. Displ. F. O. (Degrees)	Angl. Displ. R. O. (Degrees)
3.21 h	875	21.0	1.13	20		1.9			0	
						1.6			0	
3.21 a	1190	17.8	1.43	24			10.0			90
3.21 b	1320	16.8	1.55	29	10.2	11.4		90	90	
3.21 c	1480	15.6	1.69	25	16.2		11.2	180		90
3.21 d	1640	14.5	1.80	23	17.6	9.3		180	0	
3.21 e	1640	14.5	1.80	28	19.0	6.9		180	0	
3.21 f	1740	14.0	1.85	27	22.2		10.8	90		90
3.21 g	1830	13.4	1.90	26	18.0	10.7		180	0	
3.21 i	2480	10.8	2.13	16	24.6	6.1		270	0	
3.21 j	2860	10.6	2.75	14	16.9	4.0		180	0	
3.21 1b	3930	8.3	1.73	12		1.8	3.7		0	0
3.21 k	4360	7.4	1.40	11	6.3	0.5		90	0	
3.21 l	5590	5.4	0.77	8	0.5	0.4		0	0	
3.21 m	6550	4.4	0.49	7	0.3	0.0		0	0	

TABLE 4.3 Displacement of M-38A1 1/4 Ton Truck Shot 10

Position	Range (ft)	Pressure Side-on (psi)	Pressure Dynamic (psi)	Displacement Side-on (ft)	Displacement Face-on (ft)	Displacement Rear-on (ft)	Final Angular Displacement Side-on (Degrees)
3.21 t	900	78	126		Demolished	Demolished	
3.21 d	990	58	85		Demolished	Demolished	
3.21 e	1130	39	53	Demolished	Demolished		
3.21 ad	1600	12.5	14.4	Demolished			
3.21 i	1920	9.0	7.3	312 (Frame)			
3.21 af	2415	8.4	3.2	72			360
3.21 ag	2770	7.6	2.1	17.7			270
3.21 k	4380	4.0	0.5	0.5			0

TABLE 4.4 Displacement of M-35 2-1/2 Ton Truck Shot 10

Position	Range	Pressure Side-on (psi)	Pressure Dynamic (psi)	Displacement Side-on (ft)	Displacement Face-on (ft)	Displacement Rear-on (ft)	Angular Displacement Side-on (Degrees)
3.21 t	900	78	126		Demolished	Demolished	
3.21 d	990	58	85		Demolished	Demolished	
3.21 e	1130	39	53	Demolished	Demolished		
3.21 ad	1600	12.5	14.4	Demolished			
3.21 i	1920	9.0	7.3	Frame 230			
3.21 af	2415	8.4	3.2	60			540
3.21 ag	2770	7.6	2.1	8.7			90
3.21 k	4380	4.0	0.5	0.1			0

TABLE 4.5 Displacement of 57 mm Guns on Shot 10

Position	Range (ft)	Pressure		Displacement Side-on (ft)	Displacement Face-on (ft)	Displacement Rear-on (ft)
		Side-on (psi)	Dynamic (psi)			
3.21 p	645	160	430		50 44	
3.21 q	720	130	290	Tube-62 Carriage-15	10	Tube-115 Carriage-225
3.21 r	850	90	160	16	31	150
3.21 t	900	78	126	Tube-70 Carriage-18	52	Tube-290 Carriage-255
3.21 u	1045	51	73	35	48	Tube-300
3.21 v	1100	43	60	15	2	115
3.21 w	1265	27	36	21	3	25
3.21 x	1415	18	23	26	17	250
3.21 y	1240	8.6	4.9	59		55

TABLE 4.6 Displacement of 105 mm Howitzers on Shot 10

Position	Range (ft)	Pressure		Displacement Rear-on (ft)
		Side-on (psi)	Dynamic (psi)	
3.21 q	720	130	290	50
3.21 r	850	90	160	145
3.21 t	900	78	126	180
3.21 v	1100	43	60	210
3.21 w	1265	27	36	149

TABLE 4.7 Displacement of Tanks on Shot 10

Position	Range (ft)	Pressure Side-on (psi)	Pressure Dyn. (psi)	Type Tank	Displacement Side-on (ft)	Displacement Face-on (ft)	Displacement Rear-on (ft)
3.21 n	380	330		M4		54	
3.21 o	570	200		M4	overturned 122	37	
3.21 y	715	130	290	M-24		overturned 148	
3.21 u	1045	51	73	M-3	overturned 106		133
3.21 x	1415	18	23	M-7 S.P. How.	251	overturned	

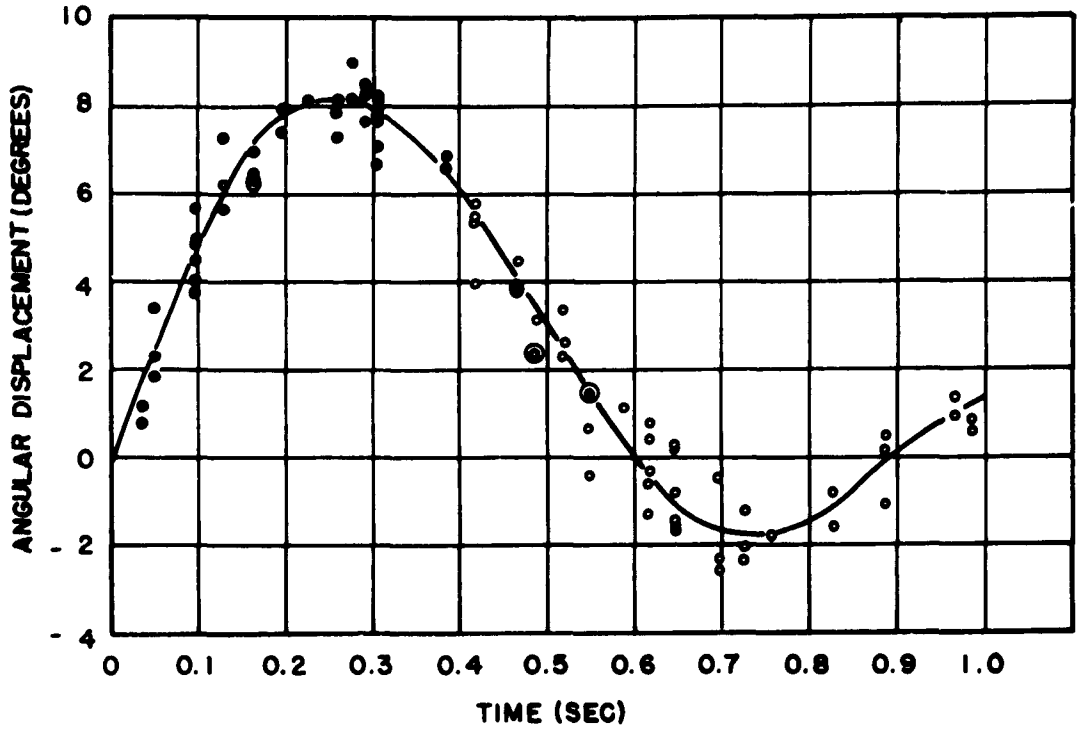

Fig. 4.1 Angular Displacement of 1/4 Ton Truck on Shot 9 at Position 3.21m (Derived from Photographs)

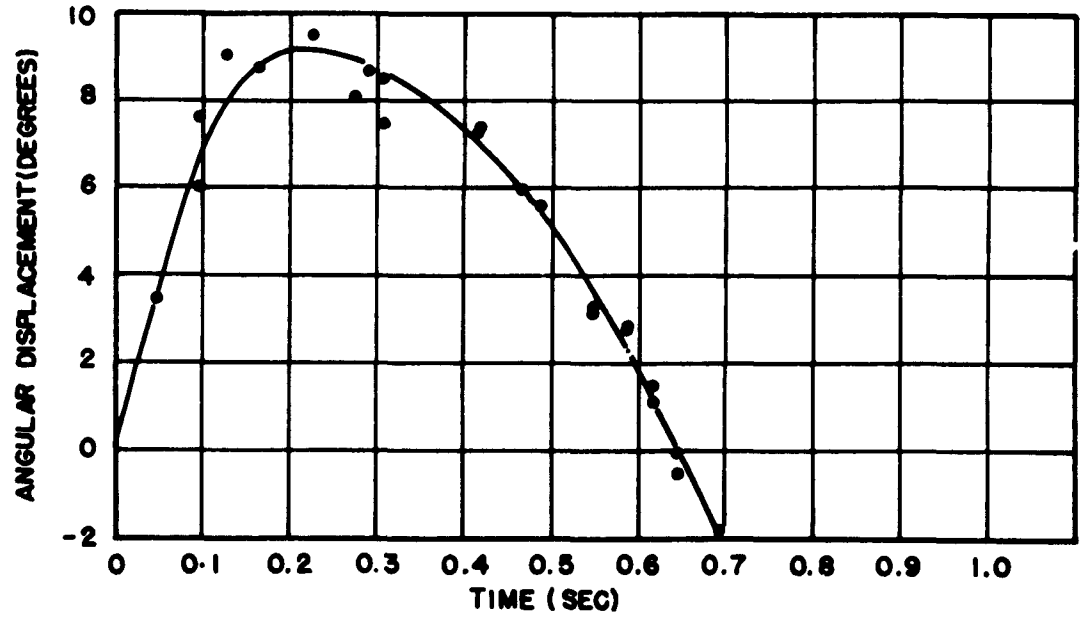

Fig. 4.2 Angular Displacement of 2-1/2 Ton Truck on Shot 9 at Position 3.21m (Derived from Photographs)

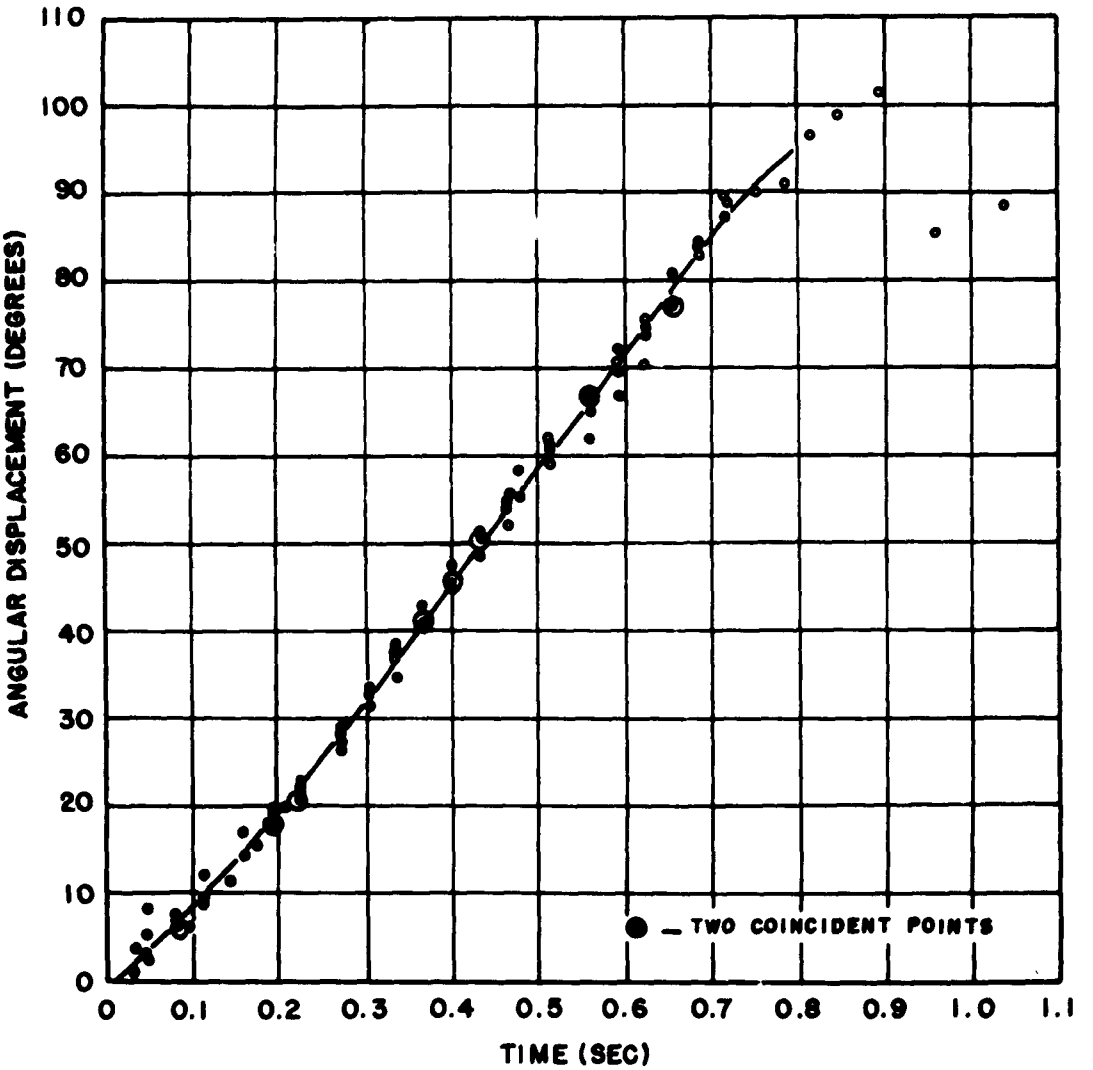

Fig. 4.3 Angular Displacement of 1/4 Ton Truck Side-on on Shot 9 At Position 3.21 K (Derived from Photographs)

shrinkage, etc. The correction necessary for the angle of tilt of the camera was examined and the conclusion was reached that the correction involved was considerably less than the magnitude of the reading errors.

For establishing the time between each frame the camera speed after shock arrival was assumed to be the same as before shock arrival. The number of frames between that frame first displaying the bomb light and the frame first indicating shock arrival was counted and compared with the arrival times as established by the electrical recording instruments. There was an uncertainty equal to the time between two frames, thus the time placement of the curves is considered accurate to + 0.05 sec.

The curves shown in Figs. 4.1 through 4.6 represent angular displacement about the longitudinal axis of the vehicles versus time as obtained from the photographs. The curves drawn through the points in the figures were drawn by eye. Sections of the curve filled by a dotted curve indicate a period when no reading could be made when dust completely obscured the view of the target. The error range with respect to the curve in Fig. 4.1 is ± 2.0 degrees; for Fig. 4.2, ± 2.0 degrees; for Fig. 4.3, ± 5.0 degrees; for Fig. 4.4, ± 7.0 degrees; and for Fig. 4.5, ± 3.0 degrees. In general, the better the visibility the lower the error range. The error range was not estimated for Fig. 4.6. At this station the camera tower was bent, and this bending may have been occurring at the times for which the points were plotted. In addition, visibility was poor. However, the points should provide an indication of the magnitude of the effects occurring during the time indicated.

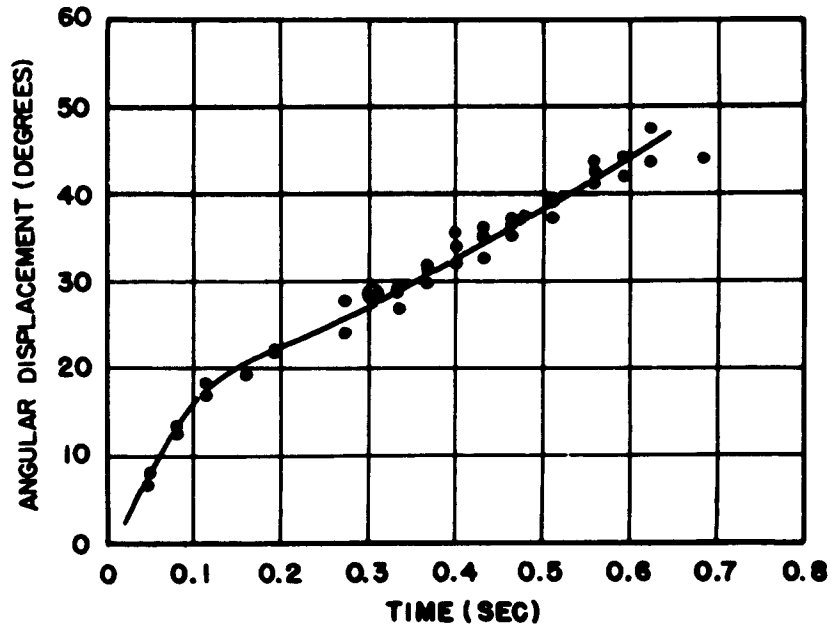

Fig. 4.4 Angular Displacement of 2-1/2 Ton Truck Side-on on Shot 9 at Position 3.21K (Derived from Photographs)

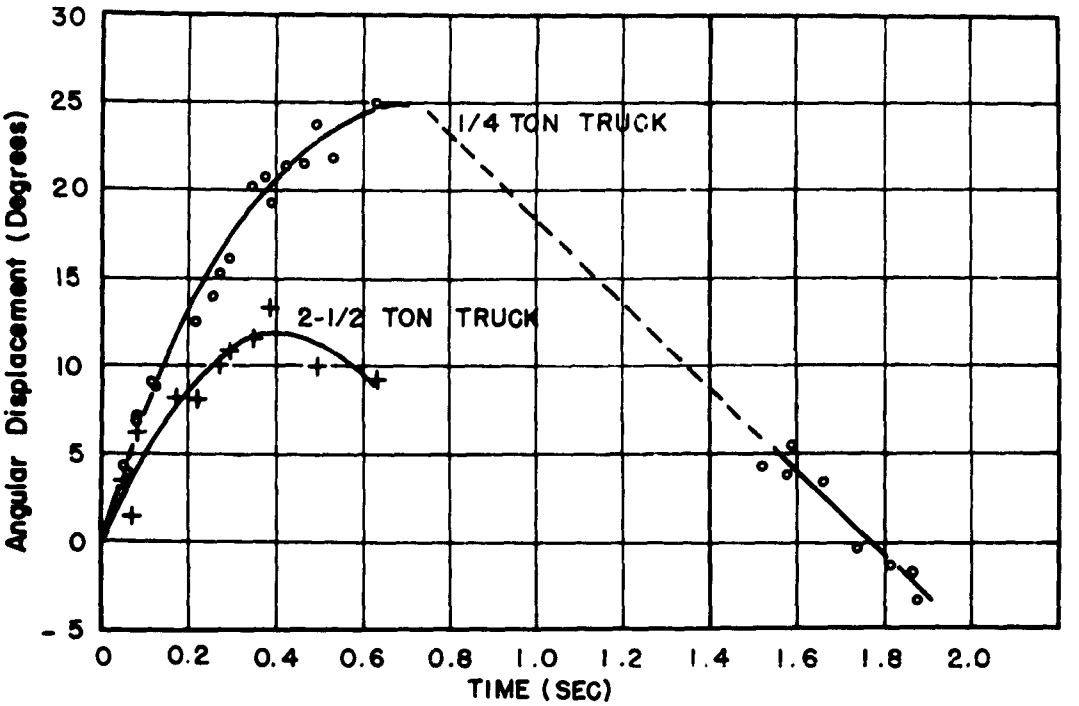

Fig. 4.5 Angular Displacement of Vehicles Side-on on Shot 10 at Position 3.21K (Derived from Photographs)

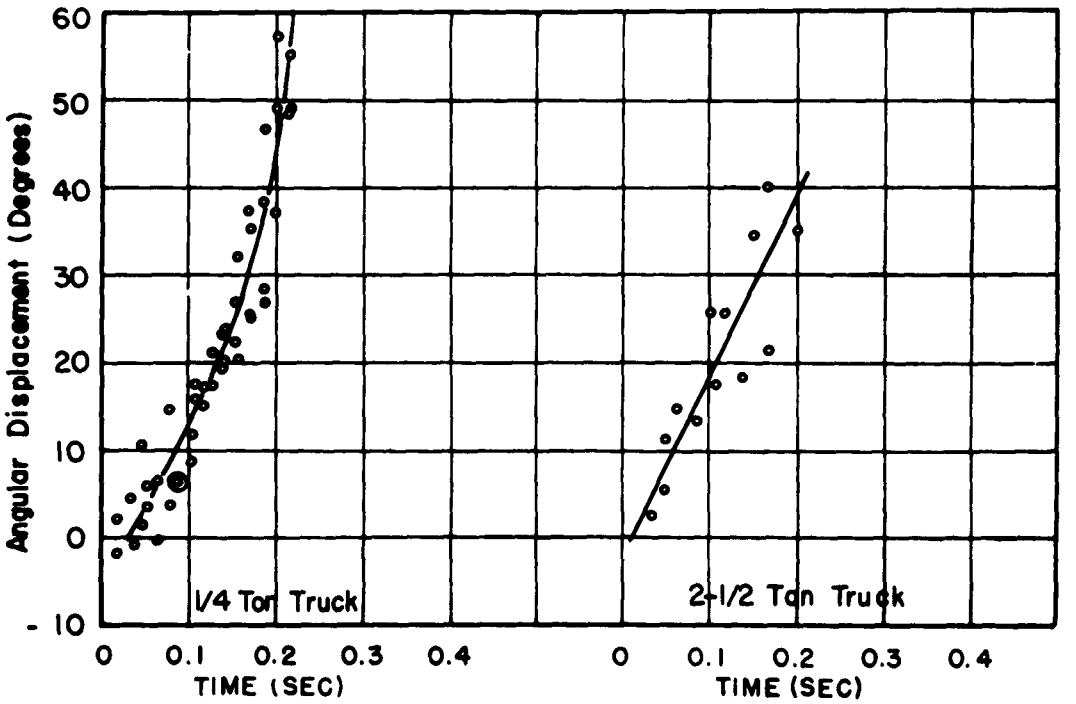

Fig. 4.6 Angular Displacement of Vehicles Side-on on Shot 10 at Position 3.21AF (Derived from Photographs)

CHAPTER 5

DISCUSSION OF RESULTS

5.1 GENERAL

The damage to vehicles exposed in Shot 9 was within the realm of statistical estimation of damage and agreed to a fair degree of accuracy with predicted effects based on the BRL method. In Shot 10, the damage to all of the equipment exposed as a function of measured overpressures greatly exceeded the predictions. Items in side-on orientation in both shots were more vulnerable to blast than either face-on or rear-on orientation.

Although many of the vehicles were turned over, the over-all damage in Shot 9 was to the sheet metal components of the vehicle and considered to be between light and moderate. The vehicle at the closest station to ground zero sustained less damage than those further away.

The cause for the extensive damage observed on Shot 10 of UPSHOT-KNOTHOLE appeared to be due to the occurrence of dynamic pressures higher than expected for the overpressures measured. The investigations thus far conducted indicate that the damage observed on Shot 10 can be attributed to dynamic pressures predicted from the so-called ideal curve. This ideal overpressure-distance curve for Shot 10 as constructed for this report is shown in Fig. 5.1. This curve is a composite of all available sources of data (references 13, 14, 15, and 16). The overpressure distance curves as measured for Shots 9 and 10 are shown in the same figure. The dynamic pressures measured on Shot 10 reported by F. H. Shelton and C. D. Broyles of Sandia Corporation[17] are said to be no higher than expected for ideal shock waves. However, after conducting shock tube tests[18] on dust laden shock waves the above report (reference 17) was later refuted by Sandia Corporation. The present opinion of Sandia apparently is that any agreement between ideal and measured dynamic pressures on UPSHOT-KNOTHOLE 10 is merely a coincidence. The dynamic pressure measured on Shot 11 agree well within limits of experimental accuracy with the dynamic pressure predicted from ideal curve (see Summary Report WT-782). This value is approximately 2.6 times larger than the dynamic pressure predicted from the measured overpressure.

A calculation made by C. W. Lampson on the organ pipes exposed in Shot 11 of UPSHOT-KNOTHOLE indicated that the dynamic pressure could be higher by a factor of 3.7 times than the dynamic pressure computed from the measured overpressure. The analysis employed was based on static loading since only the order of magnitude of the drag pressures acting on pipes was desired. The analysis is as follows:

F_d - drag force per unit area - $1/2\ \rho u^2 C_d$

Where: $1/2\ \rho u^2 = Q$ - dynamic pressure

C_d = drag coefficient

Bending moment of a pipe at failure is:

$M_o = \frac{I}{C} S$ Where: $\frac{I}{C}$ = section modulus - in^3

S = maximum fiber stress, yield point - lb in^{-2}

S = 31,000 psi for wrought iron

$\frac{I}{C} = \frac{\pi}{32} \frac{(d_1^4 - d_2^4)}{d_1}$ Where: d_1 = outside diameter of pipe

d_2 = inside diameter of pipe

For 3 in. pipe: $d_1 = 3.5$ in.

$d_2 = 3.068$ in.

$\frac{I}{C} = 1.74\ in^3$ and $M_o = 54{,}000$ in.-lb

For 3 in. pipe: $d_1 = 2.375$ in.

$d_2 = 2.067$ in.

$\frac{I}{C} = 0.57\ in^3$ $M_o = 17.680$ in.-lb

Bending moment of pipe due to drag forces is:

$M_d = 1/2\ F_d\ d_1\ L^2$ $\frac{M_d}{F_d} = 1/2\ d_1\ 2$

For 3 in. pipe, 10 ft long: L = 120 in. $\frac{M_d}{F_d} = 25{,}200$

For 3 in. pipe, 5 ft long: L = 60 in. $\frac{M_d}{F_d} = 6300$

For 2 in. pipe, 5 ft long: L = 60 in. $\frac{M_d}{F_d} = 4150$

For 2 in. pipe, 3 ft long: $L = 36$ in. $\frac{M_d}{F_d} = 1540$

If $M_d = M_o$ then $F_d = \frac{M_o}{1/2\, d_1\, L^2}$

Therefore: for 3 in. pipe, 10 ft long $F_d \geq \frac{54,000}{25,200} = 2.14$ psi

for 3 in. pipe, 5 ft long $F_d \geq \frac{54,000}{6,300} = 8.56$ psi

for 2 in. pipe, 5 ft long $F_d \geq \frac{17,680}{4,150} = 4.25$ psi

for 2 in. pipe, 3 ft long $F_d \geq \frac{17,680}{1,540} = 11.25$ psi

But the 3 in. pipe, 10 ft long, was bent and
the 2 in. pipe, 5 ft long, was bent — Hence: $F_d > 4.25$ psi

The 3 in. pipe, 5 ft long, was not bent and
2 in. pipe, 3 ft long, was not bent — Hence: $F_d < 8.56$ psi

If $C_d = 0.5$ as it is approximately for circular cylinder

Then 17.1 psi $> Q >$ 8.5 psi where $Q = 1/2\ \rho u^2$

at $d = 3435$ ft horizontal distance, location of organ pipes
$P_s = 9.5$ psi measured
$q = 2.43$ computed

Suppose $Q = 9$ psi

Then $\frac{Q}{q} = \frac{9}{2.43} = 3.7$ times the computed drag.

The drag coefficient used in the above calculations is more satisfactory for dust free air than for dust laden air, in which case the value of drag coefficient could approach unity. In using the value unity, the dynamic pressure Q is:

$$8.56 \text{ psi} > Q > 4.25 \text{ psi}$$

The predicted overpressure at $d = 3435$ ft based on the ideal curve scaled to test altitude ($P_o = 11.91$ psi) is 14.65 psi. The dynamic pressure computed for an overpressure of 14.65 psi is 5.5 psi which is within the order of magnitude of the dynamic pressure calculated above.

Tabulated below is a comparison of measured overpressures and dynamic pressures computed from actual measured overpressures of Shot 10 with those of the so-called ideal curve at corresponding distances. Damage is also indicated for 1/4 ton trucks. The overpressure and dynamic pressure of the ideal curve have been corrected to an atmospheric condition of 12.80 psi corresponding to the test altitude.

Item	Dist (Ft)	Measured P-D Curve		Ideal P-D Curve		Damage	
		P_s	P_d	P_s	P_d	Degree	Echelon of Maintenance
1/4 ton truck	1600	12.0	3.65	26.5	14.8	Severe	Salvage
1/4 ton truck	1920	9.3	2.15	18.8	8.3	Severe	Salvage
1/4 ton truck	2415	8.5	1.82	11.7	3.3	Severe	Depot
1/4 ton truck	2770	7.8	1.62	8.8	1.97	Light-Moderate	Organ.

From the above table, for a change of dynamic pressure of 0.33 psi, computed from measured P-D curve, damage varied from a completely dismembered vehicle to one which remained intact. For this large variation of damage it appears that the change in dynamic pressure is too small and it is more reasonable that a change of dynamic pressure of 5 psi corresponding to the ideal curve would be required to cause the large variation of effect.

The measured pressure-distance curve of Shot 9 corresponds favorably with pressures of an ideal curve and the measured pressure-distance curve of Shot 10 indicates a close relationship at very high overpressures and at pressures less than 8 psi with pressures of an ideal curve. The measured pressures between 10 and 30 psi of Shot 10 are less by approximately 45 to 100 per cent than the pressures of the ideal curve. It is within this region that the damage as a function of the measured pressures exceed the expected damage. As stated previously, the resulting damage to vehicles on Shot 9 was predicted to a fair degree of accuracy using the BRL method. It is shown in section 5.3 that the BRL method predicted the lethal radius of damage to vehicles in Shot 10 to a fair degree of accuracy when pressure values of the ideal curve are used. A direct comparison of damage on Shot 9 with that of Shot 10 can only be made at pressures (corresponding to an ideal curve) less than 10 psi and at these pressure levels, damage to vehicles on both shots was similar. No comparison can be made at higher pressure levels since on Shot 9, above 10.6 psi, equipment was placed in the regular reflection region and the resulting force causing damage within this region differs from the resulting force causing damage withi the mach region at corresponding pressure levels.

The foregoing discussions suggest, therefore, that in spite of the lowering of pressures the damage was equivalent to that expected from dynamic pressures expected from overpressures of the ideal curve.

5.2 STATISTICAL ESTIMATION OF DAMAGE

Since the results of Shots 9 and 10 have indicated wide discrepancies in damage as a function of measured overpressure, a resurvey was made of all exposure tests whereby damage was correlated with dynamic pressures. The survey included the equipment exposure results of Shots 9 and 10 as well as those of the Desert Rock[19] exposures.

Accurate values of the dynamic pressure acting on each target were desirable for the correlation with damage. However, the values derived for each target cannot be considered very accurate due to the uncertainties in the measured dynamic pressures and actual flow conditions. For

most shots the theoretical limit of regular reflection was assumed in order to ascertain whether item was placed in the regular reflection region or the Mach region.

Measurements of dynamic pressure on Shot 9 indicated no major deviations from the values expected. Therefore in the Mach region of Shot 9 the actual measured overpressures were used to calculate the dynamic pressures (using atmospheric pressure at ground level) by means of the following relation:

$$P_d = \frac{2.5\ Ps^2}{Ps + 7\ Po} \qquad (5.1)$$

The horizontal component of dynamic pressures within the regular reflection region of Shot 9 were obtained from theoretical calculations available at BRL. These calculations were based on procedures described in references 20 and 21 for the treatment of the reflection of plane shocks. For the particular height of burst a plane wave of overpressure corresponding to the free air TNT overpressure curve was assumed incident at each point along the ground plane, and the quantities of interest were calculated. The resulting curve for dynamic pressure in the regular reflection region terminated at a point about 10 per cent higher than the dynamic pressure curve computed for the Mach region. Since some lowering of the theoretical values from imperfect reflection seemed reasonable, the complete curve in the regular reflection region was lowered 10 per cent to match into the Mach region curve. The resulting curve for dynamic pressure is shown in Fig. 5.2.

Apparently the Mach stem on Shot 9 formed early. However, the exact nature of the flow during this early formation period seems uncertain. Figures 5.23 and 5.24 display the theoretical dynamic pressure on Shot 9, the height of the Mach stem, and the displacements for the 1/4 ton truck and the 2 1/2 ton truck in the several orientations plotted versus ground range. The displacements of the vehicles generally continue to increase through the region where the Mach stem is eight feet high, and then level off and decrease to low values as ground zero is approached. However, at a Mach stem height of 4 ft where the displacements reach a maximum, the displacements are considerably less than what they should be for a Mach pressure equivalent to that overpressure experienced at that range. At a range of 875 ft and a computed dynamic pressure of 1.0 psi the displacements were essentially equivalent to those obtained at about 1.0 psi dynamic pressure in the Mach region. Because of the uncertainty concerning the actual flow at vehicle level the computed curve shown in Fig. 5.2 was used for the analysis, providing a consistent use of ideal or near ideal curves in the analysis.

Since the applicability of the theoretical relations concerning dynamic pressure to Shot 10 was questionable, an ideal pressure-distance curve was constructed as indicated in Section 5.1. The dynamic pressures for Shot 10 were computed from this curve using Equation 5.1, and the resulting curve is shown in Fig. 5.2.

The values of peak dynamic pressures were obtained from Porzel's curves[14] except the JANGLE underground shot, for which the curves do not apply, and for TUMBLER Shot 3, which is off the chart. These theoretical curves, shown in Fig. 5.3, were considered the best available at the

time of the analysis. The 2 psi and 1.5 psi iso-pressure curves were constructed by Sandia Corporation (reference 18). The values of dynamic pressure for the JANGLE underground shot and TUMBLER Shot 3 were calculated using Equation 5.1 applied to the overpressure curves of each of the two shots. In many cases there was considerable uncertainty as to the position of the Desert Rock Targets, which increased the possible errors in pressures assigned.

To each observation of damage two classifications for damage were assigned. That is, (1) damaged items were classified in terms of echelon of maintenance and time to restore to combat use, and (2) damaged items were classified in terms of light, moderate, and severe damage according to the procedure indicated in Section 2.2.

In the statistical analysis of the data, both classifications of damage were considered as a function of dynamic pressure. In addition, the analysis included organizational maintenance (6 hours and zero hours) as a function of measured overpressures. The results of the analysis are shown in Tables 5.1 and 5.2. The values of the estimated parameters of the normal distribution are for random orientation. It is pointed out that in some cases the nature of the data was such that the estimates for standard deviation σ could not be computed. This implies that if further sampling was to be effected for these cases, the probability of damage would indicate a region of sharp demarcation for that specific category of damage.

The probability of damage curves for light, moderate, and severe damage for various items as a function of dynamic pressure are shown in Figs. 5.4, 5.5, 5.6 and 5.7. In these figures, the probability for moderate damage was obtained from the following relationship:

$$P(r)\ (M) = 1 - P(r)\ (S) - P(r)\ (L)$$

where:

$P(r)\ (S)$ = Probability for severe damage

$P(r)\ (L)$ = Probability for light damage

In Figs. 5.3 and 5.4, a contradiction might seem to arise from the straight line drawn indicating the zero to 100 per cent probability for light damage. However, it is within this region that the standard deviation σ could not be computed and if more samples were available within this region the curve for damage would take the shape of a steep rising curve, which would indicate a region of sharp demarcation between light and moderate damage. The probability curve Fig. 5.3 is for all tanks (light and medium) considered collectively. In the observations of results, there was no apparent differences in damage to light tanks or medium tanks.

The additional curves of Figs. 5.8 through 5.12 indicate the proportion of the various items that will not be combat usable as a result of organizational maintenance (6 hours after exposure) and immediately after exposure (zero hours) as a function of dynamic pressure. Only those curves were plotted where the standard deviations were computed. The proportion of items that will not be combat usable as a function of measured overpressure were not plotted. This analysis was conducted for future reference.

The Height of Burst iso-damage curves shown in Figs. 5.13, 5.14, 5.15, and 5.16 have been constructed using the information obtained from the probability of light, moderate, and severe curves and Porzel's Height of Burst curves (Fig 5.3) for dynamic pressure. For lack of data, each of the iso-damage curves was extended arbitrarily to the axis of the Height of Burst from approximately 300 ft horizontal distance. In these curves, the value μ indicates the mean value of dynamic pressure for light and severe damage. Care must be taken in the interpretation of the maximum probability for moderate damage curve. The maximum probability for moderate damage is the peak of the moderate curves indicated in Figs. 5.4 through 5.7.

It is pointed out again, that the results only suggest that the significant parameter to be associated with damage is the dynamic pressure of the experimental TNT curve or the ideal curve.

5.3 BRL PREDICTION METHOD FOR DAMAGE

The predicted effects of Shot 9 compared favorably with damage to vehicles in side-on orientation but did not compare with damage to vehicles in face-on orientation. Nearly all of the vehicles in face-on orientation were immediately combat usable. The tabulation below presents the predicted lethal radius and distances from ground zero where damage was noted to be moderate and light to vehicles in side-on orientation.

Item	Predicted L.R. for Moderate or 60% C.E. (ft)	Dist. from G.Z. Moderate Damage (ft)	Distance from G.Z for Light Damage (ft)
1/4 Ton Truck	2970	2480	3060
2-1/2 Ton Truck	3230	2480	2860

A tabulation is also made of the results of Shot 10 and compared with the predicted effects for severe damage (10% C.E.) using values from Fig. 7 of TM 23-200 as well as the predicted effects using values from an ideal curve (TNT, P_s vs D). These include side-on orientation only.

Item	Predicted L.R. (TM 23-200) Severe Damage (ft)	Predicted L.R. Ideal Curve Severe Damage (ft)	Dist from G.Z. Severe Damage (ft)	Dist from G.Z. Moderate Damage (ft)
1/4 Ton Truck	1420	1620	1920	2415
2-1/2 Ton Truck	1430	1690	1920	2415
Medium Tank	880	1090	1045	1415
Gun, 57 mm	810	920	1415	2140

The results of Shot 10, except for the 57 mm guns are approximately within 15 per cent of the predicted effects based on the ideal curve.

The large discrepancy noted between the predicted effects and resulting damage to guns is not surprising since the information about this particular type of equipment from prior exposures was limited to a greater extent than the information about vehicles or tanks.

5.4 THE ARF PREDICTION METHOD

As indicated originally the development of the ARF method for predicting the response of free targets was based on the assumption that a satisfactory correlation of the response parameters and the resulting damage could be found. At this time the statistical correlation of the various response parameters such as the displacement with the damage obtained on the test has not been completed, and the response data have been only partially reduced. Therefore, no conclusive statement can be made at this time concerning the basic assumption on which the ARF method was based, and the discussion of the success of the prediction of the response parameters must be limited. It is anticipated that a satisfactory correlation of some parameter will be realized.

Since the predictions obtained by application of the ARF method are derived from the predicted pressure-time curves, the success of the predictions for a given target will depend upon the success in predicting the pressure-time curve for that target. The pressure-distance curve predicted and the pressure-distance curve measured for Shot 9 with respect to actual ground zero are the same within the limits of error, and the predicted pressure-time curve for the measured overpressure at a given target was used for comparison of the data.

The comparison of the angular displacements as obtained from photography and the displacements calculated assuming rotation only are shown for the 1/4 ton truck in Fig. 5.17 and for the 2-1/2 ton truck in Fig. 5.18. The calculated displacements are shown by the dotted curves, and the data obtained from the films are shown by the heavy lines. The displacement of the 1/4 ton truck on Shot 9 evidently follows the predicted curves closely. However, sliding occurred at both 7.4 psi and 4.4 psi on Shot 9, and therefore the displacement measured should be less than that which would have been measured if no sliding had occurred. The vehicle at 3.21k on Shot 10, was prevented from sliding by an obstruction and experienced greater displacement at 4.0 psi than was realized at 4.4 psi on Shot 9. Thus the ARF method as applied underestimated the angular displacement of the 1/4 ton truck that would have occurred for rotation only.

The angular displacements shown in Fig. 5.18 for the 2-1/2 ton truck on Shot 9 were found to be about twice as great as the values predicted for a given time. In addition, sliding occurred at both stations photographed on Shot 9, and hence for rotation only the actual displacement recorded should have been larger. The curve resulting for the 2-1/2 ton truck at 3.21k on Shot 10 is not extremely different from the curve for 4.4 psi on Shot 9, although the curve for Shot 9 should be higher than that for Shot 10, because of the higher pressure, and the longer duration. The ARF method as applied underestimated the angular displacement of the 2-1/2 ton truck placed side-on on Shot 9 and Shot 10 for the stations photographed.

The values for the displacement of the center of gravity of the 1/4 ton truck face-on, shown in Fig. 5.19, are scattered about the curve calculated for a coefficient of friction of 1.0. However, the value of the coefficient of friction estimated for sliding face-on based on tests in Nevada and at the Aberdeen Proving Ground was 0.32. The predicted displacements based on this value, then, are considerably higher than those displacements actually obtained. The face-on orientations in the range listed apparently experienced little rotation, and hence the conditions for which the calculations were made should have been approached closely. The curve for the measured displacements is similar to those calculated but corresponds to an improper value for the coefficient of friction.

The 1/4 ton trucks and 2-1/2 ton trucks side-on whose displacements are shown in Fig. 5.20 and Fig. 5.22 all rotated to some degree, and hence any sliding that occurred can be considered less than that which would have occurred had no rotation taken place. The vehicles represented by the three upper points in each figure overturned. Since in performing such large angular displacements a greater area was exposed to the air flow, the displacements resulting may be still further increased above that obtained for sliding only. Considering the increased area exposed in the higher displacements and the variation to be expected in μ, the side-on sliding for the 1/4 ton truck and the 2-1/2 ton truck agrees fairly well with that predicted. Percentagewise the agreement is poor, since the variation in the total displacement with the coefficient of friction is large.

The displacements of the center of gravity of the 2-1/2 ton truck face-on are shown in Fig. 5.21. These displacements apparently occurred under conditions approaching those for which the calculations were made, i.e., no rotation. The points lie closest to the curve for $\mu = 0.25$. Since the appropriate value of μ for this case was $\mu = 0.4$, the prediction calculations underestimate the actual displacement occurring.

To summarize: For Shot 9 the vehicles side-on experienced angular displacements exceeding at a given time those calculated by the ARF method by 100 per cent or more at those stations photographed.

For the vehicles side-on on Shot 9 the linear sliding displacements were found to be about as expected when possible variations in μ and the increased displacements for large angular displacements were considered.

For the vehicles face-on on Shot 9 the results were conflicting. The calculations for the 1/4 ton truck overestimated the displacements resulting and the calculations for the 2-1/2 ton truck underestimated the displacements resulting by amounts greater than would be expected for a normal variation in μ.

For Shot 10 the only orientation employed for which data were obtained was the side-on. The displacements at the two positions furthest from ground zero were comparable to those obtained on Shot 9. At all stations the angular displacements were in excess of those on Shot 9 and hence exceeded the calculated values even more. The linear displacements obtained on Shot 10 were much greater than any obtained on Shot 9.

Figures 5.25 and 5.26 present the displacements of the centers of gravity of the 1/4 ton truck and the 2-1/2 ton truck side-on on Shot 9 and Shot 10 plotted versus overpressure. The calculated displacements assuming sliding only are given by the curves for various assumed values of the coefficient of friction μ. The decline in displacements on Shot 9 for pressure occurring in the regular reflection region is evident. The displacements for Shot 10 plotted against measured overpressure depart extremely from the calculated curves. However, if the displacements are plotted at those pressure levels that would have occurred at each station in the absence of disturbing effects the results are more comparable to the calculated values and the values obtained in the Mach region on Shot 9.

TABLE 5.1 - Parameters of the Normal Distribution for Probability of Light and Severe Damage as a Function of Dynamic Pressure

Item	Damage	Mean μ	Std. Dev. σ
1/4 Ton Truck	Light	2.1	0.64
	Severe	3.63	1.10
2-1/2 Ton Truck	Light	2.02	0.98
	Severe	6.75	2.72
Tanks	Light	$10.8 < \mu < 14$	No overlap
	Severe	50.2	18.5
57 mm Gun	Light	4.9	Trivial overlap
	Severe	23.4	10.5

TABLE 5.2 - Parameters of the Normal Distribution for Probability of Organizational Maintenance (6 hours and 0 hours) as a function of Overpressure and Dynamic Pressure

Item		Time (hrs)	Mean μ	Std. Dev. σ
1/4 Ton Truck	P_s	6	19.5	8.4
	"	0	10.8	7.2
	P_d	6	9.1	4.85
	"	0	2.1	1.7
2-1/2 Ton Truck	P_s	6	22.8	10.6
	"	0	10.2	10.5
	P_d	6	$2.75 < \mu < 3.20$	No overlap
	"	0	1.7	0.94
Tanks	P_s	6	42.4	29.8
	"	0	14.7	4.7
	P_d	6	29.9	19.2
	"	0	9.41	4.1
57 mm Gun	P_s	6	16.8	4.9
	"	0	13.0	7.8
	P_d	6	$4.9 < \mu < 18.5$	No overlap
	"	0	$2.0 < \mu < 2.6$	No overlap

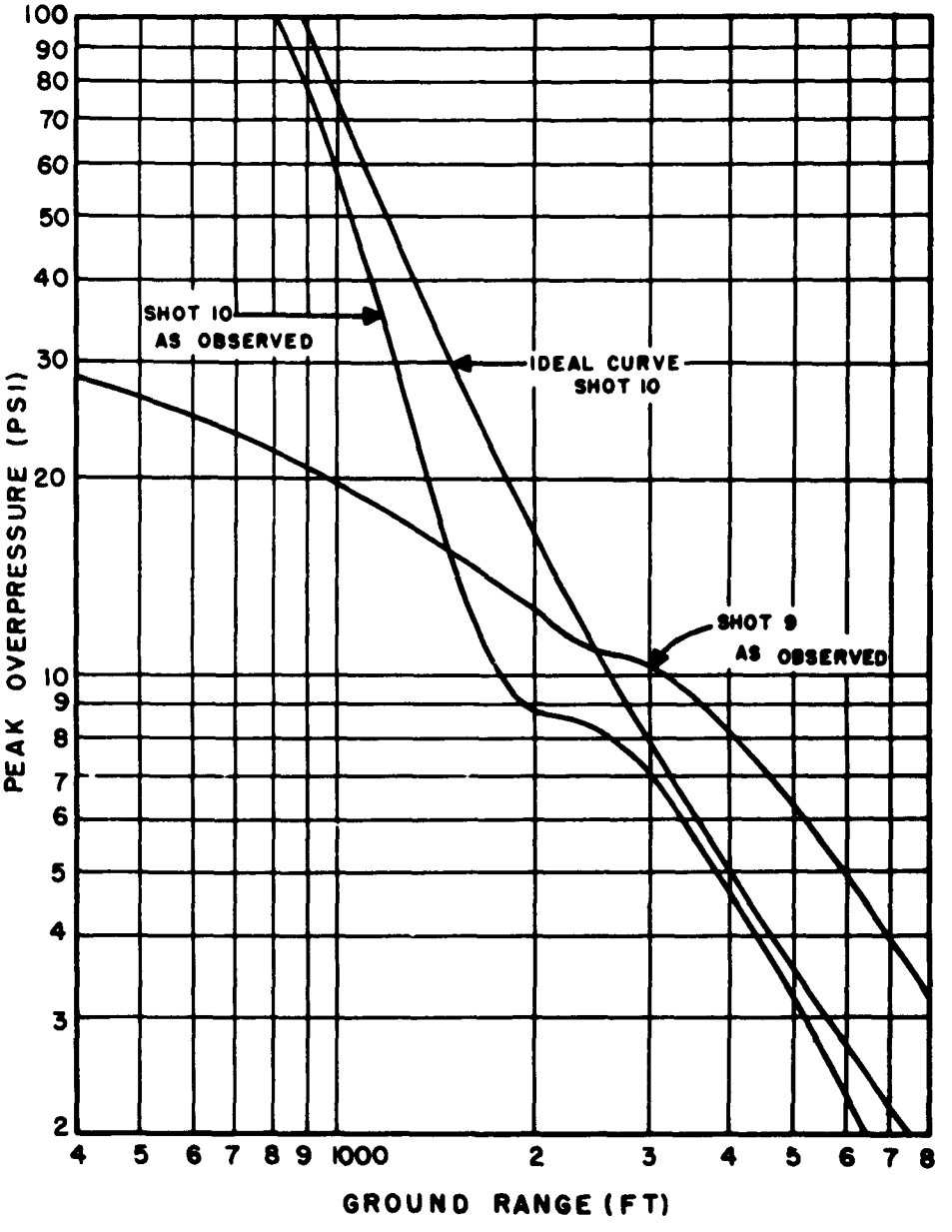

Fig. 5.1 Ground Level Overpressure vs Ground Range for Shots 9 and 10 (As Observed and Ideal Curves)

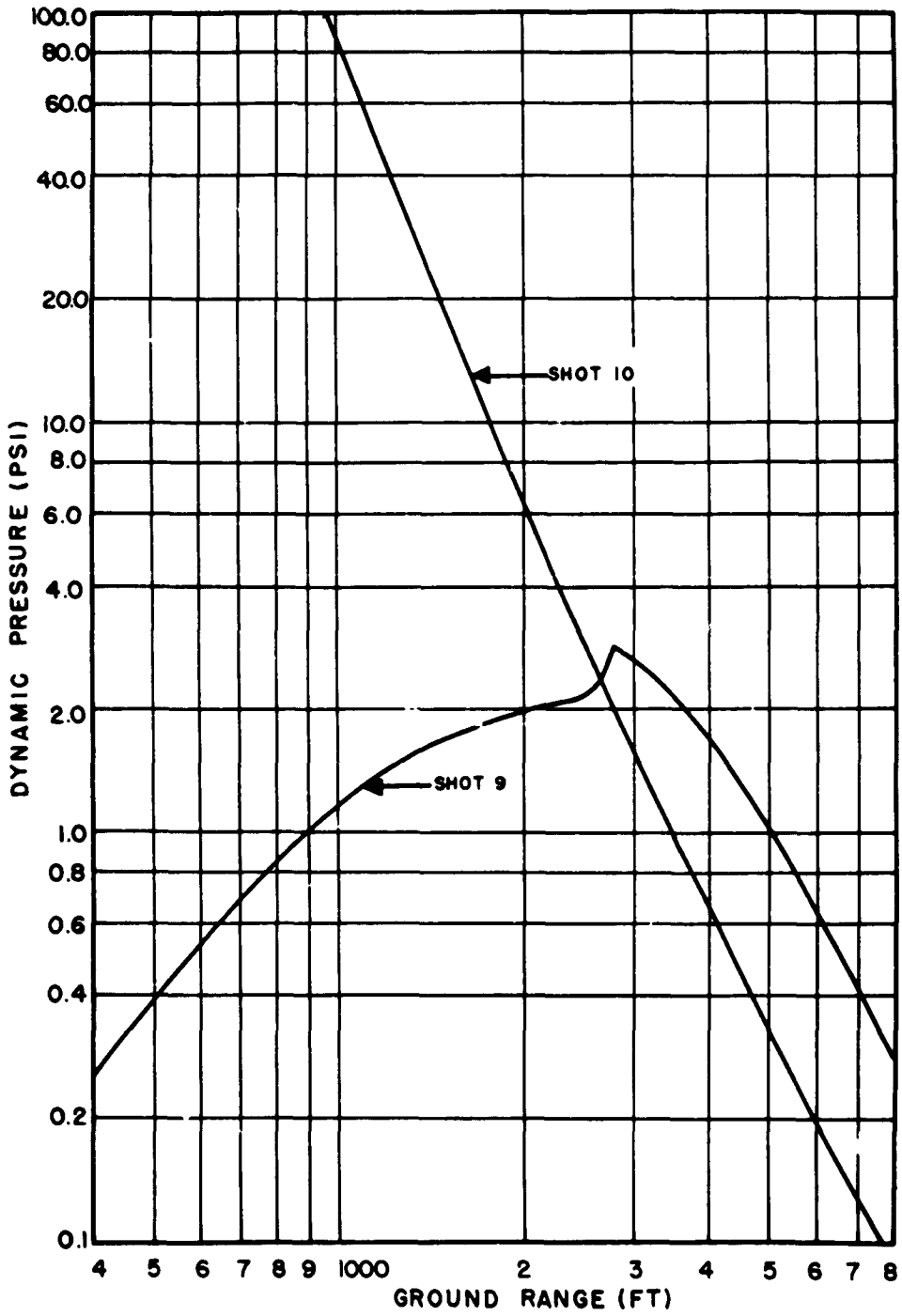

Fig. 5.2 Dynamic Pressure for Shots 9 and 10 Calculated from Ideal Curves and as Measured Overpressures

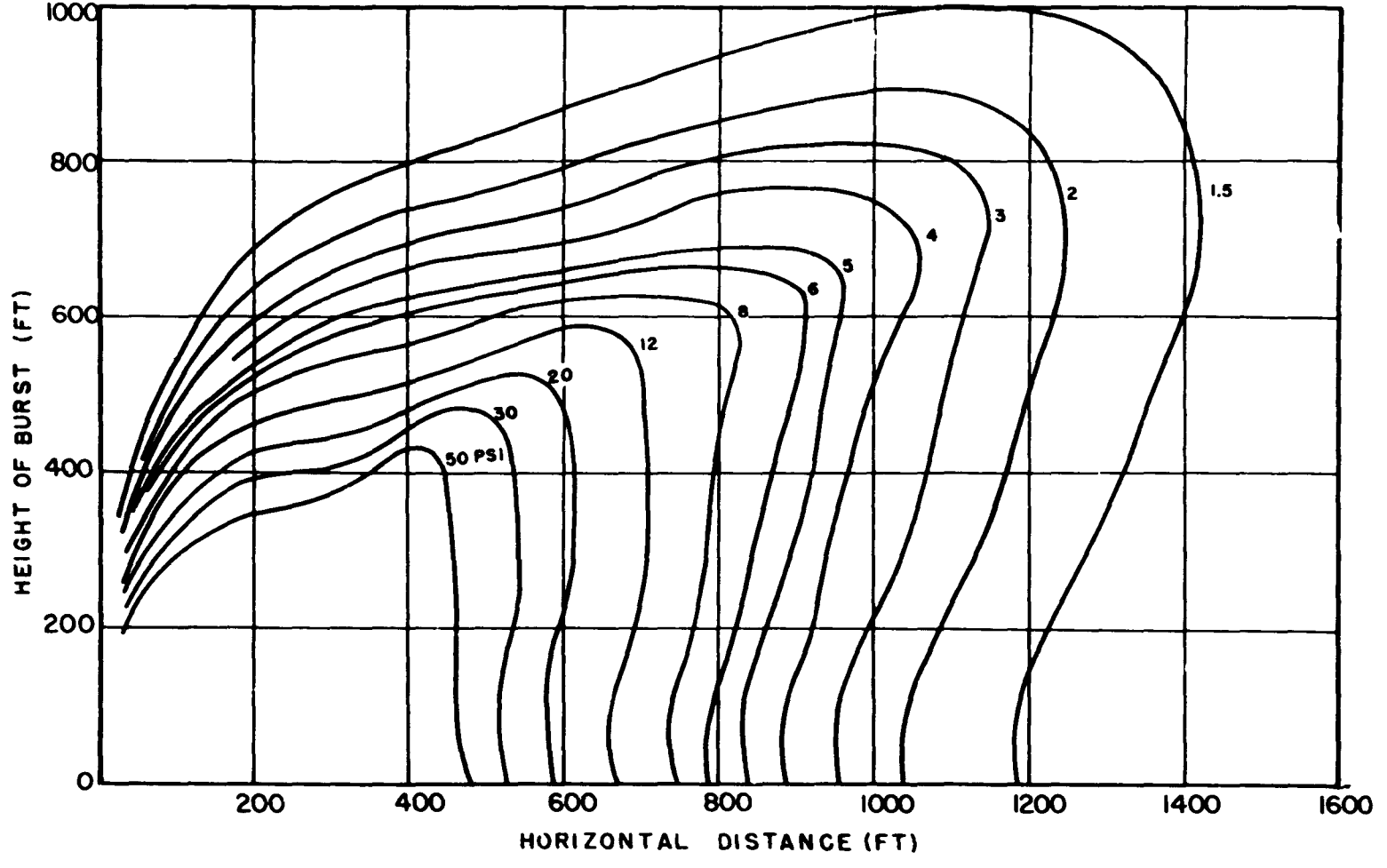

Fig. 5.3 Height of Burst vs Horizontal Distance for Dynamic Pressure (Porzel) - (Scaled to 1 KT at Sea Level)

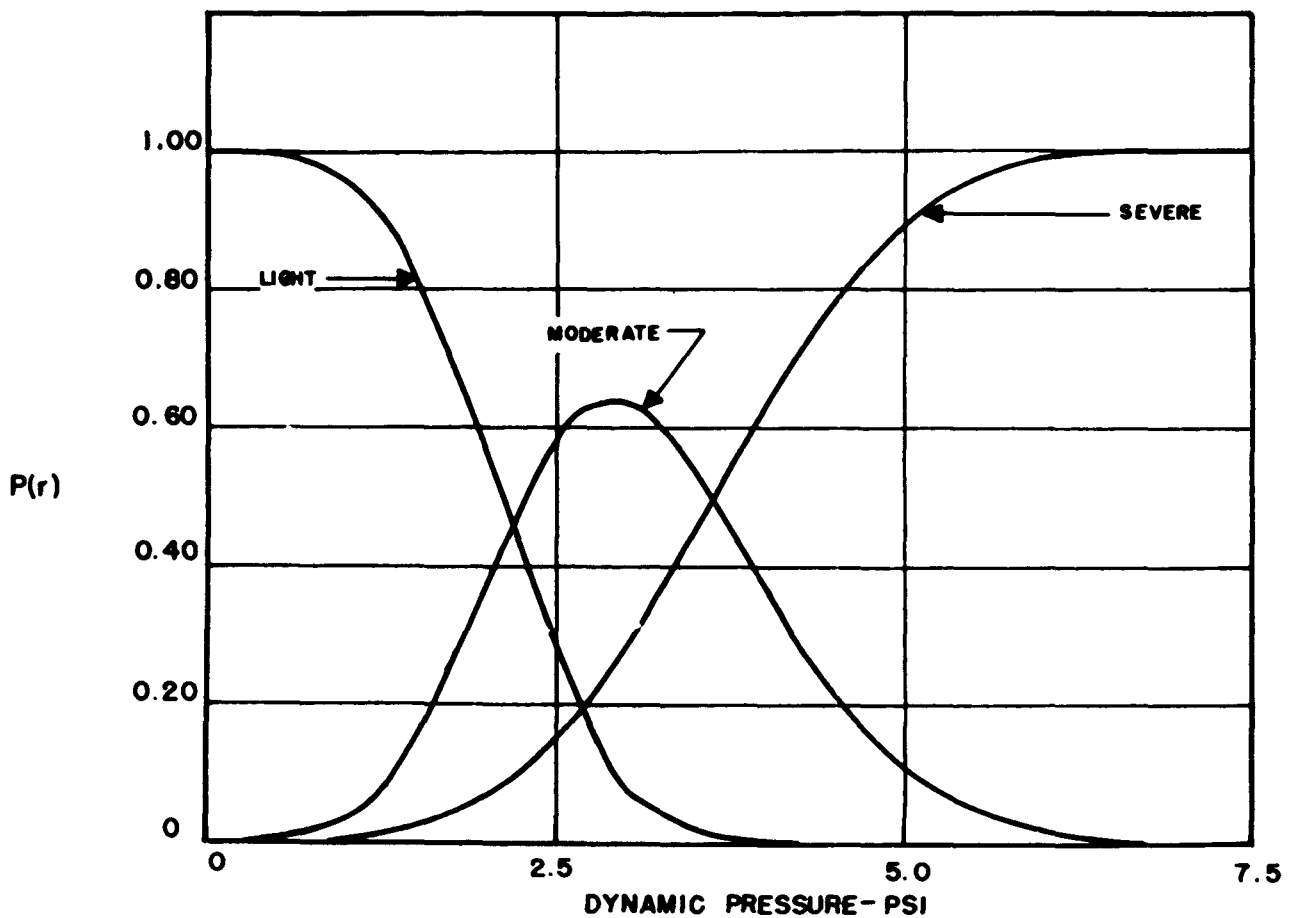

Fig. 5.4 Probability of Damage For 1/4 Ton Trucks vs Dynamic Pressure

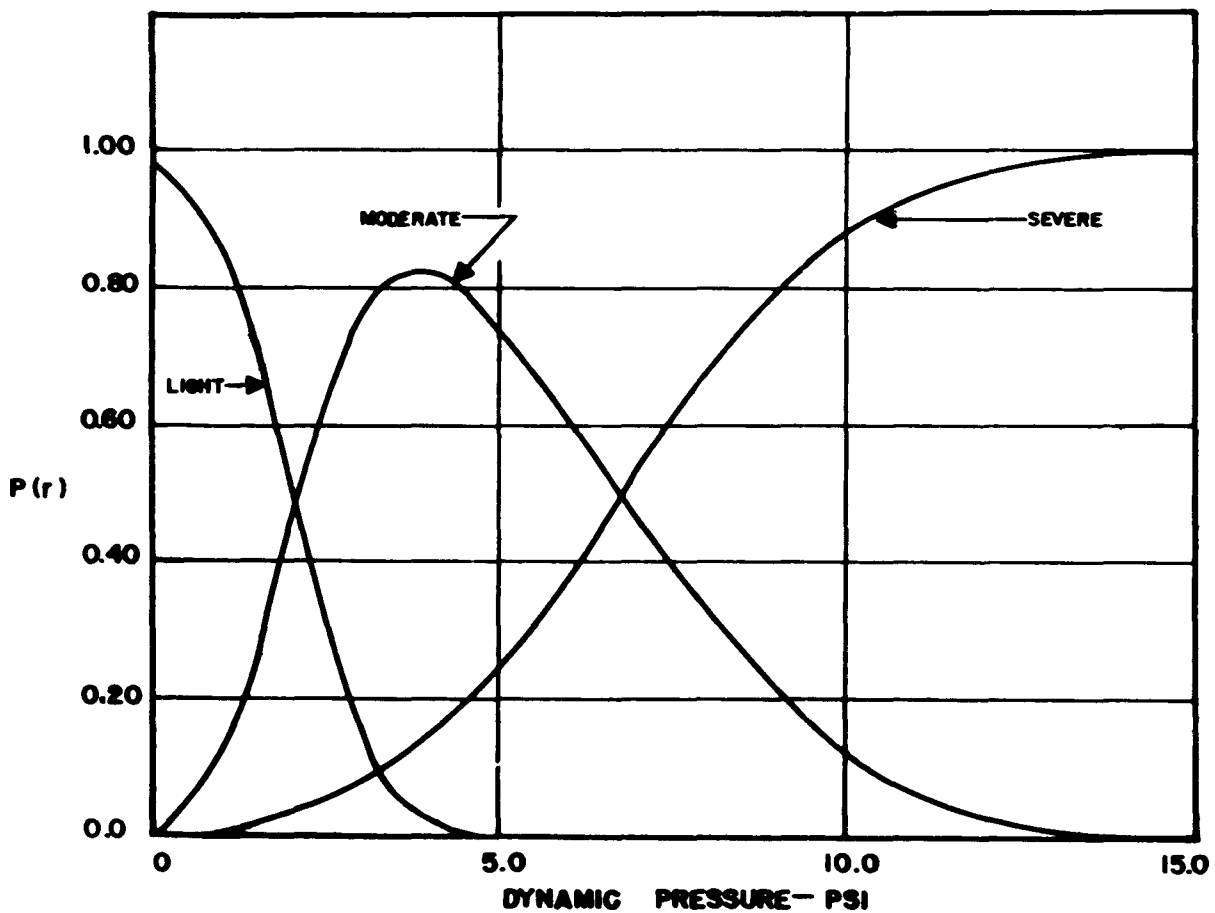

Fig. 5.5 Probability of Damage for 2-1/2 Ton Truck vs Dynamic Pressure

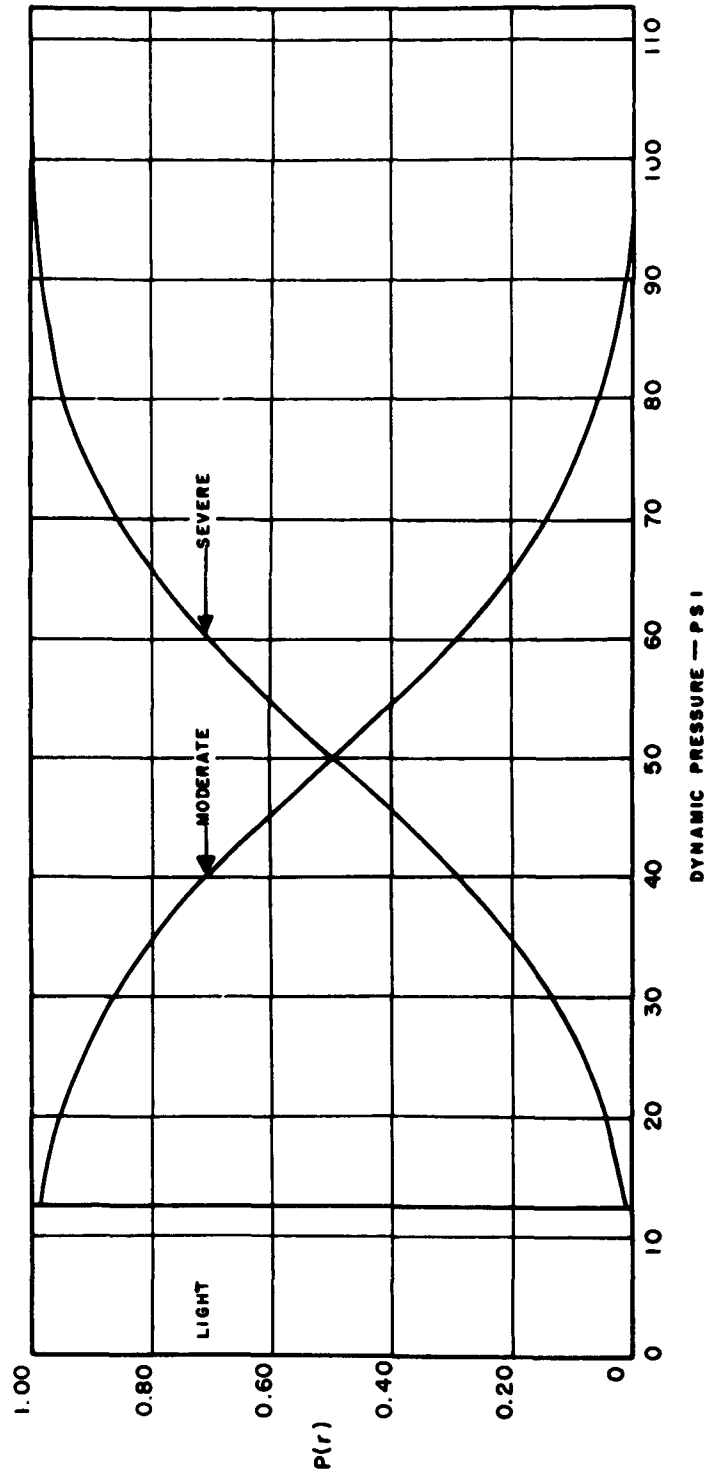

Fig. 5.6 Probability of Damage for Tanks vs Dynamic Pressure

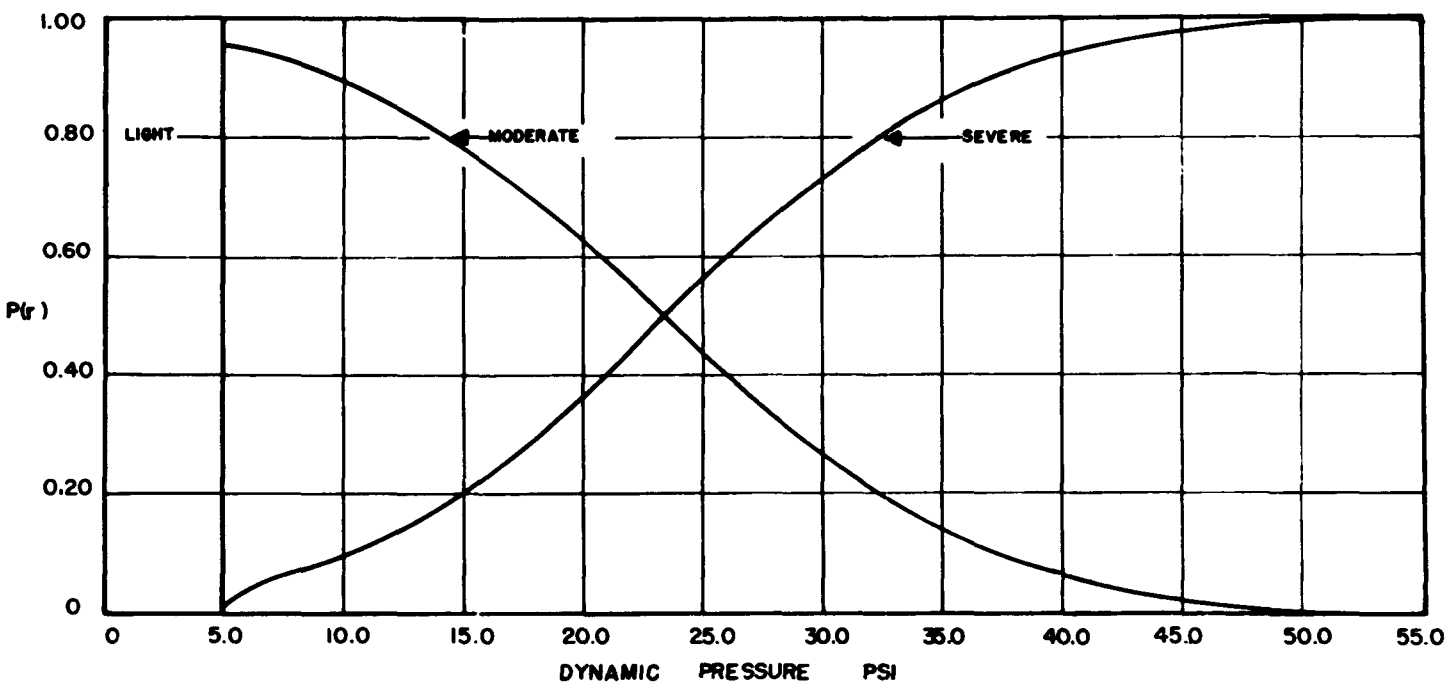

Fig. 5.7 Probability of Damage for 57 mm Guns vs Dynamic Pressure

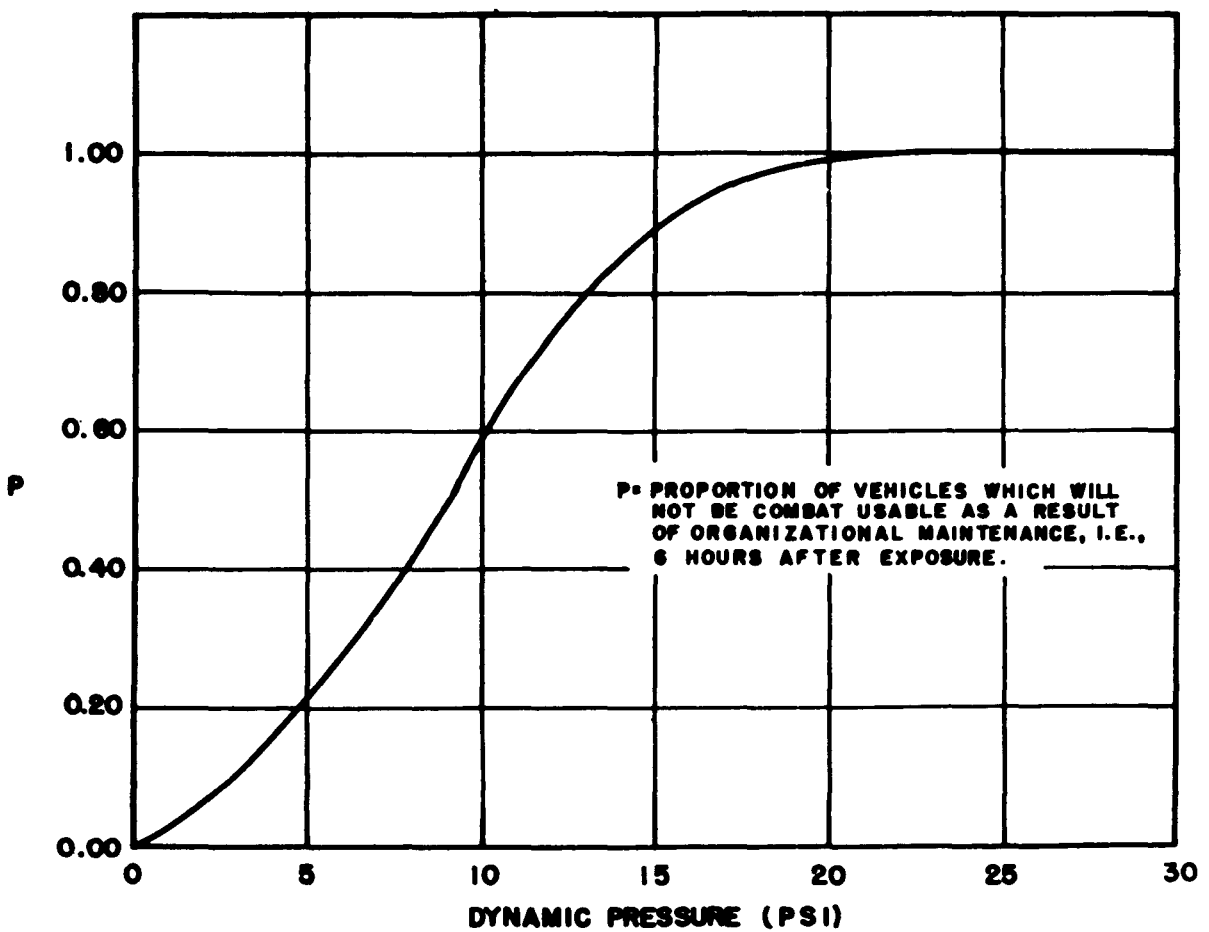

Fig. 5.8 Probability of Damage vs Dynamic Pressure (1/4 Ton Truck) (6 Hours)

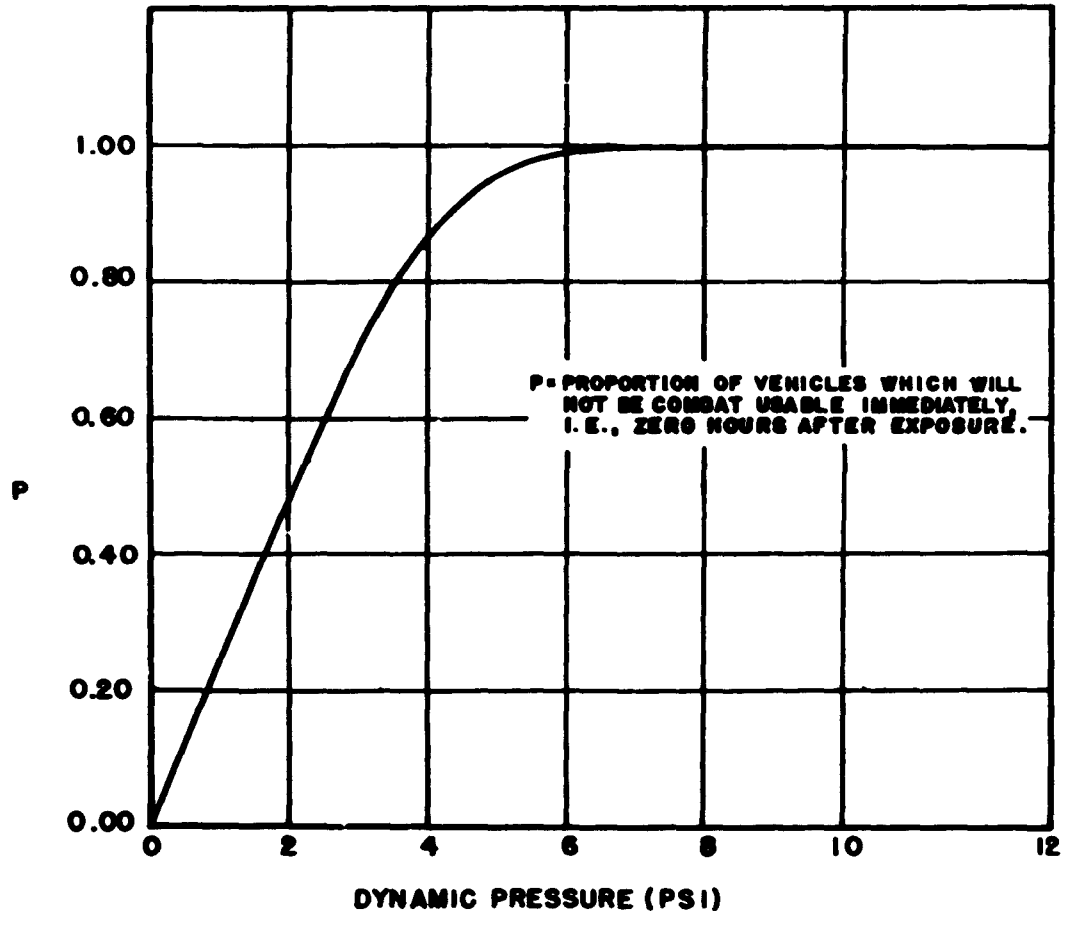

Fig. 5.9 Probability of Damage vs Dynamic Pressure (1/4 Ton Truck) (0 Hours)

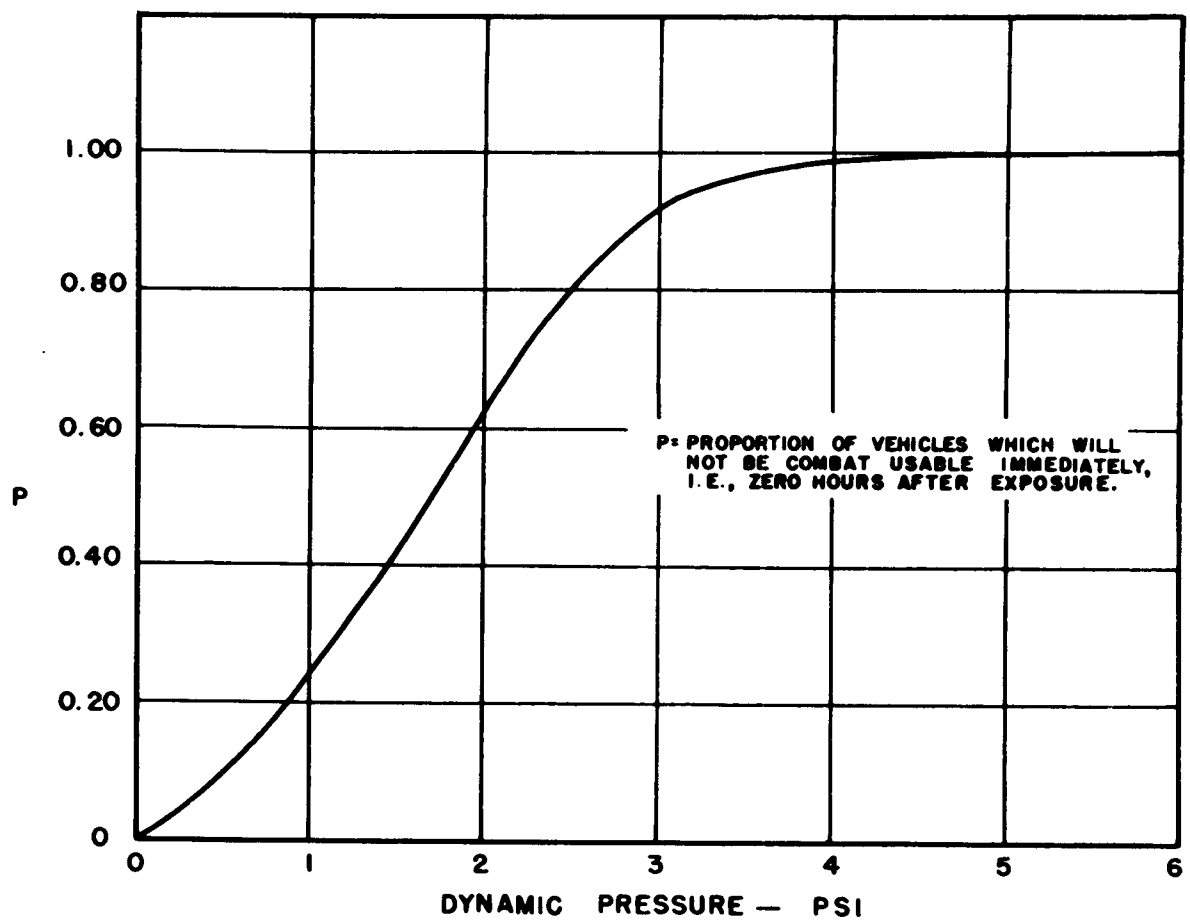

Fig. 5.10 Probability of Damage vs Dynamic Pressure 2-1/2 Ton Truck (0 Hours)

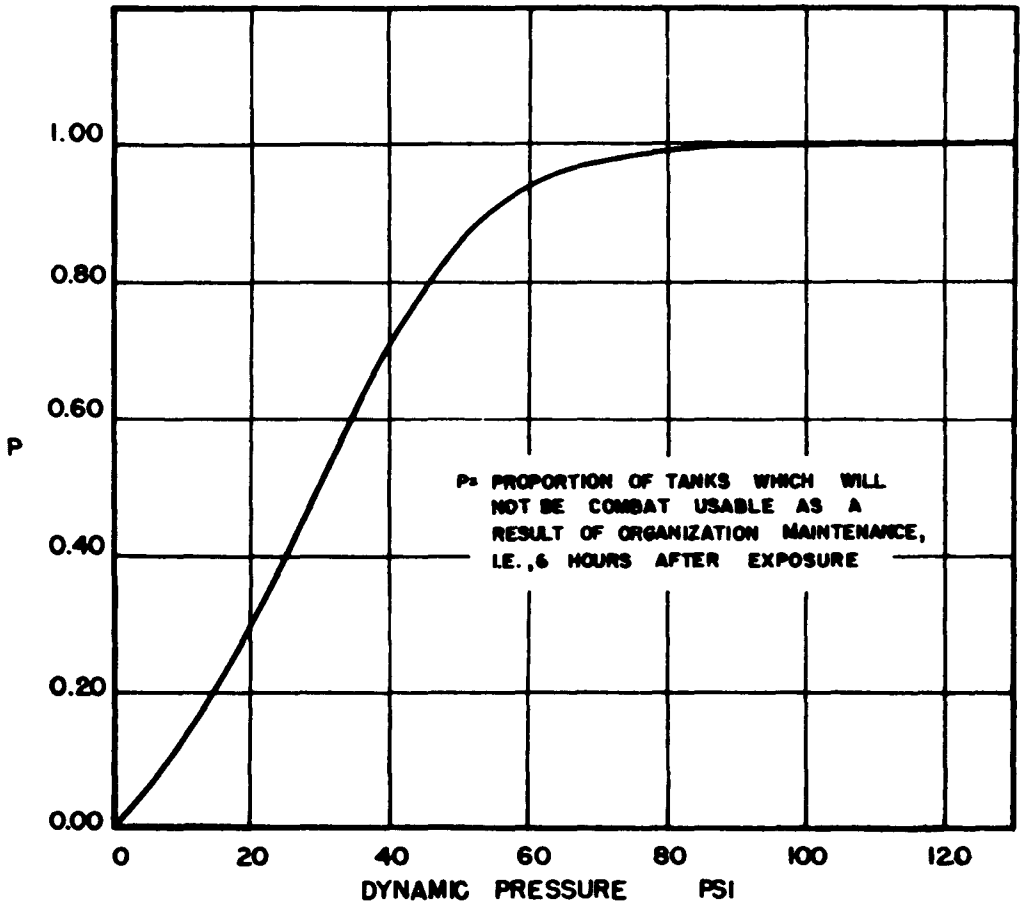

Fig. 5.11 Probability of Damage vs Dynamic Pressure Tanks (6 Hours)

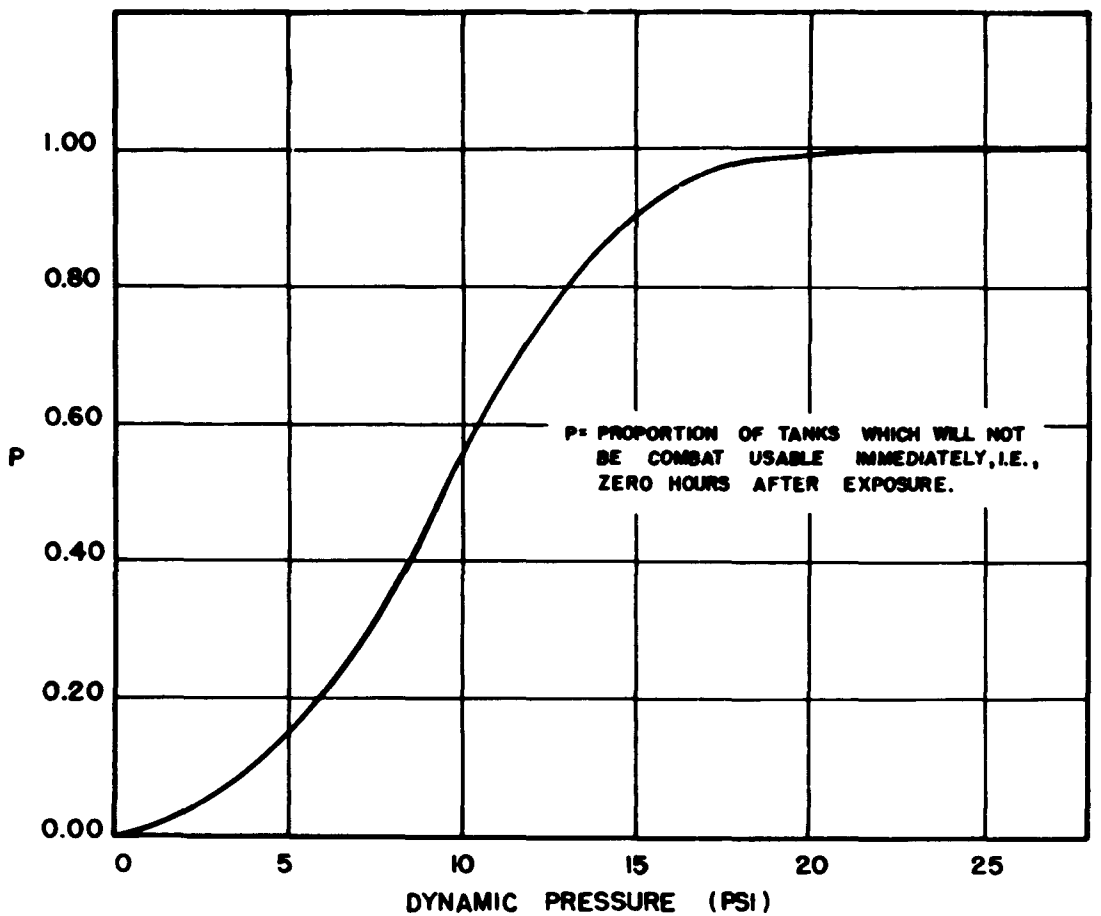

Fig. 5.12 Probability of Damage vs Dynamic Pressure (Tanks) (0 Hours)

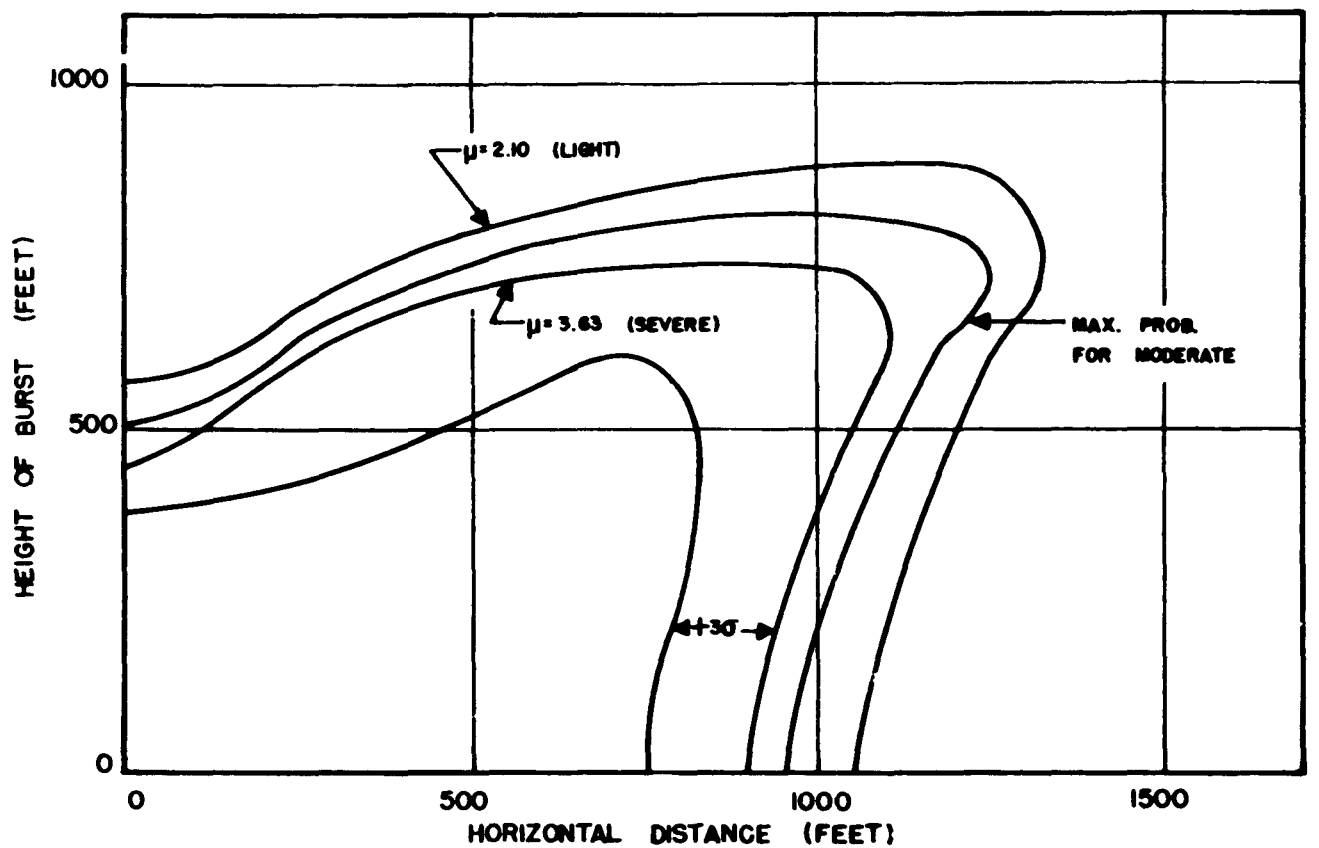

Fig. 5.13 Height of Burst vs Distance from Ground Zero for Various Damage to 1/4 Ton Trucks (Scaled to 1 KT Sea Level)

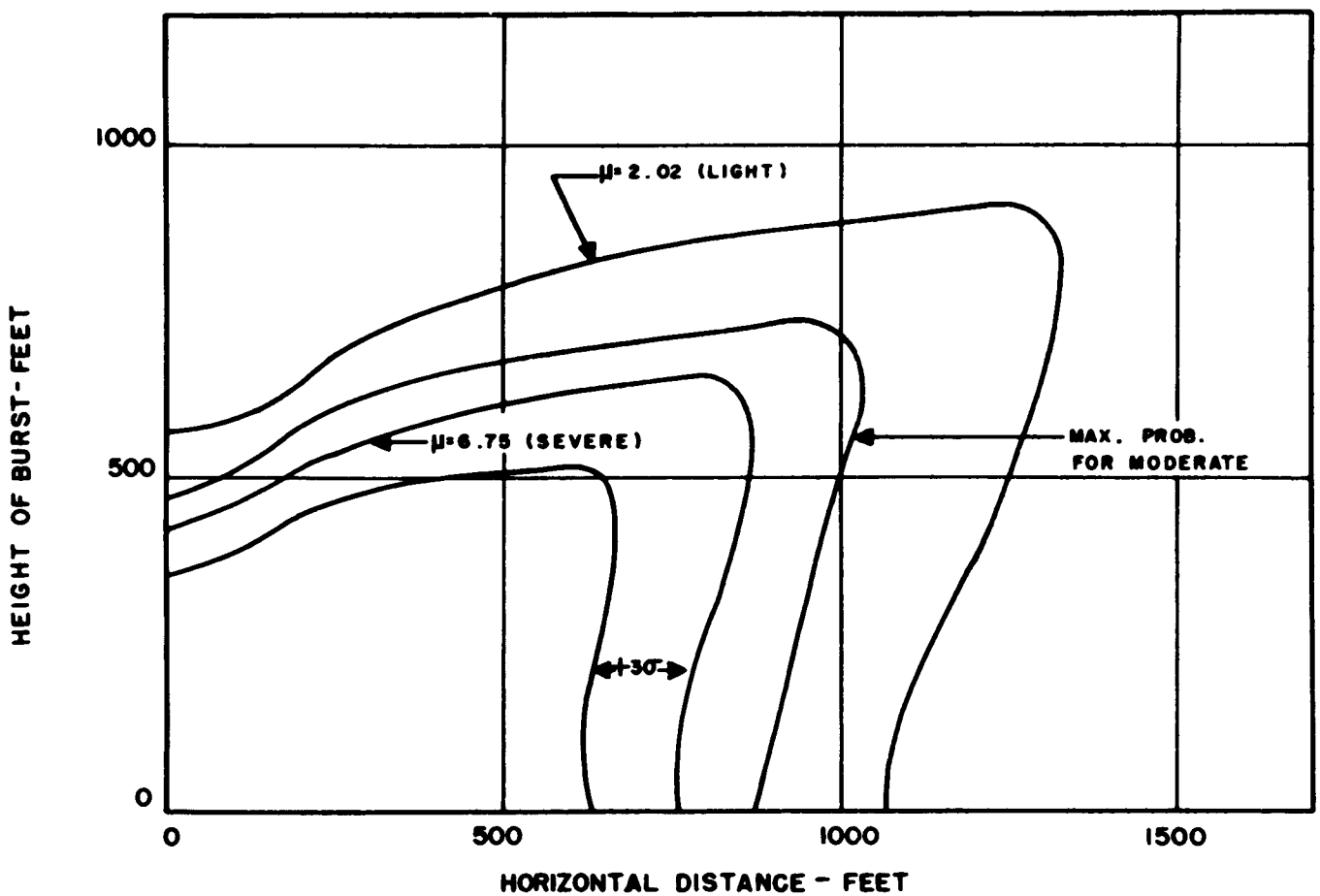

Fig. 5.14 Height of Burst vs Distance From Ground Zero For Various Damage to 2-1/2 Ton Trucks (Scaled to 1 KT Sea Level)

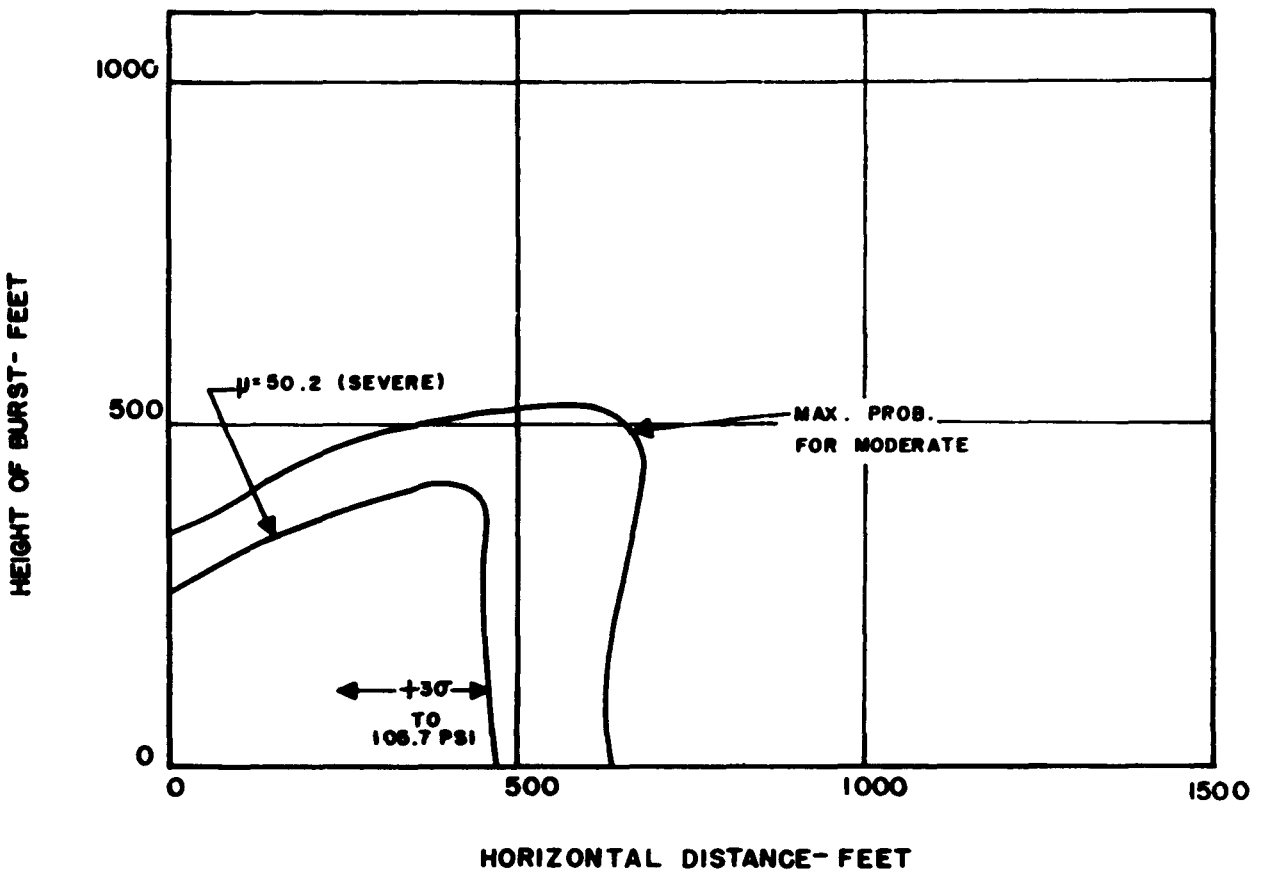

Fig. 5.15 Height of Burst vs Distance From Ground Zero for Various Damage to Tanks (Scaled to 1 KT Sea Level)

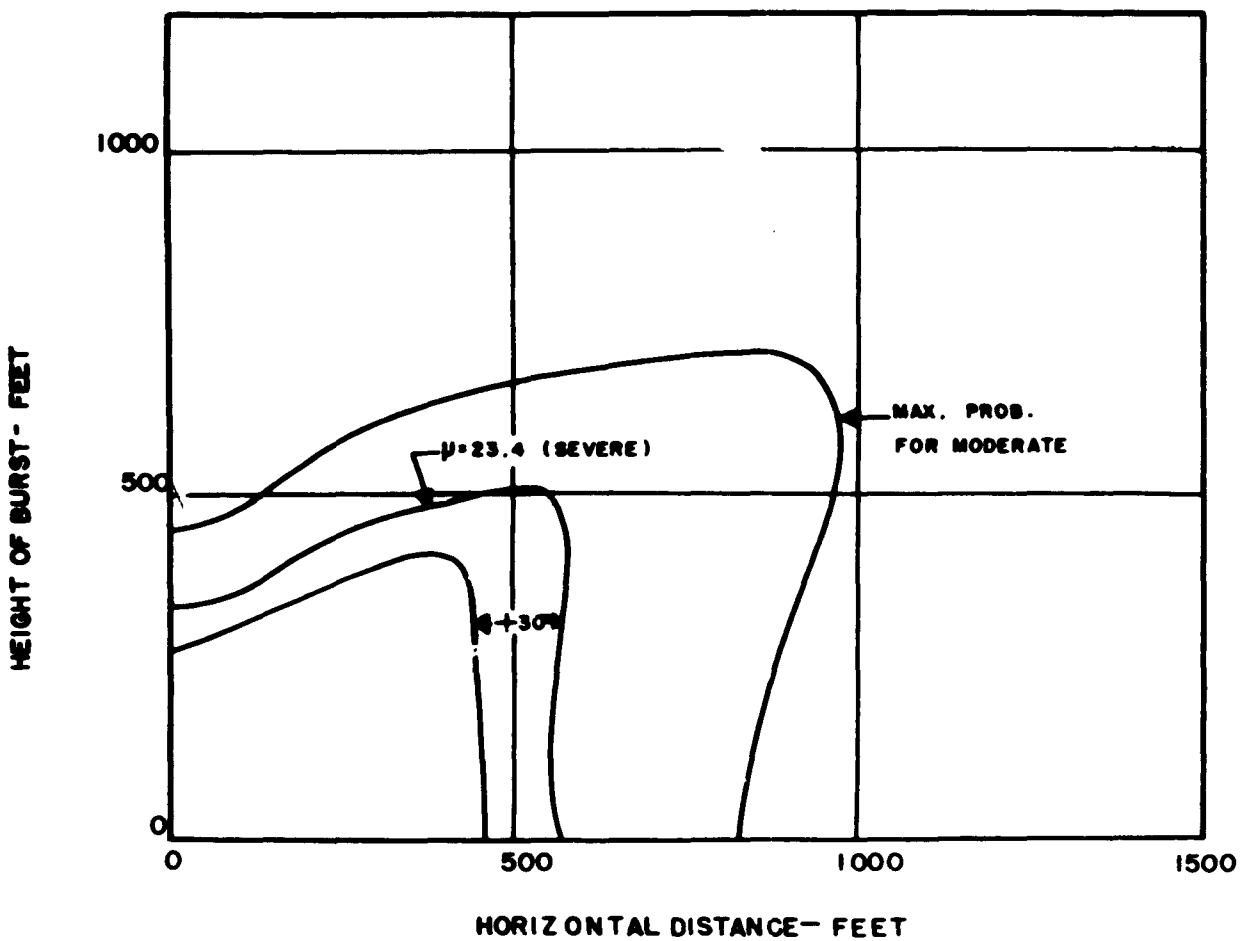

Fig. 5.16 Height of Burst vs Distance From Ground Zero for Various Damage to 57 mm Guns (Scaled to 1 KT Sea Level)

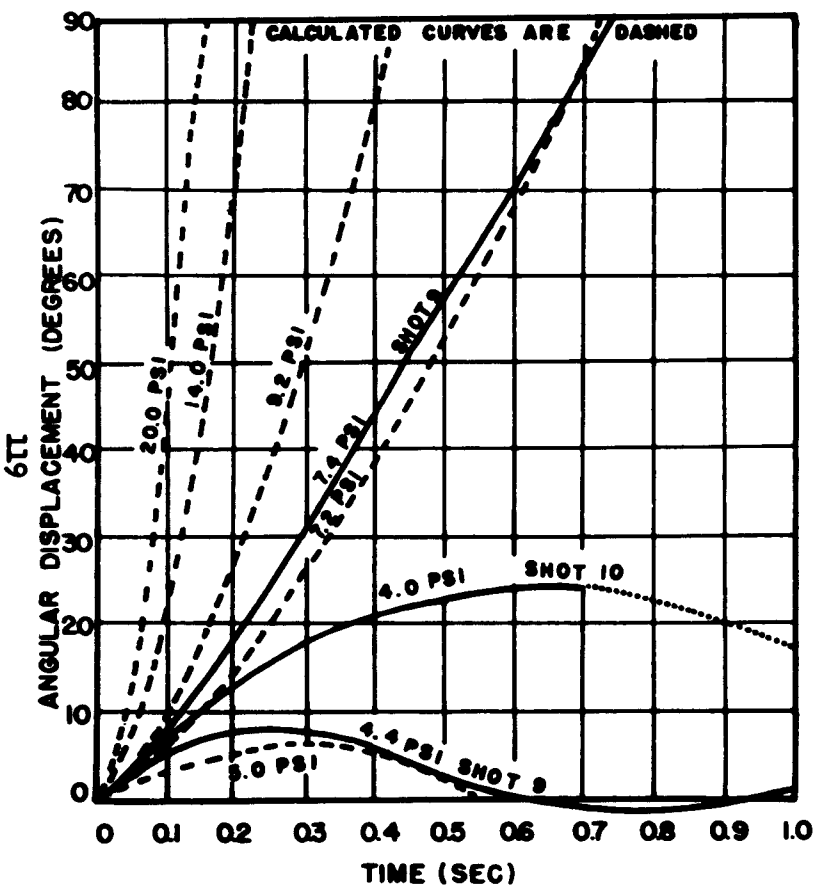

Fig. 5.17 Comparison of Angular Displacement of 1/4 Ton Truck Side-on with Calculated Angular Displacements

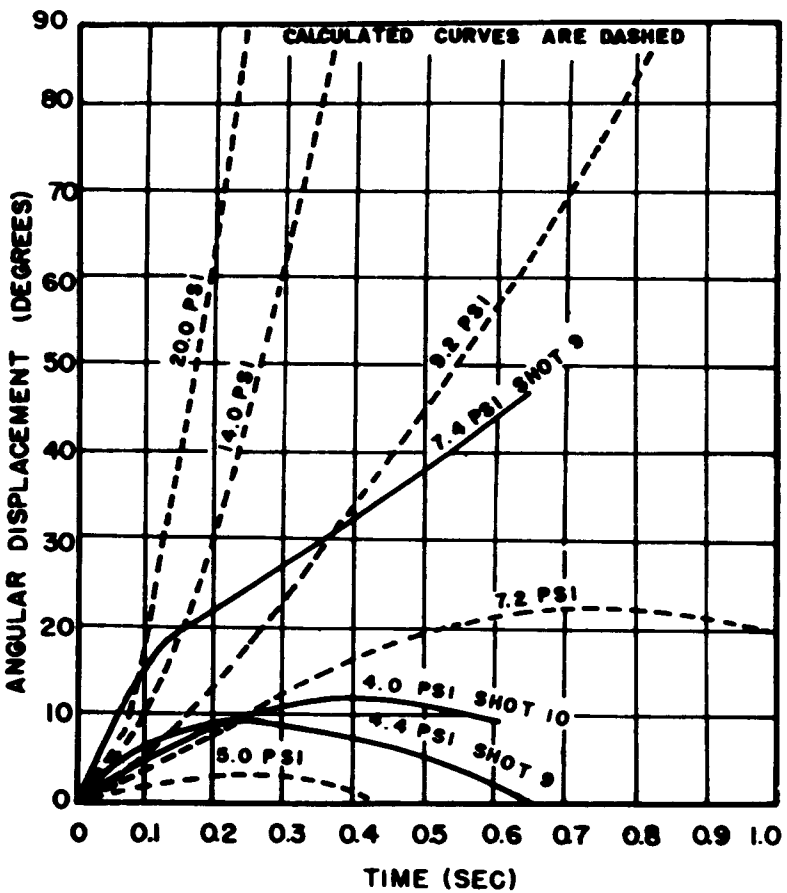

Fig. 5.18 Comparison of Angular Displacement of 2-1/2 Ton Truck Side-on with Calculated Angular Displacements

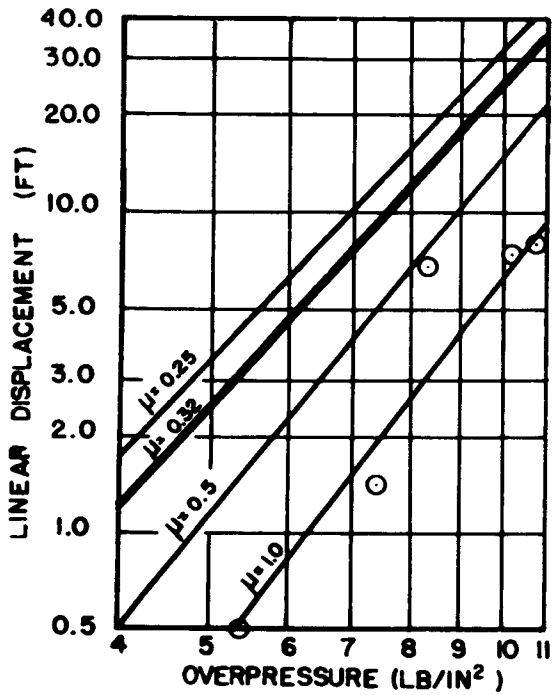

Fig. 5.19 Displacements of Center of Gravity of 1/4 Ton Truck Face-on Compared To Calculated Sliding Displacements (Shot 9)

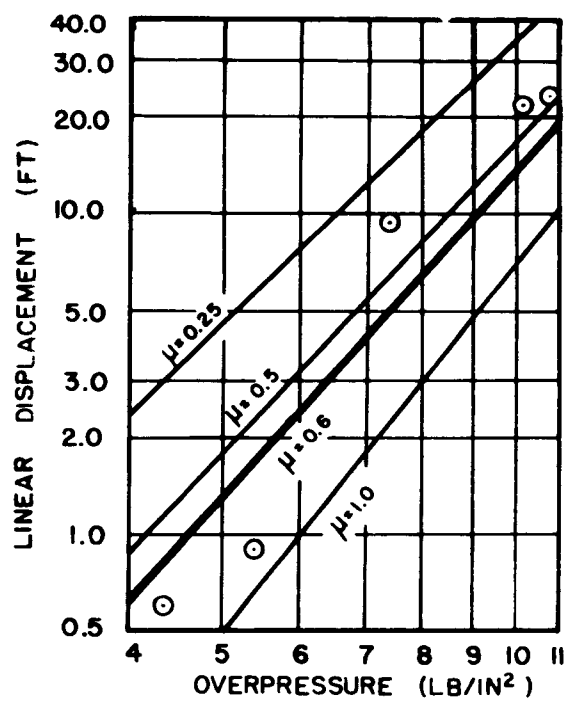

Fig. 5.20 Displacements of Center of Gravity Of 1/4 Ton Truck Side-on Compared To Calculated Sliding Displacements (Shot 9)

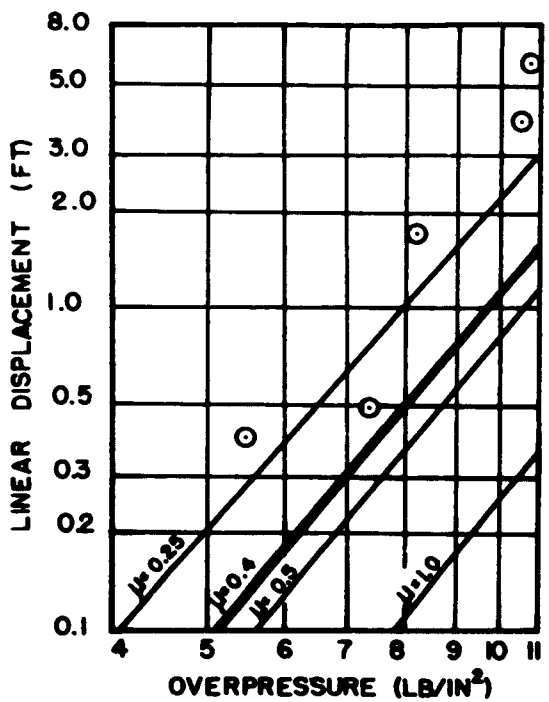

Fig. 5.21 Displacements of Center of Gravity of 2-1/2 Ton Truck Face-on Compared To Calculated Sliding Displacements (Shot 9)

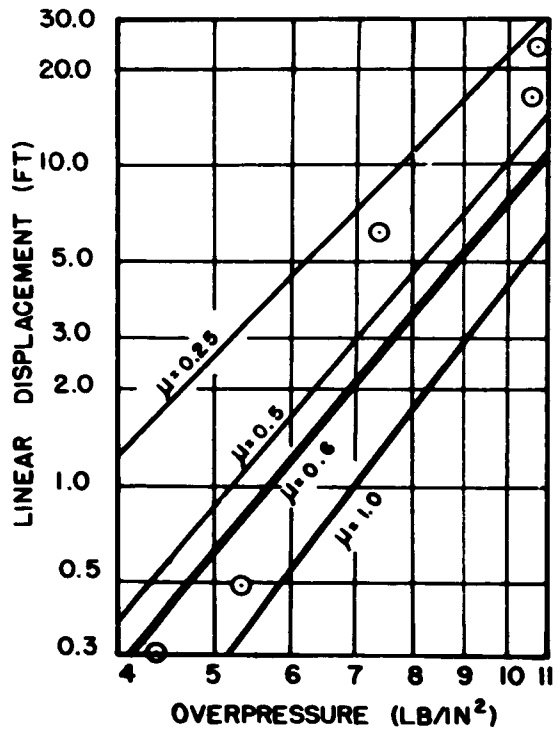

Fig. 5.22 Displacements of Center of Gravity of 2-1/2 Ton Truck Side-on Compared To Calculated Sliding Displacements (Shot 9)

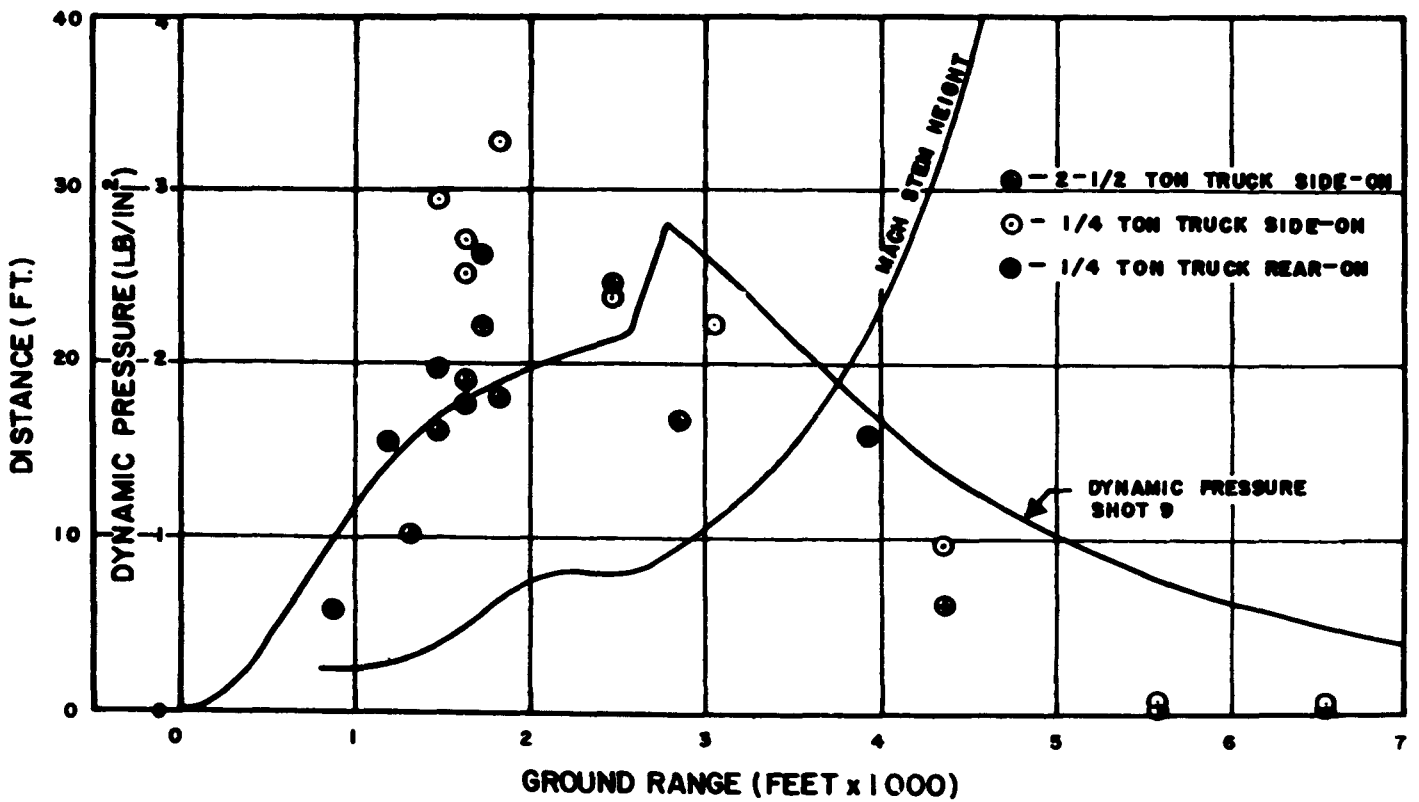

Fig. 5.23 Displacements of Center of Gravity of Trucks Side-on and Rear-on vs Ground Range for Shot 9, Dynamic Pressure vs Ground Range for Shot 9, and Mach Stem Height vs Ground Range for Shot 9

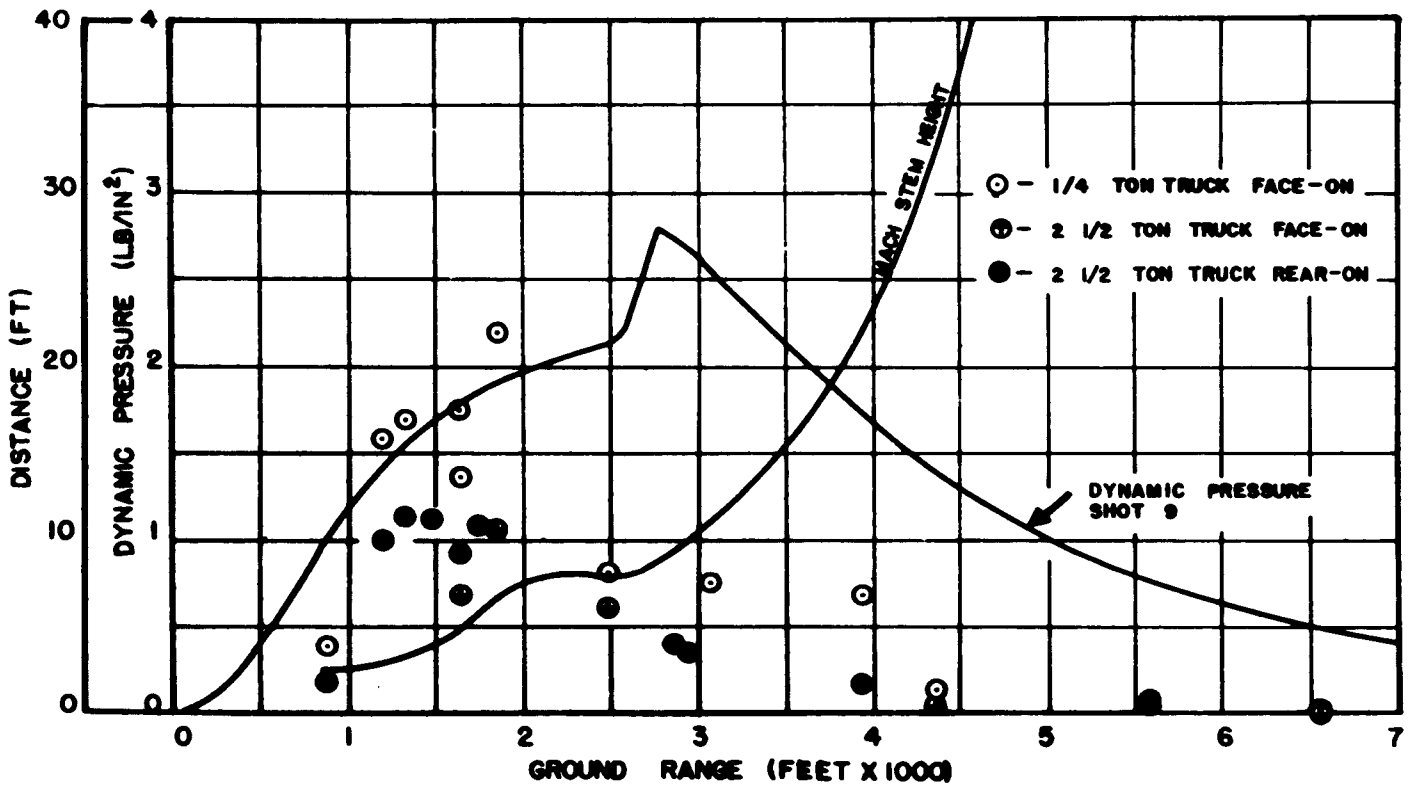

Fig. 5.24 Displacements of Center of Gravity of Trucks Face-on and Rear-on vs Ground Range for Shot 9, Dynamic Pressure vs Ground Range for Shot 9, and Mach Stem Height vs Ground Range for Shot 9

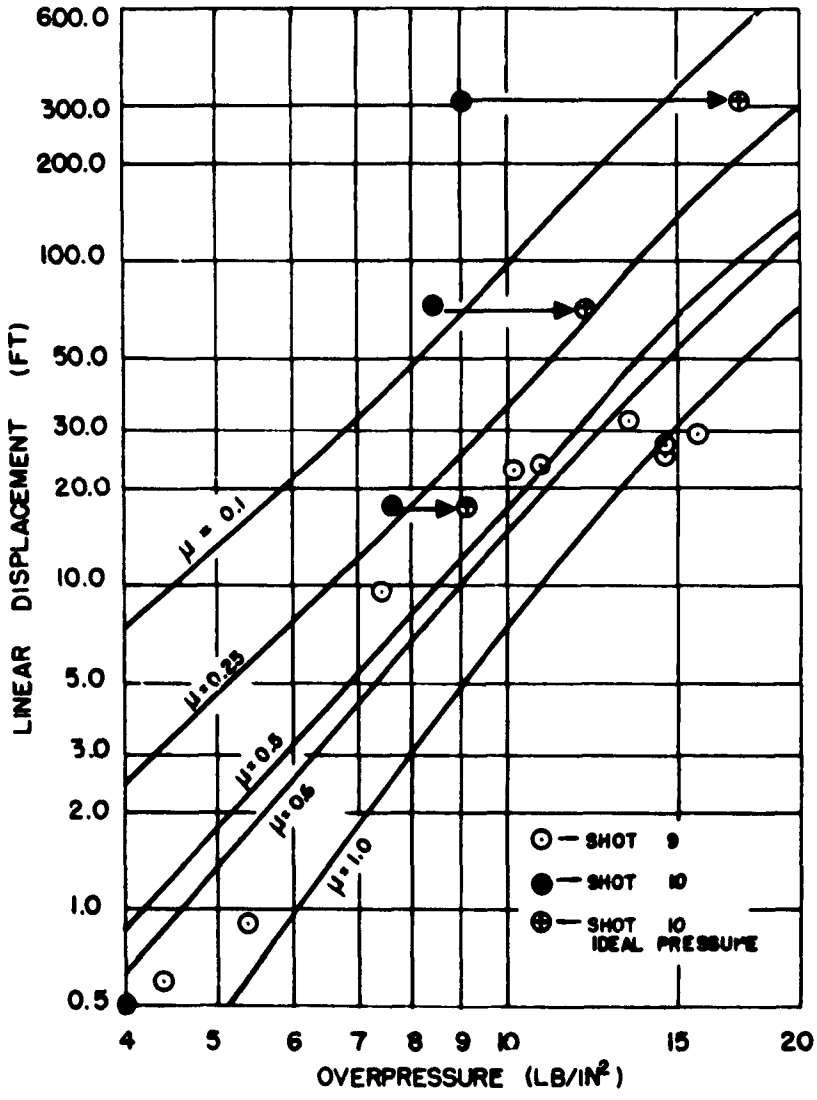

Fig. 5.25 Displacements of the Center of Gravity of the 1/4 Ton Truck on Shot 9 and Shot 10 vs Overpressure and Calculated Sliding Displacements vs Overpressure for a Mach Wave

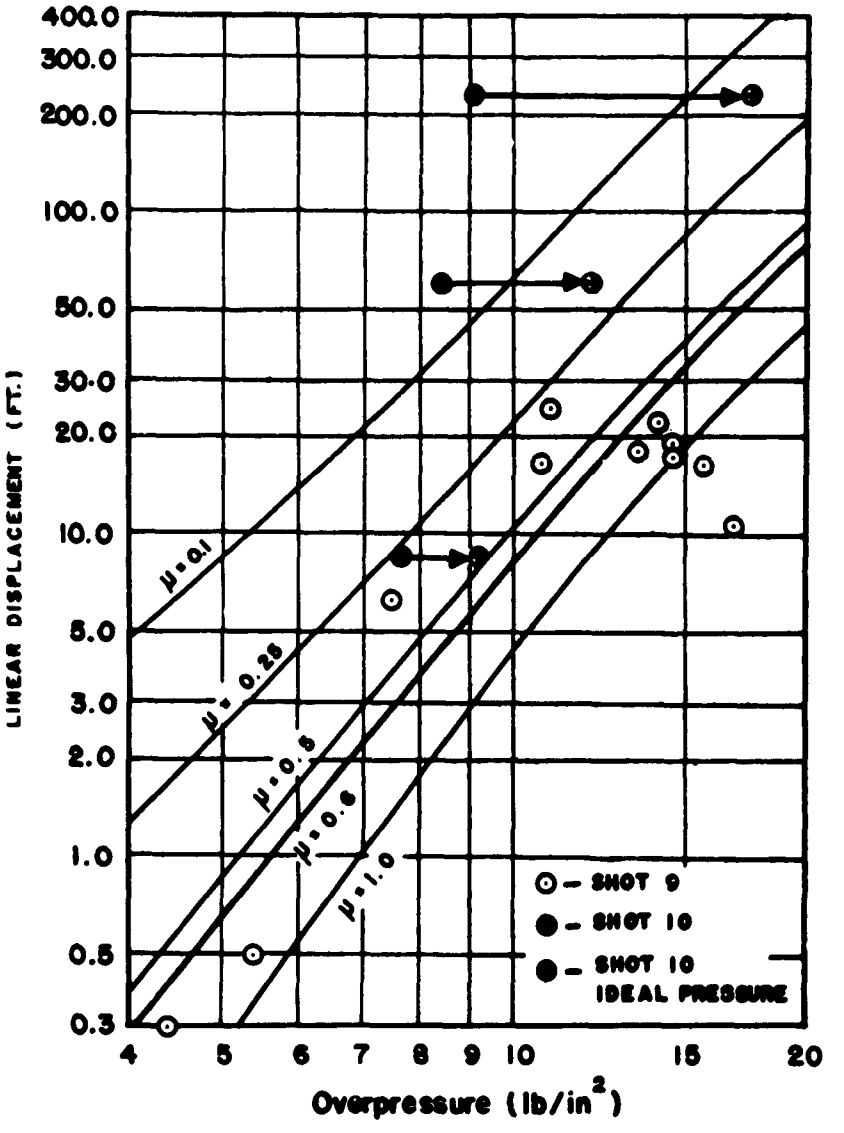

Fig. 5.26 Displacements of the Center of Gravity of the 2-1/2 Ton Truck on Shot 9 and Shot 10 vs Overpressure and Calculated Sliding Displacements vs Overpressure for a Mach Wave

CHAPTER 6

CONCLUSIONS AND RECOMMENDATIONS

6.1 CONCLUSIONS

The general conclusions drawn from Equipment Exposure Tests during UPSHOT-KNOTHOLE are as follows:

1. The two levels of burst height for Shot 9 and Shot 10 were unique in that they provided a comparison of damage resulting from overpressures within the regular reflection region with that damage resulting from corresponding overpressures within the Mach region. The results indicate that damage within the regular reflection region will be equivalent to or less than the damage resulting from equal overpressures within the Mach region.

2. The region of interest for damage criteria is the Mach region since it is within this region that damage to equipment will be maximized.

3. In most cases, equipment exposed in side-on orientation are most vulnerable to blasts and equipment in face-on orientation are least vulnerable.

4. The probability curves obtained from statistical analysis provides a criteria for predicting damage only to the type of equipment tested. If necessary, for lack of other information, it is felt that these probability curves can be applicable to other equipment of similar size, shape, and weight.

5. The BRL prediction method was partly verified and partly contradicted. The information gathered from this test along with information from previous exposures will allow, with modifications of the BRL method, prediction of damage not only to the type of equipment tested in Shots 9 and 10, but will allow extrapolation to other ordnance items as well. Modification of this method will take into account dynamic pressure, orientation of item and damage in terms of light, moderate, and severe.

6. The calculations employing the ARF prediction method provided the proper order of magnitude for the results obtained on Shot 9. The displacements obtained on Shot 10 when compared with those predicted are excessive and the calculated values apply reasonably well only when the ideal pressures are assumed.

6.2 RECOMMENDATIONS

The importance of dynamic pressures as related to drag type target has been established in these tests. Some regions of uncertainties do exist regarding the values of measured dynamic pressures. In future atomic tests measurements of dynamic pressures and drag pressures should be made along with side-on pressures. In addition 1/4 ton trucks used as response gages should be exposed in order that the basic blast measurements can be correlated with the actual damage sustained. It is not necessary that new 1/4 ton trucks be exposed.

There exists at this time a total of 107 observations of damage to 1/4 ton trucks exposed under varying conditions. Upon establishing the value of forces inflicting damage in future tests an insight can be gained on the causes of the effects of previous tests where anomalies were present.

On the supposition that atomic tests will include troop indoctrination programs, whereby equipment will be exposed, it is recommended that the damage evaluation be in accordance with the procedure described herein. It is of importance to consider the time required for repairing a given damage from the standpoint of combat use only. In this manner a continuous effort can be made to increase the reliability of the present damage criteria.

With regard to engineering and design problems concerning ordnance equipment, the following has been submitted by H. D. Duppstadt (Item a) and C. D. Montgomery (Item b) who were engineering consultants to this project:

a. Within pressure regions where vehicles are not dismembered, damage can be decreased and vehicles put into combat use more readily by providing the vehicles with (1) roll-over safety bars and (2) flexible mountings for engine and transmission components that are reinforced to withstand very high separating forces.

Much of the damage is inflicted to vehicles as a result of overturning. A properly attached roll-over safety bar on the vehicle would absorb some of the impact with the ground and effectively minimize damage to the body as well as prevent bending of the steering wheel and steering columns. The present flexible mountings for engine and transmission components are dependent on rubber bonded to steel. These mountings perform their intended function satisfactorily in normal operation but when forces of certain magnitude are applied in an opposite direction as a result of overturning, separation occurs. If the flexible mountings were redesigned whereby steel interlocks were incorporated then higher forces would be required before separation of components would occur.

b. Previous testing has shown the weapon's effects on the components of many of the older vehicles (Light Tank M24 and Medium Tanks M26 and M46). Since many of the major components are similar to the new production tank designs, repetition of component testing should be avoided. Possible predicted effects can be made on some of the components such as engine and transmission, tracks and roadwheels and suspensions of the new type vehicles. The new vehicles which are typical and and likely to be found in a tactical area are: 90 mm Gun Tank M48 and 155 mm Self-Propelled Vehicle T97. Effects on components of new

vehicles for which information is lacking are: Armor (Hull and Turret), gun and gun mountings and optical devices and fire control. Information is needed which would yield experimental design data for future consideration of tank designs.

APPENDIX A

TABLE A.1 Maintenance Echelons Howitzer 105 mm

Damage	To Restore to Combat Use (hr)	Echelon	To Restore to Original Condition (hr)	Echelon
Axle	8	Depot	8	Depot
Equalizer	8	Depot	8	Depot
Trails	1	Field	1	Field
Wheels	1	Org.	1	Org.
Brakes	1	Field	1	Field
Top Carriage	4	Field	4	Field
Pintle Pin & Bushing	55	Depot	5	Depot
Traversing Worm	1	Field	1	Field
Traversing Rack	1	Field	1	Field
Elevating Mechanism		Field		
Handwheels	1/2	Field	1/2	Field
Cross shaft	2	Field	2	Field
Mechanism housing	2	Field	2	Field
Cradle	3	Field	3	Field
Elevating Arcs	1	Field	1	Field
Equilibrator	3/4	Field	3/4	Field
Shields	1	Org-Field	1	Field
Recoil Mechanism	1	Field	4	Depot
Barrel	1/2	Field	1/2	Field
Breech Mechanism	1	Field	1	Field
Firing Mechanism	1/4	Field	1	Field
Sighting Equipment	1	Field	1	Field

TABLE A.2 Maintenance Echelons - Track-Laying, Armored, Combat Vehicles

Component	To Restore to a Combat Usable Condition (hr)	Echelon	To Restore to a Rebuilt/New Condition (hr)	Echelon
Main Armament	8	Depot	8	Depot
Co-axle Machine Gun	1	Org.	1	Org.
Stowage & Ready Racks (Turret) (Incl. Turret Floor)	16	Field	16	Field
Sighting Equip. for Main Gun & Co-axle MG	1	Org.	1	Org.
Periscope Holder	2	Org.	2	Field
Vision Blocks	2	Org.	2	Org.
Radio	8	Org.	8	Org.
Interphone Junction Box	1	Org.	1	Org.
Turret	8	Depot	8	Depot
Tracks, rec'd whole	6	Org.	6	Org.
Tracks, rec'd in sections	12	Org.	12	Org.
Roadwheels (each)	1	Org.	1	Org.
Support Rollers (each)	1	Org.	1	Org.
Driving Sprockets (2 on 1 side)	4	Org.	4	Field
Driving Sprockets and Hub	6	Org.	6	Field
Track Idlers (plus time to break & repair track - 4 hrs.)	1	Org.	1	Org.
Hatch	3	Field	3	Field
Exterior Stowage Boxes	1	Org.	1	Org.
Fender (each)	2	Org.	2	Org.
Headlights	1	Org.	1	Org.
Driving Controls - Adjust	1	Org.	1	Org.
Instrument Panel & Connections	2	Field	2	Depot
Seats (one)	1	Org.	1	Field
Bow MG Ball Mount	2	Field	2	Depot
Main Engine	36	Depot	36	Depot
Auxiliary Engine	4	Org.	4	Org.
Fuel Tank (plus time to remove & replace Main Engine-36 hrs.)	2	Depot	2	Depot
Cooling System & Fans	12	Field	12	Depot
Fans only (M-46's)	8	Field	8	Depot
Final Drive or Cross Drive	40	Depot	40	Depot
Rear End Final Drive	30	Depot	30	Depot

NOTE: This type of vehicle has no frame, the armored hull serves in place of a frame. If the hull becomes warped or bent, the only thing to do is to salvage the vehicle or to find another destroyed vehicle that has the desired piece of armor in good condition, then by welding patch up one of the two vehicles. Then you have a vehicle that will serve for a short time.

APPENDIX B

Moments of Inertia of the Vehicles

The moments of inertia of the vehicles were obtained by calculation. To find the moment of inertia of a vehicle about a selected axis, the vehicle was divided into various parts. Using a weight analysis chart and body builder's diagram, a weight and distance from an arbitrary axis (chosen for convenience) were assigned for each part. After idealizing the shape of the part, the moment of inertia of the part about the arbitrary axis was obtained using the relation:

$$Ia = I_{cg} + (w/g)d^2$$

I_{cg} = moment of inertia about center of gravity of part.

d = distance from c.g. of part to arbitrary axis.

I_a = moment of inertia of part about arbitrary axis.

w = weight of part.

g = acceleration due to gravity.

The resulting values for all parts were summed to obtain the moment of inertia of the vehicle about the arbitrary axis.

The moment of inertia of the vehicle about its center of gravity was found using the same expression:

$$Ia_t = Icg_t + (w_t/g)d^2$$

Then: $$Icg_t = Ia_t - d^2(w_t/g) \qquad (B.1)$$

Where: Ia_t = moment of inertia of vehicle about arbitrary axis.

Icg_t = moment of inertia of vehicle about c.g. of vehicle.

d = distance from arbitrary axis to axis through c.g.

w_t = weight of vehicle.

g = acceleration due to gravity.

The same expression B.1 was used to calculate the moment of inertia of the vehicles about the expected axes of rotation. These axes were aa, through the most forward point of contact of the front wheels with the ground, perpendicular to the longitudinal axis of the vehicle; bb, the axis through the most rearward point of contact of the rear wheels with the ground, perpendicular to the longitudinal axis of the vehicle; and cc, through the outer point of contact of the wheels on one side with the ground, parallel to the longitudinal axis of the vehicle. The values resulting from the calculations are shown in Table B.1.

TABLE B.1 Calculated Moments of Inertia - M-135 and M38A1

M-135 2-1/2 ton truck:	M38A1 1/4 ton truck:
Axis perpendicular to side	Axis perpendicular to side
Icg = 12,600 slug - ft^2	Icg = 790.6 slug - ft^2
Iaa = 35,770 slug - ft^2	Iaa = 2032 slug - ft^2
Ibb = 40,580 slug - ft^2	Ibb = 2203 slug - ft^2
Axis parallel to side	Axis parallel to side
Icg = 2272 slug - ft^2	Icg = 172.9 slug - ft^2
Icc = 9291 slug - ft^2	Icc = 983.7 slug - ft^2

APPENDIX C

TABLE C.1 Damage Evaluation

Project: 3.21 Date of Evaluation: 5/11/53

Item: No. 42 Truck, cargo, 2-1/2 ton 6x6 M-35 Date of Exposure: 5/9/53

Range: 3.21 j - 2860 ft Orientation: Side-on

Immediately Combat Usable: No.

Remarks: Vehicle was turned upside down. Righted by use of a wrecker. Oil and water checked, levels found to be correct. Vehicle was started and driven to the assembly area.

Man-hours to restore to Combat Usability: 1/2 hr

Class of Maintenance to Restore to Combat Usability: Organizational.

Man-hours to Completely Restore: 24 hr

Class of Maintenance to Completely Restore: Field

Was Vehicle operated? Yes

How many miles: 15-1/2 miles. Operation was satisfactory.

Remarks: Engine top panel torn off, hinge assemblies and both hold down catch assemblies broken. Left engine side panel blown off, hinge assg. broken, right engine side panel bent and hinge assemblies broken and bent. Cab windshield blown out, inner and outer frames smashed. Cab frame assembly smashed and torn off. Left door assembly bent, hinges sprung and glass assembly broken. Companion seat and back rest cushion assembly badly burned. Cargo body sides, front and end gate bent. Cargo body racks w/troop seats, end and intermediate bow tubes bent and broken. The damage to this vehicle was superficial.

TABLE C.2 Damage Evaluation

Type of Vehicle: Truck, Cargo, 2-1/2 ton 6x6 M35 Date of Evaluation: 5/14/53

USA No. 41209451 Position: 3.21 j - 2860 ft

Component	Remarks	Man-Hours Req. to Restore CU*	Man-Hours Req. to Restore Completely
1. Bumpers and Guards			
Front	No damage		
Rear	No damage		
2. Cooling System			
Radiator & Mounting parts	No damage		
Radiator Baffles and Shroud	No damage		
Lines, Fittings, and Thermostat	No damage		
Water Pump	No damage		
Fan and Fan Belts	No damage		
3. Springs & Shock Absorbers			
Front Springs, Shackes, and Attaching Parts	No damage		
Rear Springs and Attaching Parts	No damage		
Shock Absorbers and Parts	No damage		
Torque Rods	No damage		
4. Front Axle			
Front Axle Assembly	No damage		
Front Axle Housing	No damage		

* Combat Usable

TABLE C.2 Damage Evaluation (Cont'd)

Component	Remarks	Man-Hours Req. to Restore CU*	Man-Hours Req. to Restore Completely
Front Axle Differential	No damage		
Front Axle Sterring Knuckles, Arms, Bearings and Shims	No damage		
Front Axle Shafts, Universal Joint and Flanges	No damage		
5. Wheels, Hubs, and Drums			
Wheel Assembly, Studs, Nuts, Seals, Hubs, & Drums	No damage		
Tires and Tubes	No damage		
6. Hood, Fenders, and Running Boards			
Fenders, Running Boards, and Attaching Parts	Left front fender slightly bulged. Left rear running board hanger bent down about 3". Right rear running board hanger bent downward slightly. Left engine side panel w/hinge assemblies torn off and missing.		1-1/2
Hood and Attaching Parts	Engine top panel blown off, hinge assemblies twisted and broken. Both hold down catch assemblies broken		1
7. Electrical System			
Generator & Regulator	No damage		
Starter & Controls	No damage		
Distributor	No damage		
Spark Plug & Cables	No damage		

* Combat Usable

TABLE C.2 Damage Evaluation (Cont'd)

Components	Remarks	Man-Hours Req. to Restore CU Completely
Instrument Cluster, Gages, Circuit Breakers, and Switches.	Instrument cluster panel bent out slightly	1/2
Head, Tail and Marker Lights.	Left headlight lens scorched	1/2
Sending Units	No damage	
Horn and Button	Horn circuit breaker relay broken loose from fire wall	1/6
Batteries & Cables	Electrolyte drained out of batteries	1/6
Chassis and Wiring Harness	Insulation covering on right front headlight wiring frayed	1/4
Trailer Coupling (Electric)	No damage	
8. Engine		
Engine	No damage	
Cylinder Head & Block	No damage	
Oil filter	No damage	
Crankcase Breather & Filler	No damage	
Oil Pan, Oil Lines, and Level Gage	No damage	
Intake & Exhaust Manifold, & Heat Control	No damage	
Air Compressor	No damage	
9. Controls		
Steering Mechanism	Steering gear jacket and shaft bent slightly, but still operable.	2
Steering Wheel	Sterring wheel bent & charred	1/2

TABLE C.2 Damage Evaluation (Cont'd)

Components	Remarks	Man-Hours Req. to Restore CU Completely
10. Body and Cab		
Cab Frame	Rear of cab assembly bent inward slightly. Cab frame assembly smashed & destroyed. Right side of instrument panel buckled inward. Right front corner of cab assembly bent forward about 1-1/2 in.	6-2/3
Doors, Glass & Handles	Right & left door assemblies bent, upper & lower hinge assemblies bent. Both door glass assemblies broken.	2
Windshield, Cowl Ventilator, & Attaching Parts	Cab windshield blown out. Inner & outer frames mashed & destroyed. Left & right cowl ventilators w/hinge assemblies bent & sprung. Top cowling ripped from fire wall & cab.	1
Cab Floor & Parts	No damage	
Cab Seats & Parts	Driver's seat & backrest cushion assembly scorched. Companion seat & back rest cushion assembly burned partially. Companion seat leg broken & seat cushion assembly torn loose from inward.	1-1/2
Stowage Racks, Boxes, and Straps	Tool box w/door and hinge assembly bent and mashed inward.	1/2
Cargo Body, & Troop Seats	Cargo body and troop seats, left side of cargo body bent inward about 9 in.	1

TABLE C.2 Damage Evaluation (Cont'd)

Components	Remarks	Man-Hours Req. to Restore CU	Completely
	Right side of cargo body bent inward about 2-1/2 in. Cargo body endgate bent bent outward slightly. Handles bent down. Front of cargo body bent down and out about 1-1/2 in. Left front hold down bracket & bolts bent slightly. Left side cargo body sill missing. Left rear splash shield w/ brackets bent slightly. Left & right cargo body racks w/troop seats, end & intermediate bow tubes smashed & destroyed. Front cargo body rack w/stakes bent and broken.		
11. Miscellaneous Body and Cab Parts			
Canvas Items, Bows and Curtains	Cab Paulin w/rope assembly torn off & destroyed		1/2
Mirrors, Windshield Wipers, and Reflectors	Right rear view mirror broken. Extension tube bent. Right & left windshield wiper motors w/ arms & blades missing. Left front & left side amber reflectors scorched.		1
Speedometer	No damage		
Air Storage Tanks	No damage		
12. Frame and Brackets			
Frame Assembly and Brackets	No damage		

TABLE C.2 Damage Evaluation (Cont'd)

Components	Remarks	Man-Hours Req. to Restore CU	Completely
	Right side of cargo body bent inward about 2-1/2 in. Cargo body endgate bent bent outward slightly. Handles bent down. Front of cargo body bent down and out about 1-1/2 in. Left front hold down bracket & bolts bent slightly. Left side cargo body sill missing. Left rear splash shield w/ brackets bent slightly. Left & right cargo body racks w/troop seats, end & intermediate bow tubes smashed & destroyed. Front cargo body rack w/stakes bent and broken.		
11. Miscellaneous Body and Cab Parts			
Canvas Items, Bows and Curtains	Cab Paulin w/rope assembly torn off & destroyed		1/2
Mirrors, Windshield Wipers, and Reflectors	Right rear view mirror broken. Extension tube bent. Right & left windshield wiper motors w/ arms & blades missing. Left front & left side amber reflectors scorched.		1
Speedometer	No damage		
Air Storage Tanks	No damage		
12. Frame and Brackets			
Frame Assembly and Brackets	No damage		

TABLE C.2 Damage Evaluation (Cont'd)

Components	Remarks	Man-Hours Req. to Restore CU Completely
Pintles & Towing attachments	No damage	
Spare Wheel Carrier	No damage	
13. Exhaust System		
Muffler	No damage	
Exhaust & Tail Pipe	No damage	
14. Fuel System		
Carburetor	No damage	
Fuel Pump & Priming Pump	No damage	
Air Cleaner	No damage	
Fuel Tank, Lines, Fittings	No damage	
Governor	No damage	
Accelerator, Throttle, and Choke Controls	No damage	
15. Propeller Shaft Assembly		
Propeller Shafts (all units)	No damage	
Pillow Blocks	No damage	
16. Rear Axle		
Rear Axle Assembly	No damage	
Rear Axle Housing	No damage	
Rear Axle Differential	No damage	
Rear Axle Shaft	No damage	

TABLE C.2 Damage Evaluation (Cont'd)

	Components	Remarks	Man-Hours Req. to Restore CU	Completely
17.	Transmission			
	Transmission Assembly	No damage		
18.	Transfer			
	Transfer Assembly	No damage		
	Transfer Case, Plugs, Cover, & Gaskets	No damage		
	Shift Levers	No damage		
19.	Brakes			
	Hand Brakes	No damage		
	Service Brakes	No damage		
	Hydraulic System Master Cylinder, Assembly, Lines, Fittings, and Clips	No damage		
20.	Paint	Scorched		4
	Lubrication			1

TABLE C.3 Shot 9

Position	psi	Range (ft)	Item	Orientation	Degree of Damage	Damage Description	To Restore to Combat Use	
							Man Hours	Maint. Echelon
3.21 a	17.8	1195	2-1/2T	RO	L	Truck turned on right side Hydrostatic lock, no windshield glass.	1/2	Org.
3.21 a	17.8	1195	1/4T	RO	S	Vehicle turned upside down and burned.	33-11/12	Depot Salvage
3.21 a	17.8	1195	1/4T	FO	L	Vehicle turned on Left side, fenders and body smashed, no windshield glass.	1/3	Org.
3.21 b	16.8	1320	2-1/2T	FO	L	Truck lying on left side, fenders & body bent, no windshield glass.	1/2	Org.
3.21 b	16.8	1320	2-1/2T	SO	L	Truck turned over on right side. Radiator leaking from overflow pipe. Sheet metal body parts bent and torn. No windshield glass.	3/5	Org.
3.21 b	16.8	1320	1/4T	FO	L	Sheet metal on body bent & torn, paint scorched, no windshield glass.	-	-
3.21 c	15.6	1480	2-1/2T	RO	M	Truck turned upside down. Sheet metal bent & torn, body smashed, no windshield glass.	1-1/2	Org.

TABLE C.3 Shot 9 (Cont'd)

Position	psi	Range (ft)	Item	Orientation	Degree of Damage	Damage Description	To Restore to Combat Use	
							Man Hours	Maint. Echelon
3.21 c	15.6	1480	2-1/2T	SO	M	Truck turned upside down, steering wheel bent. Body smashed, no windshield glass. Sheet metal bent and torn.	1-1/2	Org.
3.21 c	15.6	1480	1/4T	SO	M	Vehicle started but stopped immediately and would not start again. Body & fenders bent & torn, no windshield glass.	2	Org.
3.21 c	15.6	1480	1/4T	RO	M	Vehicle turned on right side. Right rear wheel well badly bent, interfered with tire. Body & fenders bent & torn, no windshield glass.	1	Org.
3.21 d	14.5	1640	2-1/2T	FO	L	Hood & Cowl blown off, no windshield glass, body and fenders bent.	-	Org.
3.21 d	14.5	1640	2-1/2T	SO	M	Truck turned upside down, hydrostatic lock, body bolts sheared on one side, body and fenders bent, no windshield glass, windshield frame bent.	1	Org.

TABLE C.3 Shot 9 (Cont'd)

Position	psi	Range (ft)	Item	Orientation	Degree of Damage	Damage Description	To Restore to Combat Use	
							Man-Hours	Echelon Maint.
3.21 d	14.5	1640	1/4T	SO	L	Vehicle lying on left side, cowl & hood bent & torn, fenders bent, no windshield glass.	1/3	Org.
3.21 d	14.5	1640	1/4T	FO	L	Body & Cowl bent, fenders bent, fan and radiator top bent.	-	Org.
3.21 e	14.5	1640	2-1/2T	SO	M	Truck overturned, hydrostatic lock, hood & cowl bent and torn. Intermediate axle bent.	1-1/2	Org
3.21 e	14.5	1640	2-1/2T	FO	L	Hood blown off, splash shield bent back into one tire of a dual pair.	-	Org.
3.21 e	14.5	1640	1/4T	FO	L	Body bent & scorched, hood blown off. Windshield glass broken & windshield frame bent.	none	Org.
3.21 e	14.5	1640	1/4T	SO	L	Vehicle turned on side, body bent and scorched, hood off.	1/2	Org.
3.21 f	14.0	1740	2-1/2T	RO	L	Truck turned on right side; hood, cowl, & body bent & torn. No windshield glass, windshield frame bent. Batteries low.	1/2	Org.

TABLE C.3 Shot 9 (Cont'd)

Position	psi	Range (ft)	Item	Orientation	Degree of Damage	Damage Description	To Restore to Combat Use	
							Man-Hours	Maint. Echelon
3.21 f	14.0	1740	2-1/2T	SO	M	Truck turned on left side; steering column & wheel bent, body bolts sheared; body, cab, hood, & cowl bent & torn. No windshield glass, windshield frame bent, intermediate axle bent.	1	Org.
3.21 f	14.0	1740	1/4T	RO	L	Vehicle turned on right side, body, hood & windshield frame bent, windshield glass broken. Battery leaking from top.	1/2	Org
3.21 f	14.0	1740	1/4T	SO	L	Vehicle upside down, hood blown off, body & cowl bent & torn. Body bent.	1/2	Org.
3.21 f	15.4	1500	90 mm	FO	L	Elevation meter broken. Indicator glass broken.	1	Field
3.21 g	13.4	1830	2-1/2T	FO	L	Body, hood & cowl bent (torn). Paint scorched, speedometer broken.	1/2	Org
3.21 g	13.4	1830	2-1/2T	SO	M	Body, hood & cowl bent & torn. Left front body bolts sheared off. Steering wheel bent. One differential case leaking.	1-5/6	Org

TABLE C.3 Shot 9 (Cont'd)

Position	psi	Range (ft)	Item	Orientation	Degree of Damage	Damage Description	To Restore to Combat Use	
							Man-Hours	Maint. Echelon
3.21 g	13.4	1830	1/4T	SO	M	Vehicle lying on side. Hydrostatic lock. Body, hood, & cowl bent & torn. Radiator grill bent, steering difficult.	1	Org.
3.21 g	13.4	1830	1/4T	FO	M	Vehicle upside down, hole in radiator core from missile damage. Body, hood and cowl bent & torn. No windshield glass.	2	Org.
3.21 h	21.0	875	2-1/2T	FO	L	Hood blown off & bent; cowl torn, windshield glass broken, windshield frame broken, body bent.	-	Org.
3.21 h	21.0	875	2-1/2T	FO	L	Hood blown off & bent, cowl torn, windshield glass broken, windshield frame broken, body bent.	-	Org.
3.21 h	21.0	875	1/4T	RO	L	Seats scorched, instrument glass smoky, tool box bent, windshield glass blown off & broken.	-	Org.
3.21 h	21.0	875	1/4T	FO	L	Hood blown off, cowl torn, windshield glass broken & paint scorched.	-	Org.
3.21 i	10.8	2480	2-1/2T	SO	M	Truck turned on side, body, fenders, hood & cowl bent & torn. Cab badly bent.	1-1/6	Org.

TABLE C.3 Shot 9 (Cont'd)

Position	psi	Range (ft)	Item	Orientation	Degree of Damage	Damage Description	To Restore to Combat Use	
							Man-Hours	Maint. Echelon
3.21 i	10.8	2480	2-1/2T	FO	L	Body, hood & cowl bent & torn. Plastic headlights melted. Body corner support broken.	-	Org.
3.21 i	10.8	2480	1/4T	FO	L	Fender bent, cowl & hood bent, body bent. Windshield glass broken.	-	Org.
3.21 i	10.8	2480	1/4T	SO	M	Vehicle upside down. Hood blown off. Hydrostatic lock in one cylinder. Cowl & body bent. Windshield glass broken, frame (W/S) bent.	1-1/2	Org.
3.21 j	10.6	2860	2-1/2T	FO	L	Windshield glass blown out, cowl torn, hood blown off. Body scorched.	-	Org.
3.21 j	10.6	2860	2-1/2T	SO	L	Truck lying on side, windshield glass broken. Windshield frame bent, hood blown off, cowl torn. Body bent & scorched.	1/2	Org.
3.21 ia	10.2	3060	1/4T	FO	L	Hood blown off. Windshield glass blown out, windshield frame bent. Body & seats scorched.	-	Org.

TABLE C.3 Shot 9 (Cont'd)

Position	psi	Range (ft)	Item	Orientation	Degree of Damage	Damage Description	To Restore to Combat Use	
							Man-Hours	Maint. Echelon
3.21 i	10.8	2480	2-1/2T	FO	L	Body, hood & cowl bent & torn. Plastic headlights melted. Body corner support broken.	-	Org.
3.21 i	10.8	2480	1/4T	FO	L	Fender bent, cowl & hood bent, body bent. Windshield glass broken.	-	Org.
3.21 i	10.8	2480	1/4T	SO	M	Vehicle upside down. Hood blown off. Hydrostatic lock in one cylinder. Cowl & body bent. Windshield glass broken, frame (W/S) bent.	1-1/2	Org.
3.21 j	10.6	2860	2-1/2T	FO	L	Windshield glass blown out, cowl torn, hood blown off. Body scorched.	-	Org.
3.21 j	10.6	2860	2-1/2T	SO	L	Truck lying on side, windshield glass broken. Windshield frame bent, hood blown off, cowl torn. Body bent & scorched.	1/2	Org.
3.21 ia	10.2	3060	1/4T	FO	L	Hood blown off. Windshield glass blown out, windshield frame bent. Body & seats scorched.	-	Org.

TABLE C.3 Shot 9 (Cont'd)

Position	psi	Range (ft)	Item	Orientation	Degree of Damage	Damage Description	To Restore to Combat Use	
							Man Hours	Maint. Echelon
3.21 ia	10.2	3060	1/4T	SO	L	Vehicle upside down, steering wheel bent, hood blown off, body & cowl bent & torn, paint scorched.	1/2	Org.
3.21 ib	8.3	3930	2-1/2T	FO	L	Hood blown off, cowl torn, windshield glass blown out, windshield frame bent. Body and Cab bent.	-	Org.
3.21 ib	8.3	3930	2-1/2T	RO	L	Body bent, hood bent, glass broken.	-	Org.
3.21 ib	8.3	3930	1/4T	RO	L	Hood blown off. Steering wheel bent, seats scorched, windshield glass blown out. Windshield frame bent.	-	Org.
3.21 ib	8.3	3930	1/4T	FO	L	Hood blown off, hood, cowl, & windshield frame bent, windshield glass blown out.	-	Org.
3.21 k	7.4	4360	2-1/2T	SO	L	Truck lying on left side. Body, hood, & cab bent. Windshield glass broken.	1/2	Org.
3.21 k	7.4	4360	2-1/2T	FO	L	Hood, steering wheel, & cab bent. Cowl torn, seats scorched. Windshield glass broken.	-	Org.

TABLE C.3 Shot 9 (Cont'd)

Position	psi	Range (ft)	Item	Orientation	Degree of Damage	Damage Description	To Restore to Combat Use	
							Man-Hours	Maint. Echelon
3.21 k	7.4	4360	1/4T	SO	L	Hood blown off and bent. Windshield, frame and body bent. Windshield glass blown out. Vehicle lying on right side.	1/3	Org.
3.21 k	7.4	4360	1/4T	FO	L	Hood blown off & bent. Windshield frame & cowl bent. Windshield glass broken out. Paint & seats scorched.	-	Org.
3.21 l	6.3	5590	2-1/2T	FO	L	Windshield glass blown out. Hood blown off. Headlight lens scorched.	-	Org.
3.21 l	6.3	5590	2-1/2T	SO	L	Hood, body, & cab bent. Windshield glass cracked. Brake master cylinder defective but workable.	-	Org.
3.21 l	6.3	5590	1/4T	FO	L	Cowl bent, windshield glass blown out.	-	Org.
3.21 l	6.3	5590	1/4T	SO	L	Hood latch broken, steering wheel scorched.	-	Org.
3.21 l	6.8	5200	90 mm AA Gun	FO	L	Paint scorched, elevating hand wheels jammed by indicator dial. Weapon extremely dirty.	4-1/2	Org.
3.21 m	4.4	6550	2-1/2T	SO	L	Hood blown open, right door panel bent. Paint scorched.	-	Org.

TABLE C.3 Shot 9 (Cont'd)

Position	psi	Range (ft)	Item	Orientation	Degree of Damage	Damage Description	To Restore to Combat Use	
							Man-Hours	Maint. Echelon
3.21 m	4.4	6550	2-1/2T	FO	L	Cowl bent, windshield glass cracked. Tail pipe pulled out of muffler.	-	Org.
3.21 m	4.4	6550	1/4T	SO	L	Hood catch latch loosened.	-	Org.
3.21 m	4.4	6550	1/4T	FO	L	Windshield broken.	-	Org.

TABLE C.4 Shot 10

Position	psi	Range (ft)	Item	Orientation	Degree of Damage	Damage Description	To Restore to Combat Use	
							Man-Hours	Maint. Echelon
3.21 n	330	380	Tank M4	FO	S	Pushed into ground, tracks blown off, over half of road wheel assembly blown off in damage.	32	Depot Salvage
3.21 o	200	570	Tank M4	SO	S	Turned over, turret damaged extensively after being separated from the hull. Tracks damaged.	167	Depot Salvage
3.21 o	200	570	Tank M24	FO	S	Pushed to rear. Turret damaged extensively, engine mount broken.	28	Depot Salvage
3.21 p	160	645	57 mm Gun	FO	S	Trails badly bent, wheels blown off, shields blown off, recoil mechanism not operating.	11	Field Salvage
3.21 p	160	645	57 mm Gun	FO	S	Trails badly bent, right wheel blown off, left wheel, spindle, & right wheel spindle bent. Pintle pin bent, shields & sighting equipment blown off.	14	Field Salvage
3.21 q	130	715	57 mm Gun	RO	S	Top & bottom carriage separated, both wheels blown off, left trail missing, right trail bent & twisted, shields & sighting equipment blown off.	13	Field Salvage
3.21 q	130	715	57 mm Gun	FO	S	Trails bent & twisted, right wheel blown off, shields & sighting equipment blown off, recoil housing & cradle twisted.	12.5	Field Salvage

TABLE C.4 Shot 10 (Cont'd)

Position	psi	Range (ft)	Item	Orientation	Degree of Damage	Damage Description	To Restore to Combat Use	
							Man-Hours	Main. Echelon
3.21 q	130	715	M24 Tank	FO	S	Turret blown off, hull caved in, tracks blown off.	148	Depot Salvage
3.21 q	130	715	57 mm Gun	SO	S	Top carriage, left wheel, shields, & sighting equipment blown off. Right wheel & trails bent & twisted.	12	Field Salvage
3.21 q	130	715	105 mm How.	RO	S	Trails and gun-cradle rails badly bent & twisted. Equilibrators blown off, firing base bent, left wheel missing.	21-1/4	Depot Salvage
3.21 q	130	715	90 mm Gun	FO	S	Tube, rails & cradle blown or knocked from mount, firing platform bent & twisted. Director blown into small pieces.	45	Depot Salvage
3.21 r	90	850	57 mm Gun	RO	S	Trails bent & twisted, right wheel, shields, & sighting equipment blown off, left wheel, recoil piston rod, & cradle bent, elevating arc teeth stripped.	16	Field Salvage
3.21 r	90	850	57 mm Gun	SO	S	Trails bent & twisted, right wheel, shields, & sighting equipment blown off, elevating mechanism housing bent.	11	Field Salvage
3.21 r	90	850	57 mm Gun	FO	S	Trails bent & twisted left, wheel shields ' sighting equipment blown off, recoil housing bent, elevating arc's teeth stripped.	13	Field Salvage

TABLE C.4 Shot 10 (Cont'd)

Position	psi	Range (ft)	Item	Orientation	Degree of Damage	Damage Description	To Restore to Combat Use	
							Man-Hours	Maint. Echelon
3.21 r	90	850	105 mm How.	RO	S	Trails bent & twisted, right wheel, spindle & cradle bent, equilibrator bent, left spindle bracket broken.	13	Field Salvage
3.21 t	78	900	57 mm Gun	RO	S	Trails bent & twisted, left wheel & shield blown off, right wheel, pintle pin, & recoil mechanism bent, sights scorched.	11	Field Salvage
3.21 t	78	900	57 mm Gun	SO	S	Trails bent & twisted, right & left wheel spindles, right wheel & pintle bent, elevating mechanism jammed, shields blown off, hole in recoil mechanism.	12.5	Field Salvage
3.21 t	78	900	57 mm Gun	FO	S	Trails bent & twisted, cradle bent, recoil mechanism dented, & shields blown off.	7	Field Salvage
3.21 t	78	900	105 mm	RO	S	Trails bent & twisted, cradle		Salvage

TABLE C.4 Shot 10 (Cont'd)

Position	psi	Range (ft)	Item	Orientation	Degree of Damage	Damage Description	To Restore to Combat Use	
							Man-Hours	Maint. Echelon
3.21 d	58	995	1/4T	FO	S	Vehicle blown into pieces	-	Salvage
3.21 d	58	995	1/4T	RO	S	Vehicle blown into pieces	-	Salvage
3.21 d	58	995	2-1/2T	FO	S	Truck blown into pieces	-	Salvage
3.21 d	58	995	2-1/2T	RO	S	Truck blown into pieces	-	Salvage
3.21 u	51	1045	M4 Tank	RO	S	Turret inoperable, tracks broken, road wheels torn off.	69	Depot Salvage
3.21 u	51	1045	M4 Tank	RO	S	Pushed to rear into ground, turret jammed, engine mounts broken, tracks & road wheels broken & bent.	70	Depot Salvage
3.21 u	51	1045	57 mm Gun	RO	S	Trails bent & twisted, wheel & shields blown off, left wheel & breech operating lever bent.	11	Field Salvage
3.21 u	51	1045	57 mm Gun	SO	S	Trails bent & twisted, right wheel, left trunion cap, shields, & sighting equipment sheared &/or blown off, pintle pin & cradle bent, recoil housing dented.	11.5	Field Salvage
3.21 u	51	1045	57 mm Gun	FO	S	Both trails bent & twisted, elevating mechanism will not function, housing spring shields & sighting equipment blown off.	7	Field Salvage

TABLE C.4 Shot 10 (Cont'd)

Position	psi	Range (ft)	Item	Orientation	Degree of Damage	Damage Description	To Restore to Combat Use	
							Man-Hours	Maint. Echelon
3.21 v	43	1100	105 mm How.	RO	S	Trails bent & twisted, both wheels blown off, right wheel spindle broken, elevating mechanism bent, breech cross head split.	7.5	Field Salvage
3.21 v	43	1100	57 mm Gun	RO	S	Trails bent & twisted, both wheels blown off, cradle & sleigh bent, recoil housing punctured, shields blown off.	10.5	Field. Salvage
3.21 v	43	1100	57 mm Gun	SO	S	Trails bent & twisted, right wheel sheared off, shields blown off, sight bracket broken & bent, recoil housing bent.	9.8	Field Salvage
3.21 v	43	1100	57 mm Gun	FO	S	Right trail bent & twisted, end of barrel gouged slightly, shield blown off, sighting equipment missing, sight bracket broken & bent	8.5	Field Salvage
3.21 v	43	1100	57 mm Gun	SO	S	Trails bent & twisted, right wheel & left shield blown off, right wheel spindle, pintle pin & recoil housing bent.	12	Field Salvage
3.21 v	43	1100	57 mm Gun	RO	S	Top carriage & tube blown off, botton carriage, right trail broken, left trail bent & twisted, right wheel spindle broken; left wheel spindle bent; shield blown off, sight bent.	11.3	Field Salvage

TABLE C.4 Shot 10 (Cont'd)

Position	psi	Range (ft)	Item	Orientation	Degree of Damage	Damage Description	To Restore to Combat Use	
							Man-Hours	Maint. Echelon
3.21 e	39	1130	1/4T	FO	S	Vehicle blown to pieces	-	Salvage
3.21 e	39	1130	1/4T	SO	S	Vehicle blown to pieces	-	Salvage
3.21 e	39	1130	2-1/2T	FO	S	Truck blown to pieces	-	Salvage
3.21 e	39	1130	2-1/2T	SO	S	Truck blown to pieces	-	Salvage
3.21 w	27	1265	57 mm Gun	RO	S	Trails bent & twisted, wheels, pintle pin, & bottom carriage bent, elevating arcs stripped, shields & sight bracket blown off.	8.8	Field Salvage
3.21 w	27	1265	57 mm Gun	SO	S	Trails bent & twisted, recoil housing dented; right wheel spindle bent; shields & sighting equipment blown off.	9.6	Field Salvage
3.21 w	27	1265	57 mm Gun	FO	M	Right trail bent, shields & sighting equipment blown off.	7	Field
3.21 w	27	1265	105 mm How.	RO	S	Trails dented, traversing gear case sheared off, damage to tires & sights by debris.	8.25	Field Salvage
3.21 x	18	1415	57 mm Gun	RO	S	trails broken off, wheels blown off, cradle badly bent, elevating arc burned, recoil piston rod bent, pintle pin bent.	17	Field Salvage
3.21 x	18	1415	57 mm Gun	FO	M	Left trail bent & twisted badly, right trail bent, shields bent, sight lens burned & chipped.	6.5	Field

TABLE C.4 Shct 10 (Cont'd)

Position	psi	Range (ft)	Item	Orientation	Degree of Damage	Damage Description	To Restore to Combat Use	
							Man-Hours	Maint. Echelon
3.21 x	18	1415	57 mm Gun	SO	S	Trails bent & twisted; right wheel spindle, firing linkage, and sight and bracket broken, left shield broken off, cocking handle missing.	12	Field Salvage
3.21 x	18	1415	M-7 SP How.	SO	S	Armour pushed in, tracks broken, road wheels & sprockets bent.	64	Depot
3.21 ad	12.5	1600	1/4T	SO	S	Vehicle blown to pieces	-	Salvage
3.21 ad	12.5	1600	2-1/2T	SO	S	Vehicle blown to pieces	-	Salvage
3.21 i	9	1920	1/4T	SC	S	Truck demolished, blown to pieces	-	Salvage
3.21 i	9	1920	2-1/2T	SO	S	Truck demolished, blown to pieces	-	Salvage
3.21 y	8.6	2140	57 mm Gun	RO	L	Right shield blown off, sight scorched & chipped.	0.25	Org.
3.21 y	8.6	2140	57 mm Gun	SO	L	Pintle pin bent; sight scorched & chipped.	4.5	Field
3.21 af	8.4	2415	1/4T	SO	S	Vehicle upside down, radiator pushed against fan, radiator leaking, frame bent, left side of body bent, left rear spring shackle broken, body bent & twisted.	24-1/3	Depot
3.21 af	8.4	2415	2-1/2T	SO	M	Truck upside down, hydrostatic lock, both front tires blown out; body, cab, hood & cowl bent & torn. Hole in radiator.	6	Org.

TABLE C.4 Shot 10 (Cont'd)

Position	psi	Range (ft)	Item	Orientation	Degree of Damage	Damage Description	To Restore to Combat Use	
							Man-Hours	Maint. Echelon
3.21 ag	7.6	2770	2-1/2T	SO	M	Truck lying on left side transfer case broken by flying missile. Body, cab, hood & cowl burnt & torn, chassis wiring cut several places by missiles.	5	Org.
3.21 ag	7.6	2770	1/4T	SO	L	Vehicle lying on left side, steering column & wheel bent, windshield glass broken, windshield frame bent and twisted.	0.5	Org.
3.21 a	7.2	3000	90 mm Gun	FO	L	Indicator faces broken, scales scorched (could be employed against ground targets in approximately 2 hr).	3	Org.
3.21 k	4.0	4380	1/4T	SO	L	Hood blown off, steering wheel scorched, windshield glass broken, windshield frame, dowl & body bent.	none	Org.
3.21 k	4.0	4380	2-1/2T	SO	L	Hood blown off, body & cab bent slightly, windshield glass broken, windshield frame bent.	none	Org.

TABLE C.5 Damage Evaluation

Type of Artillery: 57 mm, AT, M1
USA No. Tube No. 5671 Carriage No. 14701 Date of Evaluation: 5/30/53.
Position: 3.21 p 650 ft.
Recoil No. 9944

Component	Remarks	Man-Hours Req. to Restore CU*	Completely
Axle	No damage		
Equalizer	No applicable		
Trails	Right & left trail assemblies bent and twisted	6-1/3	6-1/3
Wheels	Right wheel disc & rim assembly w/hub & brake drum blown off, spindle bent. Left wheel disc & rim assembly bent. Wheel spindle bent.	4	4
Brakes	Right brake mechanism assembly torn off wheel spindle flange. Left hand brake lever & ratchet bent.	2	2
Top Carriage	No damage		
Pintle Pin and Bushing	Pintle pin bent, pivot battered (repair time included under trails 40 min).		
Traversing Worm	Not applicable		
Traversing Rack	Not applicable		
Elevating Mechanism - Hand Wheels	Elevating mechanism hand wheel bent & broken	1/4	1/4
Cross Shaft	Not applicable		
Housing	Elevating mechanism worm shaft bracket broken	1	1
Elevating Arcs	No damage		

* Combat Usable

TABLE C.5 Damage Evaluation (Cont'd)

Component	Remarks	Man-Hours Req. to Restore CU	Completely
Cradle	Cradle assembly bent slightly on bottom. (Repair time included under trails, 1 hr)		
Equilibrator	Not applicable		
Shields	Right and left upper shield assembly and lower shield assembly broken and blown off. (Repair time included under trails, 2 hr 40 min.)		
Sighting Equipment	Telescope and mount blown off and destroyed.		1-1/4
Recoil Mechanism	Appeared to be undamaged		
Barrel	Appeared to be undamaged		
Breech Mechanism	Full of dirt, but operable		
Firing Mechanism	Full of dirt, but operable		
General Condition	Right & left trail assemblies bent & twisted. Right wheel assembly torn off, wheel spindle bent. Left wheel assembly and spindle bent. Elevating hand wheel broken. All shields blown off and broken. Cradle assembly bent on bottom. Damage to this weapon was extensive. Dust and dirt was blown into all exposed bearing surfaces. Weapon requires cleaning, painting, and lubrication.		4

TABLE C.6 Damage Evaluation

Type of Vehicle: M4A3E8 Date of Evaluation: 5/29/53

Component	Remarks	Man-Hours Req. to Restore CU	Completely
1. Turret			
Main Gun	Appears OK		
Co-axle MG	Appears OK		
Ammunition	None installed		
Stowage & Ready Racks	Appears OK		
Sighting Equipment for Main Gun & Co-Axle MG	None installed		
Periscopes Gunners Other	None		
Vision Blocks	Sand Blasted & cloudy		1-1/2
Radios & Interphone	None installed		
Aerials	None		
External Condition	Turret jammed, will not rotate		14
Internal Condition	General disorder, but repairable	5	10
2. Hull-Exterior			
Tracks	Loose	4	4
Road wheels	Sand blasted and charred		
Support Rollers	Appears OK		
Driving Sprockets	Several bolts sheared		2

TABLE C.6 Damage Evaluation (Cont'd)

Component	Remarks	Man-Hours Req. to Restore CU	Completely
Track Idlers	Appears OK		
Hatches	Blown open. Engine door blown open		4
Stowage Boxes	IGRB Lid Missing		2
Fenders	Blown off & missing		1
Lights	None		
External Condition	Sand blasted		
3. Hull-Interior			
Driving Controls	Appears OK		
Instrument Panel and Connections	Glass broken, electrical connections broken	2	2
Seats	Broken	15	15
Bow MG	None		
Ammunition	None		
Stowage Boxes	Appears OK		
Internal Condition	General disorder and dirty - dust, etc.	4	10
4. Motive Power			
Main Engine	Engine mount broken, wiring burnt in several places. Overhead valve cover bent in about 2 in.	40	40
Auxiliary Engine	Appears OK		
Fuel Tanks	Appears OK		

TABLE C.6 Damage Evaluation (Cont'd)

Component	Remarks	Man-Hours to Restore to CU	Completely
Cooling System and Fans	Shroud bent, but fan will rotate		10
Transmission and Drive Shaft	Appear OK		
Final Drive	Appears OK		
Painting			10
Lubrication			2

APPENDIX D

D.1 STILL PHOTOGRAPHS

The photographs taken of the various items exposed in Shot 9 and Shot 10 during UPSHOT-KNOTHOLE are shown in the following figures. Many photographs have been taken of the items exposed before and after each shot, but only those are included which it is felt are of the most interest.

Fig. D.1 Pos. 3.21f Shot 9 M35 (side-on) Before Blast

Fig. D.2 Pos. 3.21 1 Shot 9 - M38A1 Before Blast

Fig. D.3 Pos. 3.21 l Shot 9 - Typical Position Before Blast

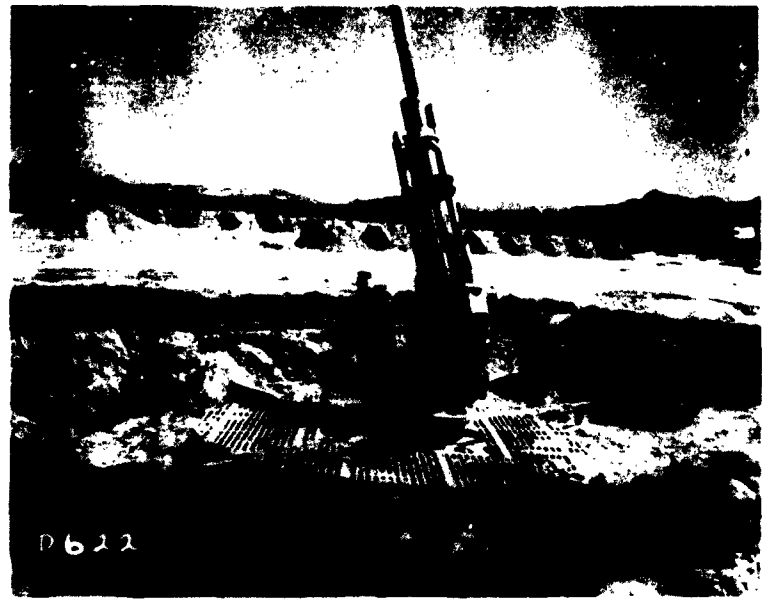

Fig. D.4 Pos. 3.21 f Shot 9 - 90 mm AA Guns Installed Before Blast

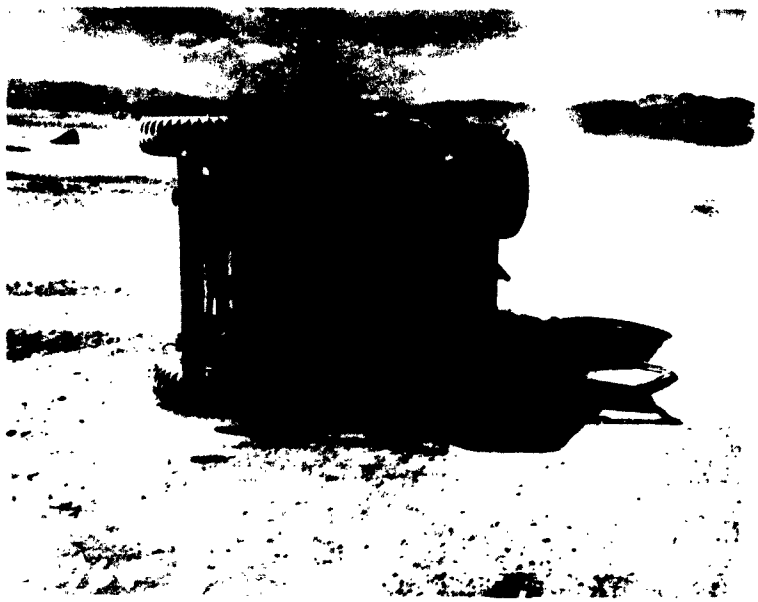

Fig. D.5 Pos. 3.21 d Shot 9 - M38A1 (Side-on) After Blast

Fig. D.6 Pos. 3.21 d Shot 9 - M38A1 (Face-on) After Blast

Fig. D.7 Pos. 3.21 e Shot 9 - M35 (Side-on) After Blast (Compare with below)

Fig. D.8 Pos. 3.21 e Shot 9 - M35 (Face-on) After Blast (Compare with above)

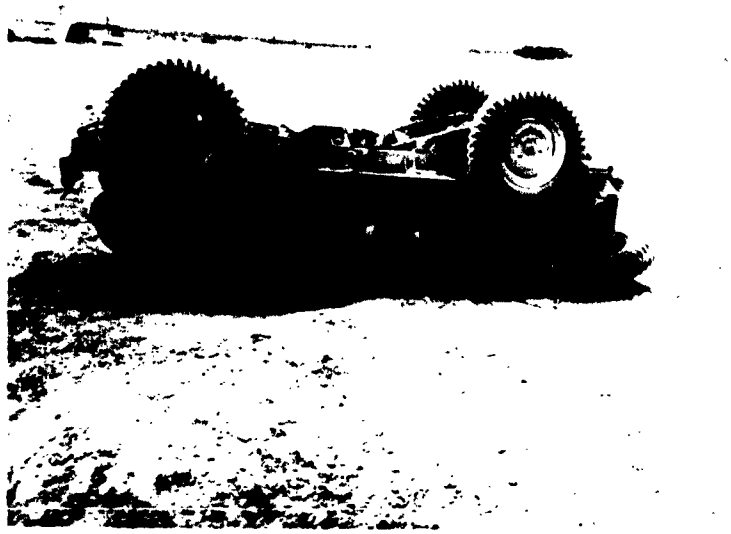

Fig. D.9 Pos. 3.21 ia Shot 9 - Dynamic Pressure = 2.6 psi computed from Measured Pressure (Compare with below)

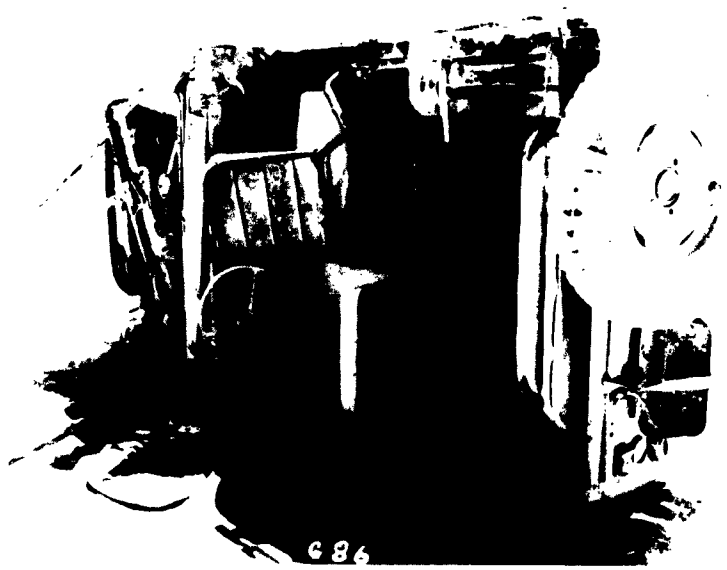

Fig. D.10 Pos. 3.21 ag Shot 10 - Dynamic Pressure = 2.0 psi computed from Ideal Curve (Compare with above)

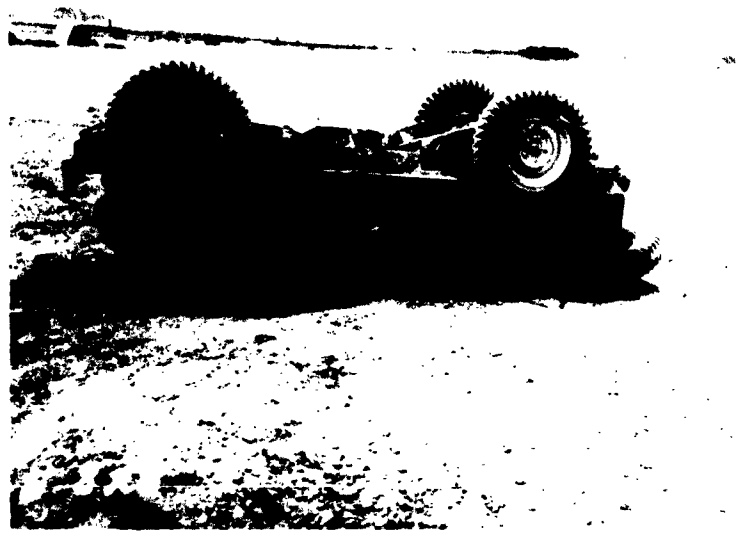

Fig. D.9 Pos. 3.21 ia Shot 9 - Dynamic Pressure = 2.6 psi computed from Measured Pressure (Compare with below)

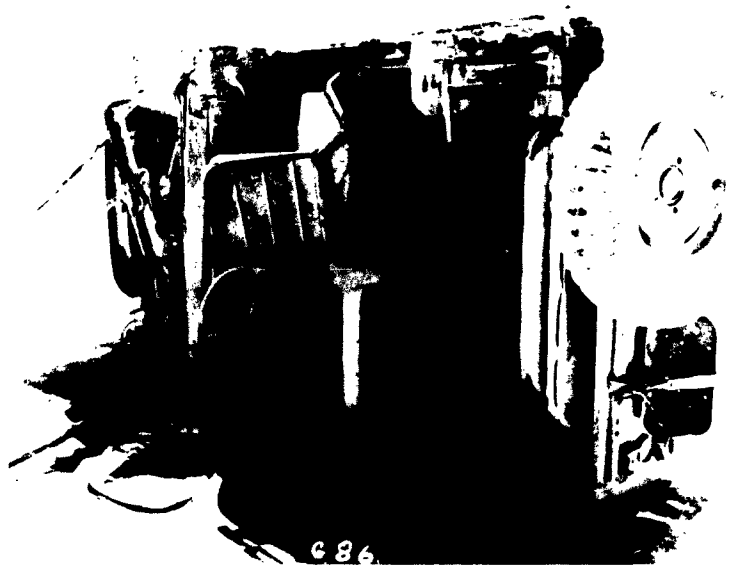

Fig. D.10 Pos. 3.21 ag Shot 10 - Dynamic Pressure = 2.0 psi computed from Ideal Curve (Compare with above)

Fig. D.7 Pos. 3.21 e Shot 9 - M35 (Side-on) After Blast (Compare with below)

Fig. D.8 Pos. 3.21 e Shot 9 - M35 (Face-on) After Blast (Compare with above)

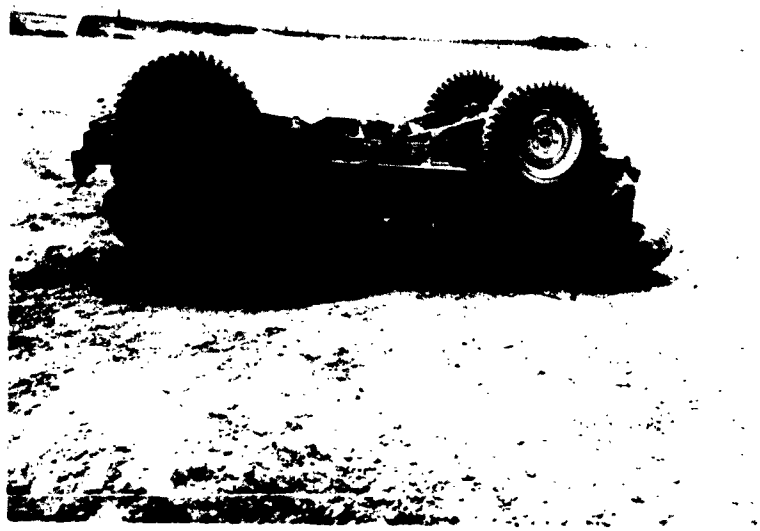

Fig. D.11 Pos. 3.21 ia Shot 9 Measured Pressure = 10.2 psi
(Compare with below)

Fig. D.12 Pos. 3.21 i Shot 10 - Measured Pressure = 9.0 psi
(Compare with above)

Fig. D.13 Uprighting Overturned M38A1 After Shot 9

Fig. D.14 Uprighting Overturned M35 After Shot 9 Using 5-Ton Wrecker

Fig. D.15 Shot 10 - 57 mm AT Gun (Emplaced) Before Blast

Fig. D.16 Shot 10 - 105 mm Howitzer, M3 (Emplaced) Before Blast

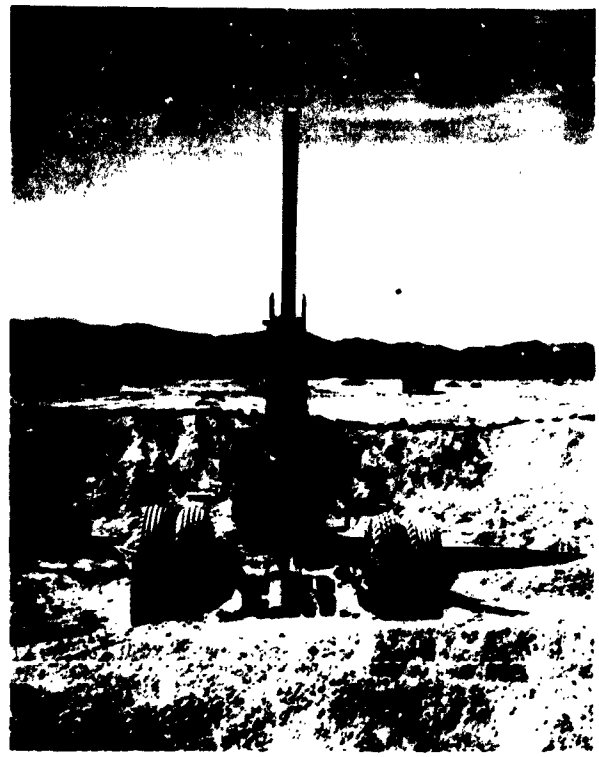

Fig. D.17 Shot 10 90 mm AA Gun (Emplaced) Before Blast

Fig. D.18 Shot 10 90 mm AA Gun (Emplaced) After Blast Struck by Debris

Fig. D.19 Pos. 3.21 p Shot 10 P_s = 160 psi 57 mm Gun After Blast Parts of Vehicle in Background

Fig. D.20 Pos. 3.21 w Shot 10 P_s = 27 psi 57 mm Gun, After Blast

Fig. D.21 Pos. 3.21 v Shot 10 P_s = 43 psi 105 mm Howitzer After Blast

Fig. D.22 Pos. 3.21 o Shot 10 P_s = 200 psi Medium Tank After Blast Turret in Rear

Fig. D.23 Pos. 3.21 u Shot 10 P_s = 51 psi Medium Tank After Blast

Fig. D.24 Pos. 3.21 n Shot 10 P_s = 300 psi Medium Tank After Blast

Fig. D.25 Pos. 3.21 e Shot 10 P_s = 39 psi 2-1/2 Ton Truck After Blast

Fig. D.26 Shot 10 Remains of 1/4 Ton Truck After Blast

REFERENCES

1. United States Department of Defense, Final Report of Atomic Bomb Tests, Vol IV, Joint Task Force I Army Ground Group (Task Group 1.4), 27 January to 30 September 1946.

2. Warren W. Berning, et al, Combat Vehicle Exposure Annex 6.3, Scientific Director's Report, Operation GREENHOUSE, August 1952.

3. BRL Memorandum Report No. 597 RD, A Report On the Prediction of Blast Effects on Ordnance Materiel at Exercise DESERT ROCK, 20 March 1952.

4. Exercise DESERT ROCK IV April - June 1952.

5. E. J. Bryant and F. E. Grubbs, Statistical Estimation of Damage to Ordnance Equipment Exposed to Nuclear Blast, BRL Memorandum Report No. 657 RD April 1953

6. Warren W. Berning, Prediction of the Effects of Atomic Weapons on Ordnance Equipment, BRL No. 847, May 1953.

7. Armour Research Foundation, Analysis of Atomic Weapon's Effects Upon Army Ground Operations Equipment, First Quarterly Report, ORO-S-80, 27 December 1950.

8. Armour Research Foundation, Analysis of Atomic Weapon's Effects Upon Army Ground Operations Equipment, Second Quarterly Report, ORO-S-81, 19 January 1951.

9. Armour Research Foundation, Analysis of Atomic Weapon's Effects Upon Army Ground Operations Equipment, Third Phase Report, ORO-S-200, 18 June 1951.

10. Armour Research Foundation, Analysis of Atomic Weapon's Effects Upon Army Ground Operations Equipment, Fourth Phase Report, ORO-S-253, Vol I, 20 November 1951.

11. Armour Research Foundation, Analysis of Atomic Weapon's Effects Upon Army Ground Operations Equipment, Fifth Phase Report, ORO, 1 July 1952.

12. Armour Research Foundation, Appendix E, Blast Loading and Structural Response, Vol I, General Blast Loading and Response, The Air Force Structures Program, Project 3.3, Operation GREENHOUSE, March 1951.

13. R. A. Eberhard and C. N. Kingery, A Coefficient of Reflection Over a Concrete Surface, BRL Report No. 860, Confidential, April 1953.

14. F. B. Porzel, Theoretical Blast Curves, Supplement to Memorandum J-17837, May 25, 1953, Theoretical Blast Curves, August 20, 1953.

15. J. D. Shreve, Jr., Pressure-Distance-Height Study of 250-lb TNT Spheres, Operation TUMBLER WT-520, April-June 1952.

16. TM 23-200 Capabilities of Atomic Weapons

17. F. H. Shelton and C. D. Broyles, New Pressure Distance Data for Low Heights of Burst and a Height-of-Burst Chart for Dynamic Pressure in the Precursor Region and for a Surface Detonation, Sandia Corporation Technical Memorandum 132-53-51, August 18, 1953.

18. C. D. Broyles, Dynamic Pressure vs. Time and Supporting Air Blast Measurements, Operation UPSHOT-KNOTHOLE WT-714, March - June 1953.

19. Exercise DESERT ROCK V, January - June 1953.

20. J. von Neumann, Oblique Reflections of Shock, Bureau of Ordnance, Explosive Research Report No. 12 (1943)

21. Courant and Friedrichs, Supersonic Flow and Shock Waves, Interscience, New York, 1948.

DISTRIBUTION

Military Distribution Categories 5-21 and 5-60

ARMY ACTIVITIES

1 Asst. Chief of Staff, G-3, D/A, Washington 25, D.C ATTN: Dep. CofS, G-3 (RR&SW)
2 Deputy Chief of Staff for Logistics, D/A, Washington 25, D.C. ATTN: Director of Research & Development
3 Chief of Ordnance, D/A, Washington 25, D.C. ATTN: ORDTX-AR
4- 6 Chief Signal Officer, D/A, P&O Division, Washington 25, D.C. ATTN: SIGOP
7 The Surgeon General, D/A, Washington 25, D.C. ATTN: Chief, R&D Division
8- 9 Chief Chemical Officer, D/A, Washington 25, D.C.
10 The Quartermaster General, CBR, Liaison Officer, Research and Development Div., D/A, Washington 25, D.C.
11- 15 Chief of Engineers, D/A, Washington 25, D.C. ATTN: ENGNB
16 Chief of Transportation, Military Planning and Intelligence Div., Washington 25, D.C.
17- 19 Commanding General, Continental Army Command, Ft. Monroe, Va.
20 President, Board #1, Headquarters, Continental Army Command, Ft. Bragg, N.C.
21 President, Board #2, Headquarters, Continental Army Command, Ft. Knox, Ky.
22 President, Board #3, Headquarters, Continental Army Command, Ft. Benning, Ga.
23 President, Board #4, Headquarters, Continental Army Command, Ft. Bliss, Tex.
24 Commanding General, U.S. Army Caribbean, Ft. Amador, C.Z. ATTN: Cml. Off.
25 Commander-in-Chief, European Command, APO 128, c/o PM, New York, N.Y.
26- 27 Commander-in-Chief, Far East Command, APO 500, c/o PM, San Francisco, Calif. ATTN: ACofS, J-3
28- 29 Commanding General, U.S. Army Europe, APO 403, c/o PM, New York, N.Y. ATTN: OPOT Div., Combat Dev. Br.
30- 31 Commandant, Command and General Staff College, Ft. Leavenworth, Kan. ATTN: ALLLS(AS)
32 Commandant, The Artillery School, Ft. Sill, Okla.
33 Secretary, The AAAGM Branch, The Artillery School, Ft. Bliss, Tex. ATTN: Lt. Col. Albert D. Epley, Dept. of Tactics and Combined Arms
34 Commanding General, Medical Field Service School, Brooke Army Medical Center, Ft. Sam Houston, Tex.
35 Director, Special Weapons Development Office, Ft. Bliss, Tex. ATTN: Lt. Arthur Jaskierny
36 Commandant, Army Medical Service Graduate School, Walter Reed Army Medical Center, Washington 25, D.C.
37 Superintendent, U.S. Military Academy, West Point, N.Y. ATTN: Prof. of Ordnance
38 Commandant, Chemical Corps School, Chemical Corps Training Command, Ft. McClellan, Ala.
39 Commanding General, Research and Engineering Command, Army Chemical Center, Md. ATTN: Deputy for RW and Non-Toxic Material
40- 41 Commanding General, Aberdeen Proving Grounds, Md. (inner envelope) ATTN: RD Control Officer (for Director, Ballistics Research Laboratory)
42- 44 Commanding General, The Engineer Center, Ft. Belvoir, Va. ATTN: Asst. Commandant, Engineer School
45 Commanding Officer, Engineer Research and Development Laboratory, Ft. Belvoir, Va. ATTN: Chief, Technical Intelligence Branch
46 Commanding Officer, Picatinny Arsenal, Dover, N.J. ATTN: ORDBB-TK
47 Commanding Officer, Army Medical Research Laboratory, Ft. Knox, Ky.
48- 49 Commanding Officer, Chemical Corps Chemical and Biological Laboratory, Army Chemical Center, Md. ATTN: Tech. Library
50 Commanding Officer, Transportation R&D Station, Ft Eustis, Va.
51 Director, Technical Documents Center, Evans Signal Laboratory, Belmar, N.J.
52 Director, Waterways Experiment Station, PO Box 631 Vicksburg, Miss. ATTN: Library
53 Director, Armed Forces Institute of Pathology, 7th Independence Avenue, S.W., Washington 25, D.C.
54 Director, Operations Research Office, Johns Hopkins University, 7100 Connecticut Ave., Chevy Chase, Md. ATTN: Library
55- 61 Technical Information Service, Oak Ridge, Tenn. (Surplus)

NAVY ACTIVITIES

62- 63 Chief of Naval Operations, D/N, Washington 25, D.C. ATTN: OP-36
64 Chief of Naval Operations, D/N, Washington 25, D.C ATTN: OP-03EG
65 Director of Naval Intelligence, D/N, Washington 25, D.C. ATTN: OP-922V
66 Chief, Bureau of Medicine and Surgery, D/N, Washington 25, D.C. ATTN: Special Weapons Defense Div.
67 Chief, Bureau of Ordnance, D/N, Washington 25, D.C.
68 Chief, Bureau of Ships, D/N, Washington 25, D.C. ATTN: Code 348
69 Chief, Bureau of Yards and Docks, D/N, Washington 25, D.C. ATTN: D-440
70 Chief, Bureau of Supplies and Accounts, D/N, Washington 25, D.C.
71- 72 Chief, Bureau of Aeronautics, D/N, Washington 25, D.C.
73 Chief of Naval Research, Department of the Navy Washington 25, D.C. ATTN: LT(jg) F. McKee, USN
74 Commander-in-Chief, U.S. Pacific Fleet, Fleet Post Office, San Francisco, Calif.
75 Commander-in-Chief, U.S. Atlantic Fleet, U.S. Naval Base, Norfolk 11, Va.
76- 79 Commandant, U.S. Marine Corps, Washington 25, D.C. ATTN: Code A03H
80 President, U.S. Naval War College, Newport, R.I.
81 Superintendent, U.S. Naval Postgraduate School, Monterey, Calif.
82 Commanding Officer, U.S. Naval Schools Command, U.S. Naval Station, Treasure Island, San Francisco, Calif.
83 Commanding Officer, U.S. Fleet Training Center, Naval Base, Norfolk 11, Va. ATTN: Special Weapons School
84- 85 Commanding Officer, U.S. Fleet Training Center, Naval Station, San Diego 36, Calif. ATTN: (SPWP School)
86 Commanding Officer, Air Development Squadron 5, VX-U.S. Naval Air Station, Moffett Field, Calif.
87 Commanding Officer, U.S. Naval Damage Control Training Center, Naval Base, Philadelphia 12, Pa. ATTN: AE Defense Course
88 Commanding Officer, U.S. Naval Unit, Chemical Corps School, Army Chemical Training Center, Ft. McClellan, Ala.
89 Commander, U.S. Naval Ordnance Laboratory, Silver Spring 19, Md. ATTN: EE
90 Commander, U.S. Naval Ordnance Laboratory, Silver Spring 19, Md. ATTN: EH

91 Commander, U.S. Naval Ordnance Laboratory, Silver Spring 19, Md. ATTN: R
92 Commander, U.S. Naval Ordnance Test Station, Inyokern, China Lake, Calif.
93 Officer-in-Charge, U.S. Naval Civil Engineering Res. and Evaluation Lab., U.S. Naval Construction Battalion Center, Port Hueneme, Calif. ATTN: Code 753
94 Commanding Officer, U.S. Naval Medical Research Inst., National Naval Medical Center, Bethesda 14, Md.
95 Director, U.S. Naval Research Laboratory, Washington 25, D.C. ATTN: Code 2029
96 Commanding Officer and Director, U.S. Navy Electronics Laboratory, San Diego 52, Calif. ATTN: Code 4223
97- 98 Commanding Officer, U.S. Naval Radiological Defense Laboratory, San Francisco 24, Calif. ATTN: Technical Information Division
99 Director, Naval Air Experimental Station, Air Material Center, U. S. Naval Base, Philadelphia, Penn.
100-101 Commanding Officer and Director, David W. Taylor Model Basin, Washington 7, D.C. ATTN: Library
102 Commander, U.S. Naval Air Development Center, Johnsville, Pa.
103 Director, Office of Naval Research Branch Office, 1000 Geary St., San Francisco, Calif.
104-110 Technical Information Service, Oak Ridge, Tenn. (Surplus)

AIR FORCE ACTIVITIES

111 Asst. for Atomic Energy, Headquarters, USAF, Washington 25, D.C. ATTN: DCS/O
112 Director of Operations, Headquarters, USAF, Washington 25, D.C. ATTN: Operations Analysis
113 Director of Plans, Headquarters, USAF, Washington 25, D.C. ATTN: War Plans Div.
114 Director of Research and Development, Headquarters, USAF, Washington 25, D.C. ATTN: Combat Components Div.
115-116 Director of Intelligence, Headquarters, USAF, Washington 25, D.C. ATTN: AFOIN-1B2
117 The Surgeon General, Headquarters, USAF, Washington 25, D.C. ATTN: Bio. Def. Br., Pre. Med. Div.
118 Deputy Chief of Staff, Intelligence, Headquarters, U.S. Air Forces Europe, APO 633, c/o PM, New York, N.Y. ATTN: Directorate of Air Targets
119 Commander, 497th Reconnaissance Technical Squadron (Augmented), APO 633, c/o PM, New York, N.Y.
120 Commander, Far East Air Forces, APO 925, c/o PM, San Francisco, Calif.
121 Commander, Strategic Air Command, Offutt Air Force Base, Omaha, Nebraska. ATTN: Special Weapons Branch, Inspection Div., Inspector General
122 Commander, Tactical Air Command, Langley AFB, Va. ATTN: Documents Security Branch
123 Commander, Air Defense Command, Ent AFB, Colo.
124-125 Commander, Wright Air Development Center, Wright-Patterson AFB, Dayton, O. ATTN: WCRRN, Blast Effects Research
126 Commander, Air Training Command, Scott AFB, Belleville, Ill. ATTN: DCS/O GTP
127 Assistant Chief of Staff, Installations, Headquarters, USAF, Washington 25, D.C. ATTN: AFCIE-E
128 Commander, Air Research and Development Command, PO Box 1395, Baltimore, Md. ATTN: RDDN
129 Commander, Air Proving Ground Command, Eglin AFB, Fla. ATTN: AG/TRB
130-131 Director, Air University Library, Maxwell AFB, Ala.
132-139 Commander, Flying Training Air Force, Waco, Tex. ATTN: Director of Observer Training
140 Commander, Crew Training Air Force, Randolph Field, Tex. ATTN: 2CTS, DCS/O
141 Commander, Headquarters, Technical Training Air Force, Gulfport, Miss. ATTN: TA&D
142-143 Commandant, Air Force School of Aviation Medicine, Randolph AFB, Tex.
144-149 Commander, Wright Air Development Center, Wright-Patterson AFB, Dayton, O. ATTN: WCOSI
150-151 Commander, Air Force Cambridge Research Center, 230 Albany Street, Cambridge 39, Mass. ATTN: CRQST-2
152-154 Commander, Air Force Special Weapons Center, Kirtland AFB, N. Mex. ATTN: Library
155 Commandant, USAF Institute of Technology, Wright-Patterson AFB, Dayton, O. ATTN: Resident College
156 Commander, Lowry AFB, Denver, Colo. ATTN: Department of Armament Training
157 Commander, 1009th Special Weapons Squadron, Headquarters, USAF, Washington 25, D.C.
158-159 The RAND Corporation, 1700 Main Street, Santa Monica, Calif. ATTN: Nuclear Energy Division
160-166 Technical Information Service, Oak Ridge, Tenn. (Surplus)

OTHER DEPARTMENT OF DEFENSE ACTIVITIES

167 Asst. Secretary of Defense, Research and Development, D/D, Washington 25, D.C.
168 U.S. National Military Representative, Headquarters, SHAPE, APO 55, c/o PM, New York, N.Y. ATTN: Col. J. P. Healy
169 Director, Weapons Systems Evaluation Group, OSD, Rm 2E1006, Pentagon, Washington 25, D.C.
170 Armed Services Explosives Safety Board, D/D, Building T-7, Gravelly Point, Washington 25, D.C.
171 Commandant, Armed Forces Staff College, Norfolk 11, Va. ATTN: Secretary
172-177 Commanding General, Field Command, Armed Forces Special Weapons Project, PO Box 5100, Albuquerque, N. Mex.
178-179 Commanding General, Field Command, Armed Forces, Special Weapons Project, PO Box 5100, Albuquerque, N. Mex. ATTN: Technical Training Group
180-188 Chief, Armed Forces Special Weapons Project, Washington 25, D.C.
189 Office of the Technical Director, Directorate of Effects Tests, Field Command, AFSWP, PO Box 577, Menlo Park, Calif. ATTN: Dr. E. B. Doll
190-196 Technical Information Service, Oak Ridge, Tenn. (Surplus)

ATOMIC ENERGY COMMISSION ACTIVITIES

197-199 U.S. Atomic Energy Commission, Classified Technical Library, 1901 Constitution Ave., Washington 25, D.C. ATTN: Mrs. J. M. O'Leary (For DMA)
200-202 Los Alamos Scientific Laboratory, Report Library, PO Box 1663, Los Alamos, N. Mex. ATTN: Helen Redman
203-205 Sandia Corporation, Classified Document Division, Sandia Base, Albuquerque, N. Mex. ATTN: Martin Lucero
206-207 University of California Radiation Laboratory, PO Box 808, Livermore, Calif. ATTN: Margaret Edlund
208 Weapon Data Section, Technical Information Service, Oak Ridge, Tenn.
209-265 Technical Information Service, Oak Ridge, Tenn. (Surplus)

ADDITIONAL DISTRIBUTION

266 Dr. N. M. Newmark, Room 111, Talbot Laboratory, University of Illinois, Urbana, Illinois

AEC, Oak Ridge, Tenn